Robust Control

For

Gantry Cranes

Giuseppe Costa
1999

Submitted in partial fulfilment for the requirements of the degree of Master of Engineering, School of Electrical Engineering and Telecommunications, University of New South Wales, Sydney, Australia.

To my wife Gabriela, my daughter Sofia Lily and our unborn baby

Acknowledgements

I would like to extend my sincere thanks to my supervisor Dr. D. J. Clements for his assistance during my thesis and his valuable comments on the style and contents of my thesis. I would also like to thank Associate Professor T. Hesketh for his comments on the contents of my thesis. Most of all I would like to thank my wife Gabriela for her love and support over the past 4 years.

Abstract

In this thesis a class of robust non-linear controllers for a gantry crane system are discussed. The gantry crane has three degrees of freedom, all of which are interrelated. These are the horizontal traverse of the cart, the vertical motion of the goods (i.e. rope length) and the swing angle made by the goods during the movement of the cart. The objective is to control all three degrees of freedom. This means achieving setpoint control for the cart and the rope length and cancellation of the swing oscillations.

A mathematical model of the gantry crane system is developed using Lagrangian dynamics. In this thesis it is shown that a model of the gantry crane system can be represented as two sub models which are coupled by a term which includes the rope length as a parameter. The first system will consist of the cart and swing dynamics and the other system is the hoist dynamics. The mathematical model of these two systems will be derived independent of the other system.

The model that is comprised of the two sub models is verified as an accurate model of a gantry crane system and it will be used to simulate the performance of the controllers using Matlab. For completeness a fully coupled mathematical model of the gantry crane system is also developed.

A detailed design of a gain scheduled sliding mode controller is presented. This will guarantee the controller's robustness in the presence of uncertainties and bounded matched disturbances. This controller is developed to achieve cart setpoint and swing control while achieving rope length setpoint control. A non gain scheduled sliding mode controller is also developed to determine if the more complex gain scheduled sliding mode controller gives any significant improvement in performance.

In the implementation of both sliding mode controllers, all system states must be available. In the real-time gantry crane system used in this thesis, the cart velocity and the swing angle velocity are not directly available from the system. They will be estimated using an alpha-beta state estimator.

To overcome this limitation and provide a more practical solution an optimal output feedback model following controller is designed. It is demonstrated that by expressing the system and the model for which the system is to follow in a non-minimal state space representation, LQR techniques can be used to design the controller. This produces a dynamic controller that has a proper transfer function, and negates the need for the availability of all system states.

This thesis presents an alternative method of solving the LQR problem by using a generic eigenvalue solution to solve the Riccati equation and thus determine the optimal feedback gains.

In this thesis it is shown that by using a combination of sliding mode and H_∞ control techniques, a non-linear controller is achieved which is robust in the presence of a wide variety of uncertainties and disturbances.

A supervisory controller is also described in this thesis. The supervisory control is made up of a feedforward and a feedback component. It is shown that the feedforward component is the crane operator's action, and the feedback component is a sliding mode controller which compensates as the system's output deviates from the desired trajectory because of the operator's inappropriate actions or external disturbances such as wind gusts and noise.

All controllers are simulated using Matlab and implemented in real-time on a scale model of the gantry crane system using the program RTShell. The real-time results are compared against simulated results to determine the controller's performance in a real-time environment.

TABLE OF CONTENTS

CHAPTER 1 INTRODUCTION

The field of non-linear control of dynamic systems is quite diverse. Extensive literature is available that covers general non-linear control. This thesis examines a specific non-linear system, the gantry crane.

Gantry cranes (overhead cranes) are used in numerous industrial applications, such as the loading and unloading of containers, nuclear waste handling facilities, factory automation and basically in any industry which requires heavy goods to be lifted and moved.

The study of the control of the crane is complex, as different industrial applications require different control systems. Some applications require a fast traversal time, and optimisation of the cart's motion is required. Others require very little or no swing of the goods as they are being moved. Some others require that all three dynamics of the crane be optimally controlled i.e. load positioning swing cancellation and load height.

Since the gantry crane system is a non-linear multivariable system, it provides a means of observing the performance of different types of controllers when applied to a non-linear multivariable system. These controllers consist of, but are not limited to linear, non-linear, adaptive and multivariable controllers. Thus, the solution to the control of the gantry crane is not limited to one specific area of control theory. By observing the performance of different classes of controllers, improvements in the control of industrial gantry cranes may be achieved.

Non-linear control is not treated in its purest form in this thesis, where the non-linear controller is derived from a non-linear model. Even though the gantry crane system is a non-linear system, the non-linear controller is derived from the linearised model of the crane.

The non-linearities in the designed controller stem from two major aspects,

1) The sliding mode controller is inherently a non-linear controller due to the discontinuous function present in the control structure.
2) Gain scheduling is used with respect to the rope length in the design of the sliding mode controller.

These two key aspects will produce a non-linear controller that will be simulated on the linearised model, and implemented in real-time on the non-linear gantry crane system.

This thesis considers not only the theoretical implications of control theory, but also the practical issues that arise in industrial applications of the gantry crane. Thus, unlike most literature that has been published, this thesis extends non-linear control to a practical implementation to compare theoretical results with practical results.

1.1 LITERATURE REVIEW

An overview of the literature that has been published in relation to *crane control* is given in this section. A literature review of the *sliding mode controller* is given in Chapter 4 and a literature review of *output feedback controllers* and *model following controllers* is given in Chapter 9.

The literature reviewed details different approaches in the control of the gantry crane system. These controllers extend from simple state feedback controllers [28], to more complex non-linear controllers [24] and [26].

Ridout [28] solved the problem of swing control and cart positioning by use of a state variable feedback design. He did not consider rope length control, which is a critical component in the practical application of the gantry crane. Ridout found that the practical implementation of the controller had to be tuned on line to achieve results that could correlate to his simulation. This means either his modelling of the crane needed to be more accurate, or the linear controller was sensitive to changes in system parameters, which is a characteristic of linear controllers.

Nguyen [26] extended Ridout's work to include rope length control. He developed a simple gain scheduled state variable feedback controller. He also details a model for the crane in which the cart dynamics are also influence by a change in the rope length. It thus can be clearly seen that he would achieve better performance if he were to schedule all feedback gains rather then just the swing angular velocity. The scheduling function is a simple division of the swing angular velocity gain by the rope length. This scheduling function appears to be derived experimentally rather then mathematically, as he does not detail the mathematical derivation. If a mathematical derivation were used, then all feedback gains would be scheduled by the rope length. Nguyen only details the robustness of the controller's operation for a finite operating region. Thus, there is no guarantee of the controller's performance over the whole operating space. Also since Nguyen's controller is basically a state variable feedback controller there is guarantee of the controllers performance in the presence of uncertainties.

Auernig and Troger [20] solved the time optimal problem of the gantry crane, but only simulation results were available, and they did not detail the proof of the concavity of maximised hamiltonian. While this is quite a valid solution there do exist flaws in this approach in that since they solved the problem analytically, they require a very accurate model. Also their controller is an open loop controller that does not cater for system imperfection and disturbances. Auernig and Troger basically developed a bang–bang controller for the crane, but a practical implementation of a bang–bang controller is strictly not feasible, as it causes excessive wear and tear on machinery and parts. Also for safety reasons a sudden and large current being switched to the motors is not desirable.

Singhose, Porter and Seering [27] proposed a method of feedforward control called input shaping to control the gantry crane. Input shaping was solely used to minimise the magnitude of the swing angle and does not address rope length control or cart positioning control. Basically input shaping requires a known command signal that produces an approximate desired response for the system. This approximate command signal may then leave residual oscillations in the swing angle. If the frequency of these oscillations is known, then a new command signal can be produced by convoluting the approximate command signal with a filter (input shaper) which cancels the residual frequencies. The impulses that constitute the shaper must have appropriate amplitude and time locations to cancel the residual oscillations. Singhose used an IIR filtering technique for the input shaping.

Convolving the command signal with a sequence of impulses forms the input shaping signal. The command signal can be derived by an analytical approach [20] or by observing an experienced crane driver.

Singhose noted that if the modelling frequency is not exact then the input shaping methods would not completely cancel the swing angle. Thus, in using input shaping, one must have a superior knowledge of the systems to generate an appropriate command signal. This is also required to position the impulse at the correct time location in order to minimise any system vibrations. In simulation this is clearly possible, but in a

practical environment that consists of noise and changing system parameters, this method would produce an ineffective control signal.

Woods and Clements [24] detail a method to achieve non-linear control of the gantry crane system by using a dynamic exact linearisation controller. This method basically transforms a non-linear system into a linear normal form, from which a linear controller is designed by means of the dynamic exact linearisation technique. A reverse transformation is then performed on the controller, such that it is a function of the correct system states. Thus, transforming the linear controller into a non-linear controller. Their work compared the non-linear controller with a linear controller that was designed when the system was linearised about it's operating points. They found that if the rope length was varied by a large amount the linear controller would be unstable, whereas the non-linear controller would be stable. This method is also a valid solution, however their work does not detail any practical implementation of the controller, nor if cart positioning and rope length control was achieved. Thus, there is no guarantee that the controller will behave similar to the simulation when it is implemented in a noisy environment.

Butler [22] proposed an adaptive model reference controller that used model decomposition to develop an adaptive controller. He presents a method that produces a reduced order controller for both cart position and swing cancellation. Butler [8] has not dealt with the hoisting system. It is also assumed that the model and system are of the same order i.e. perfect model matching. Thus, Butler (and all the papers discussed in this section) assumes that all relevant states must be measurable or observable. Clearly in practice it is not always the case that all system states are directly available.

Boustany and d'Andrea–Novel [21] and [23] describe and compare both adaptive and non-adaptive controllers that are derived from a Lyapunov approach and the dynamic feedback linearisation technique, where the adaptation is on the load mass. They show that in the non-adaptive case a controller that is designed via a Lyapunov approach does give greater stability over a larger range of masses than the linearisation technique.
In the adaptive case, they show that using the Lyapunov approach to derive an adaptive controller does not bring in any special improvements, which is to be expected since the

Lyapunov approach is very robust to parametric uncertainties. They found that an adaptive controller based on dynamic feedback linearisation produces far greater stability for a larger range of the load mass than a non-adaptive controller. Both methods of deriving adaptive controllers provide global stability, as non-linear controllers are produced, but they can be quite difficult to implement in real-time. For a complete practical solution using either of their described methods their work must be extended to include cart positioning and rope length control, which they do not address. It should be noted that they only provide experimental results and no practical consideration is given.

Burg [26] implements saturation control that was proposed by Teel [36] - [37]. Burg uses saturation control to minimise the swing angle. The controller design does not guarantee the magnitude of the swing angle, but Burg assumes that if the input force to the system can be limited by a saturation function, then swing minimisation should be achieved. In this work rope length control was also not considered. One key aspect that is noted in this paper is that in order to achieve swing minimisation, slower traverse time is required. Thus, in using the saturation method there is a trade off between settling time and swing angle.

Pieper and Surgenor [19] simulated a discrete sliding mode controller on the gantry crane system. Pieper [19] used a linear quadratic solution as a benchmark for the discrete sliding mode controller's performance. They observed that the DSMC performed just as well as the LQ controller design. In this work, rope length control was also not considered. The model used by Pieper [19] is not a scaled model of a real crane, and uses pneumatic controls for the input to the cart. Thus, Pieper and Surgenor had to use pulse width modulation in order to drive the system. A more practical solution for this apparatus would be to use time optimal control, such as the open loop method proposed in [20] or a feedback time optimal Bang-Bang controller. These methods may give fewer changes in the control input and thus reduces wear and tear on the apparatus. With PWM fast on – off functions are applied as the driving force, this may cause unnecessary swing changes, which may not be apparent in a control designed by optimal control methods.

Yu, Lewis and Huang [30] use a singular perturbation approach to separate the dynamics of the crane into two sub systems. These are, a slow system that describes the "average" motion of the cart, and a fast system that describes the oscillatory motion of the load while the cart is moving. They then use LQR techniques to design a controller for each of these two subsystems. These two controllers are then combined to form a single controller for the crane. The control of the slow system enabled the cart to be positioned and follow a desired trajectory and the control of the fast system enables the swing to be minimised. Yu, Lewis and Huang [30] only consider the cases where the load height is fixed. Thus, there is no guarantee in the controller's performance while the height of the load is being controlled to a setpoint.

All the methods discussed in the literature review require at least one, if not all five of the following assumptions.

1) All states are measurable or observable.
2) The hoisting system is not considered (i.e. the load height is fixed).
3) No practical implementation of the respective theory is documented.
4) Step changes are used to instigate a new setpoint for the cart and rope length.
5) Non-linear controllers are derived from non-linear models of the system.

This thesis will attempt to give a satisfactory control solution for the above mentioned deficiencies. This will be achieved by the use of sliding mode control techniques to develop a non-linear controller for the entire crane system using a linearised model that is robust in the presence of external disturbances and system uncertainties. Then an output feedback model reference controller will be designed and implemented to cope with the fact that not all the states are present and minimise large control signals that are caused by step changes to setpoint.

1.2 AIM

This work is driven by the observation of man-operated cranes in shipyards. Manual operation of a crane takes years of experience in order to drive the crane well. The aim of this thesis is to develop and investigate a class of ***robust non-linear controllers*** that would position the cart and the load at a predefined setpoint while cancelling the swing oscillations. These controllers must not only be mathematically sound, but they must also be a viable practical solution.

This thesis presents two levels of control automatic control and supervisory control. In the case of automatic control, the controller drives the crane either to the desired setpoint, or tracks the desired trajectory that is provided by the operator. In the case of supervisory control, the operator drives the crane and the controller observes the output of the system and compensates as the system's output strays from the desired trajectory.

In order to develop these levels of control, a robust non-linear controller that will provide safe operation of the crane in the presence of uncertainties and disturbances is required.

The following objectives (of which (2) - (4) have not been documented in other literature) are set out in order to achieve the aim of this thesis.

1) *The modelling of the gantry crane*. This thesis derives a mathematical model of the gantry crane system that has the same performance as the real-time system. Two models are developed and investigated. The first is the complete mathematical model of the gantry crane system where the cart, swing, and hoist dynamics are tightly coupled together. The second model is a loosely coupled model. The loosely coupled model is comprised of one model for the hoist dynamics and another model for the cart and swing dynamics, where the cart and swing dynamics are coupled to the hoist dynamics by the rope length. This is required in order to design and simulate the controllers discussed throughout this thesis.

2) *The design and implementation of sliding mode controller for cart positioning and swing cancellation*. A continuous sliding mode controller is designed and implemented on the real-time crane by use of a computer. In this case the rope length is set to 1 metre and is not controlled. The real-time results are compared to the simulated results and any discrepancies are discussed.

   A state variable feedback controller is designed and implemented for rope length control. Discrepancies between the real-time results and the simulated results are discussed. In this instance the cart and swing dynamics are not controlled, they are fixed.

   Since the sampling rate is very fast compared to the system dynamics it is assumed that the digital implementation can be viewed as a continuous controller. Thus, discretisation of the controller is not really an issue.

3) *The design and implementation of a gain scheduled sliding mode controller*. A gain scheduled sliding mode controller (where the scheduling parameter is the rope length) is designed and implemented. All three dynamics of the system are controlled, that is the cart position, the swing cancellation, and the rope length.

   A discussion of the discrepancies between the real-time implementation and simulation of a gain scheduled sliding mode controller and a sliding mode controller that has been designed for a fixed rope length is given. In both of these cases the rope length is controlled. Controlling the rope length while controlling the cart and swing dynamics introduces parameter fluctuations and modelling uncertainties from the varying rope length.

   These two controllers are compared to observe the robustness of the sliding mode controller in the presence of modelling uncertainties and parameter fluctuations. If reasonable results are achieved with a fixed rope length sliding mode controller, then there would be no need to implement the more complex gain scheduled sliding mode controller.

4) *An output feedback model reference controller is designed and implemented*. An alternative approach to derive an output feedback model following controller is presented. This approach consists of placing the error system (i.e. the difference between the actual system and the referenced model) into non-minimal state space representation and then using an alternative method to solve the LQR problem. This method produces a controller that consists of a feedforward component and a feedback component. This alternative approach is used to design an output feedback model referenced controller which will be implemented. Discrepancies between the simulation and the real-time implementation are discussed.

It is shown that this approach to the design of output feedback model following controllers can be extended to produce a robust non-linear controller by using a combination of H_∞ and sliding mode control techniques. This allows the controller to achieve cart setpoint, swing cancellation and rope length control in the presence of a wide range of uncertainties and disturbances.

A discussion is given on how a combination of feedforward and feedback control can be used to form a supervisory controller. The operator drives the crane (this is the feedforward component) and the sliding mode controller (which is the feedback component) compensates as the system's output strays from the desired trajectory. The system's output may stray from the desired trajectory because of the operator's inappropriate action or because of any uncertainties which lie in the system or by external disturbances. This approach means that an operator can directly influence the system's performance, where as in using the other controller forms the operator only provides the desired setpoint or trajectory and thus, the operator does not directly influence the system's performance.

CHAPTER 2 MODELLING OF CRANE DYNAMICS

In this chapter is described the derivation of a mathematical model where sub models are coupled by a term which has a small magnitude. This model will be known as the loosely coupled model. The system model can be basically broken down into three components, the motor and cart, the swing dynamics and the hoisting system. All three components mentioned mutually affect each other in determining the complete system model. A full derivation of the complete model is given in appendix A. From observing the open loop response of the complete model, it is concluded that a more accurate representation of the dynamics of the real-time system is given by a loosely coupled model. The loosely coupled model is made up of a model for the hoist dynamics and another model for the cart and swing dynamics. These two models are coupled by a term which includes the rope length as a parameter. Since the length of the rope (i.e. the distance that the goods are away from the centre of the cart) influence the swing angle which in turn influences the cart dynamics, the length of the rope is included as a measured term in the derivation of the cart and swing dynamics.

The model of the system is derived using Lagrangian dynamics and electromechanical modelling techniques. Lagrangian equations provide a means of determining the equations of motion for conservative and non-conservative systems. Since it is assumed that the system has no energy losses a conservative approach in the derivation of the Lagrangian equations can be used. The mathematical equation for determining the dynamics of a system using Lagrangian equations is given as:

$$\frac{d}{dt}\left[\frac{\partial L}{\partial \dot{q}_i}\right] - \left[\frac{\partial L}{\partial q_i}\right] = F_i \qquad \text{for } i = 1,2, \ldots..n \qquad 2.1$$

where

i = number of degrees of freedom.

F_i = net external forces acting in the direction q

q_i = set of generalised co-ordinates, where i = 1,2,3…..n

L = system Lagrangian which is comprised of the kinetic and potential energy

The Lagrangian for the system is given as:

$$L = T - U \qquad 2.2$$

where

T = Total Kinetic energy of the system

U = Total Potential energy of the system.

Since U is not a function of $\dot{q}_i$ $L=L(\dot{q}_i, q_i, t)$ and $U = (q_i, t)$

2.1 MATHEMATICAL MODELLING OF THE CART AND SWING DYNAMIC

Figure 2.1.1 gives a pictorial representation of the gantry crane. It should be noted that frictional components are not indicated on the diagram. This is because a frictionless system is assumed in the derivation of the mathematical model.

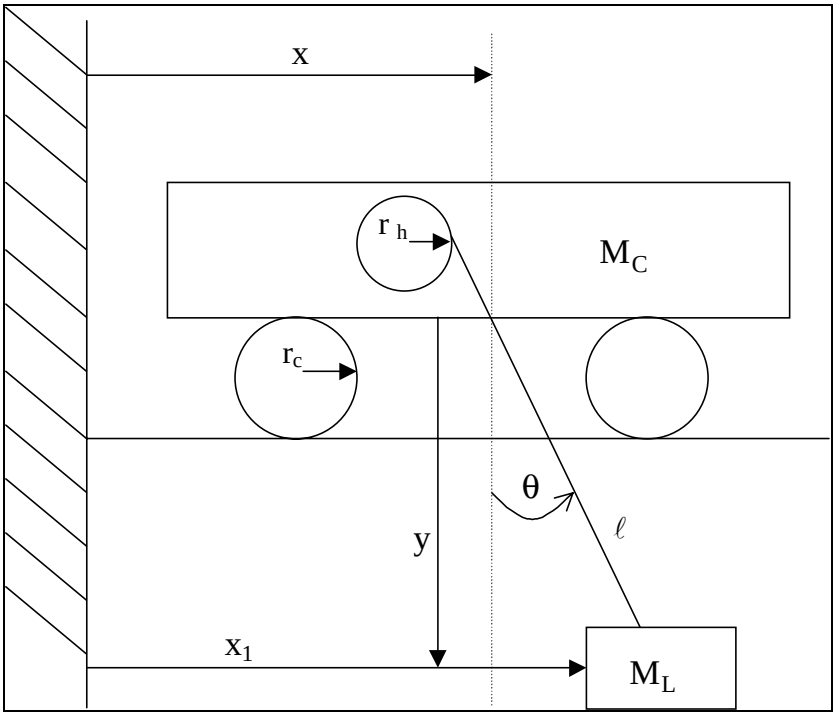

Figure 2.1.1 Diagram of the gantry crane

Before the mathematical model is developed it is necessary to define the variables that will be used.

Nomenclature

x = horizontal position of cart (m) x_1 = horizontal position of load (m)

M_C = mass of cart (kg) M_L = mass of load (kg)

y = vertical position of load (m) ℓ = length of rope (m)

θ = load angle (rad)

r_C = effective radius of cart (m) r_h = effective radius of hoist (m)

J_C = moment of inertia of cart (kg m^2) J_h = moment of inertia of hoist (kg m^2)

Kinetic Energy of Cart

$$T_1 = \frac{1}{2} M_C \dot{x}^2 \qquad 2.1.1$$

Kinetic Energy of Load (Weight)

$$T_2 = \frac{1}{2} M_L (\dot{x}1^2 + \dot{y}^2) \qquad 2.1.2$$

where

$$x_1 = x + \ell \sin\theta \qquad y = \ell \cos\theta \qquad 2.1.3$$

$$\dot{x}_1 = \dot{x}_1 + \ell\dot{\theta}\cos\theta \qquad \dot{y} = -\ell\dot{\theta}\sin\theta \qquad 2.1.4$$

Moment of Inertia of Cart

$$T_3 = \frac{1}{2} J_C \frac{\dot{x}^2}{r_C^2} \qquad 2.1.5$$

where $x = r_C \theta$

Total Kinetic Energy

$$T = \frac{1}{2} M_C \dot{x}^2 + \frac{1}{2} M_L [(\dot{x} + \ell\dot{\theta}\cos\theta)^2 + (-\ell\dot{\theta}\sin\theta)^2] + \frac{1}{2} J_C \frac{\dot{x}^2}{r_C^2} \qquad 2.1.6$$

$$T = \frac{1}{2}M_C \dot{x}^2 + \frac{1}{2}M_L[\dot{x}^2 + 2\dot{x}\ell\dot{\theta}\cos\theta + (\ell\dot{\theta})^2\cos^2\theta + (\ell\dot{\theta})^2\sin^2\theta] + \frac{1}{2}J_C\frac{\dot{x}^2}{r_C^2} \quad 2.1.7$$

Total Potential Energy

$$U = -M_L g y = -M_L g \ell\cos\theta \quad 2.1.8$$

<u>Lagrangian Equation</u>

Now that all the energy components within the system have been accounted for, the Lagrangian of the system is found by combining (2.1.7) and (2.1.8)

$$L = \frac{1}{2}M_C \dot{x}^2 + \frac{1}{2}M_L[\dot{x}^2 + 2\dot{x}\ell\dot{\theta}\cos\theta + (\ell\dot{\theta})^2\cos^2\theta + (\ell\dot{\theta})^2\sin^2\theta] + \frac{1}{2}J_C\frac{\dot{x}^2}{r_C^2} + M_L g\ell\cos\theta \quad 2.1.9$$

There is only one external force that is acting on the cart and swing dynamics and that is the force that is applied by the motor to the cart. This force only acts on the co-ordinate of x, which is linear displacement. The θ co-ordinate of the system does not have any external forces that directly act upon it.

Thus

$$\frac{d}{dt}\left[\frac{\partial L}{\partial \dot{x}}\right] - \frac{\partial L}{\partial x} = F \quad 2.1.10$$

$$\frac{d}{dt}\left[\frac{\partial L}{\partial \dot{\theta}}\right] - \frac{\partial L}{\partial \theta} = 0 \quad 2.1.11$$

Substituting (2.1.9) into (2.1.10) and evaluating for the ‘x’ co-ordinate of the system gives

$$\frac{\partial L}{\partial \dot{x}} = M_C \dot{x} + M_L \dot{x} + M_L \ell\dot{\theta}\cos\theta + J_C\frac{\dot{x}}{r_C^2} \quad 2.1.12$$

$$\frac{d}{dt}\left[\frac{\partial L}{\partial \dot{X}}\right] = M_C \ddot{x} + M_L \ddot{x} - M_L \ell\dot{\theta}\dot{\theta}\sin\theta + M_L \ell\ddot{\theta}\cos\theta + J_C\frac{\ddot{x}}{r_C^2} \quad 2.1.13$$

$$\frac{\partial L}{\partial x} = 0 \quad 2.1.14$$

$$F = M_C \ddot{x} + M_L \ddot{x} - M_L \ell\dot{\theta}\dot{\theta}\sin\theta + M_L \ell\ddot{\theta}\cos\theta + J_C\frac{\ddot{x}}{r_C^2} \quad 2.1.15$$

Similarly evaluating for the 'θ' co-ordinate of the system gives

$$\frac{\partial L}{\partial \dot{\theta}} = M_L \dot{x} \ell \cos\theta + M_L \ell^2 \dot{\theta} \qquad 2.1.16$$

$$\frac{d}{dt}[\frac{\partial L}{\partial \dot{\theta}}] = -M_L \dot{x} \ell \dot{\theta} \sin\theta + M_L \ddot{x} \ell \cos\theta + M_L \ell^2 \ddot{\theta} \qquad 2.1.17$$

$$\frac{\partial L}{\partial \theta} = -M_L \dot{x} \ell \dot{\theta} \sin\theta - M_L g \ell \sin\theta \qquad 2.1.18$$

$$0 = M_L \ddot{x} \ell \cos\theta + M_L \ell^2 \ddot{\theta} + M_L g \ell \cos\theta \qquad 2.1.19$$

2.2 MODELLING OF DC MOTOR

The DC motors on the crane system are ±13 V armature controlled DC motors. The model of the DC motor described here is based on [35]. The diagram below shows the schematic representation of the motor.

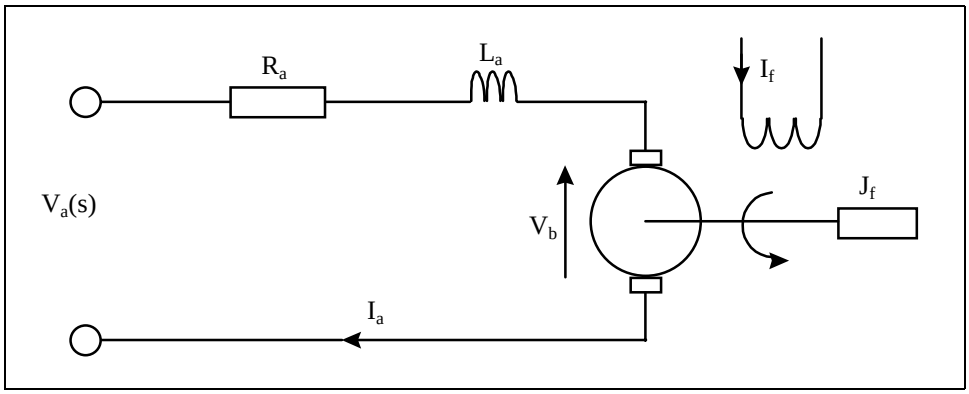

Figure 2.2.1 Schematic of an armature controlled DC motor

Nomenclature

R_a = armature resistance (Ω)

L_a = armature inductance (H)

I_a = armature current (A)

I_f = field current(A)

$V_a(s)$ = applied armature voltage (V)

V_b = generated back emf (V)

Θ = angular position of motor shaft (rad)

T = developed torque (Nm)

J_f = moment of inertia of motor Load (kg m^2)

f = viscous friction of motor and load (Nm rad^{-1} s^{-1})

The torque developed is proportional to $I_a(t)$ and the air gap flux ϕ

$$T = K_1 \phi I_a(t) = K_1 K_f I_f(t) I_a(t) \qquad 2.2.1$$

where $\phi = K_f I_f(t)$ and K_f is a constant

Since $I_f(t)$ is constant in an armature controller DC motor and K_1, K_f are also constants, then

$$T = K_c I_a(t) \qquad 2.2.2$$

The applied armature voltage is related to the armature current as follows

$$V_{a(t)} = R_a I_a(t) + L_a \frac{dI_a(t)}{dt} + V_b(t) \qquad 2.2.3$$

where $V_b(t)$ is the back emf voltage proportional to the motor's speed. Therefore

$$V_b(t) = K_{emf} \frac{d\Theta}{dt} \qquad 2.2.4$$

Taking the Laplace transform of (2.2.2)-(2.2.4) and substituting (2.2.4) into (2.2.3), the armature current can be represented as

$$I_a(s) = \frac{V_a(s) - K_b \dot{\Theta}(s)}{R_a + L_a s} \qquad 2.2.5$$

Thus substituting (2.2.5) into the Laplace transform of (2.2.2), the torque equation becomes

$$T(s) = K_C \left(\frac{V_a(s) - K_b \dot{\Theta}(s)}{R_a(1 + \frac{L_a s}{R_a})} \right) \qquad 2.2.6$$

For many DC motors the time constant L_a / R_a may be neglected as L_a is significantly smaller then R_a. Thus the equation for torque that will be used in the modelling of the system is

$$T = K_C\left(\frac{V_a - K_b\dot{\Theta}}{R_a}\right) \qquad 2.2.7$$

Since it is desired to measure linear position and velocity the following conversion is performed: $\dot{\Theta} = \frac{\dot{x}}{r_C}$ where r_C is the effective radius that converts an angular displacement into its linear equivalent.

$$T = K_C\left(\frac{V_a - K_b\frac{\dot{x}}{r_C}}{R_a}\right) \qquad 2.2.8$$

Torque is described by the following equation:

$$T = FL \text{ with SI units of (Nm)} \qquad 2.2.9$$

where *L* is described as the moment arm, i.e. the perpendicular distance between the line of rotation and the force. Since torque is the force which causes rotation it is used when one wants to use angular co-ordinates to develop a systems model. In the derivation of the Lagrangian dynamics for the cart system a linear co-ordinate system was chosen, thus (2.1.15) needs to be equated to force (linear co-ordinate) and not torque (angular co-ordinate).

The force equation can be derived by substituting (2.2.9) into (2.2.8) thus, the force equation of the motor becomes

$$F = K_I\left(\frac{V_a - K_b\frac{\dot{x}}{r_C}}{R_a}\right) \qquad 2.2.10$$

where

$K_I = K_C / L$

2.3 TOTAL SYSTEM MODEL STATE SPACE REPRESENTATION

Now that the motor has been modelled it can be combined with the cart and swing dynamics to give an overall system transfer function. Thus, combining (2.1.15) and (2.2.10)

$$K_I\left(\frac{V_a - K_b\frac{\dot{x}}{r_C}}{R_a}\right) = M_C\ddot{x} + M_L\ddot{x} - M_L\ell\ddot{\theta}\dot{\theta}\sin\theta + M_L\ell\ddot{\theta}\cos\theta + J_C\frac{\ddot{x}}{r_C^{\,2}} \qquad 2.3.1$$

$$0 = M_L\ddot{x}\ell\cos\theta + M_L\ell^2\ddot{\theta} + M_Lg\ell\cos\theta \qquad 2.3.2$$

Linearising about the operating point with the assumptions $\sin\theta \cong \theta$ $\cos\theta \cong 1$ $\dot{\theta}^2 \cong 0$ produces equations that are easier to manipulate. Thus (2.3.1) and (2.3.2) become

$$K_I\left(\frac{V_a - K_b\frac{\dot{x}}{r_C}}{R_a}\right) = M_C\ddot{x} + M_L\ddot{x} + M_L\ell\ddot{\theta} + J_C\frac{\ddot{x}}{r_C^{\,2}} \qquad 2.3.3$$

$$0 = M_L\ddot{x}\ell + M_L\ell^2\ddot{\theta} + M_Lg\ell\theta \qquad 2.3.4$$

The states of the cart and swing dynamics are defined as follows

x_1 = cart position = x

x_2 = cart velocity = $\dot{x} = \dot{x}_1$

x_3 = swing angle = θ

x_4 = swing velocity = $\dot{\theta} = \dot{x}_3$

u = the applied motor voltage = V_a

Thus (2.3.3) and (2.3.4) can be rewritten to produce the following state space equations

$$\dot{x}_2 = -\left(\frac{\frac{K_I}{R_a}\frac{K_b}{r_C}}{(M_C + \frac{J_C}{r_C{}^2})}\right)x_2 + \left(\frac{M_L g}{(M_C + \frac{J_C}{r_C{}^2})}\right)x_3 + \left(\frac{\frac{K_I}{R_a}}{(M_C + \frac{J_C}{r_C{}^2})}\right)u \qquad 2.3.5$$

$$\dot{x}_4 = \left(\frac{\frac{K_I}{R_a}\frac{K_b}{r_C}}{(M_C + \frac{J_C}{r_C{}^2})\ell}\right)x_2 - \left(\frac{g\left(M_C + M_L + \frac{J_C}{r_C{}^2}\right)}{(M_C + \frac{J_C}{r_C{}^2})\ell}\right)x_3 - \left(\frac{\frac{K_I}{R_a}}{(M_C + \frac{J_C}{r_C{}^2})\ell}\right)u \qquad 2.3.6$$

Thus (2.3.5) and (2.3.6) can be rewritten in terms of the system matrices

$$\begin{bmatrix} \dot{x}_1 \\ \dot{x}_2 \\ \dot{x}_3 \\ \dot{x}_4 \end{bmatrix} = \begin{bmatrix} 0 & 1 & 0 & 0 \\ 0 & \frac{-ab}{d} & \frac{e}{d} & 0 \\ 0 & 0 & 0 & 1 \\ 0 & \frac{ab}{d\ell} & \frac{-c}{d\ell} & 0 \end{bmatrix}\begin{bmatrix} x_1 \\ x_2 \\ x_3 \\ x_4 \end{bmatrix} + \begin{bmatrix} 0 \\ \frac{a}{d} \\ 0 \\ \frac{-a}{d\ell} \end{bmatrix}u \qquad 2.3.7$$

$$y = \begin{bmatrix} 1 & 0 & 0 & 0 \\ 0 & 0 & 1 & 0 \end{bmatrix}\begin{bmatrix} x_1 \\ x_2 \\ x_3 \\ x_4 \end{bmatrix}$$

where

$a = K_I / R_a$

$b = K_b / r_C$

$c = g(M_C + M_L + J_C / r_C{}^2)$

$d = (M_C + + J_C / r_C{}^2)$

$e = M_L g$

2.4 HOIST MODEL

Using the Lagrangian dynamics method defined previously, the hoist dynamics of the system can be derived. In the modelling of the hoist dynamics it is assumed the swing angle is zero. Thus, $y = \ell$ and the moment of inertia is small and negligible.

Kinetic Energy of Hoist

$$T_1 = \frac{1}{2} M_L \dot{y}^2 \qquad 2.4.1$$

Potential Energy of Hoist

$$U = -M_L g y \qquad 2.4.2$$

The Lagrangian for the system is now found by combining (2.4.1) and (2.4.2)

$$L = \frac{1}{2} M_L \dot{y}^2 - M_L g y \qquad 2.4.3$$

From the definition of the Lagrangian dynamics it is known that

$$\frac{d}{dt}\left[\frac{\partial L}{\partial \dot{y}}\right] - \frac{\partial L}{\partial y} = F \qquad 2.4.4$$

Substituting (2.4.3) into (2.4.4) and evaluating gives

$$\frac{d}{dt}\left[\frac{\partial L}{\partial \dot{y}}\right] = M_L \ddot{y} \qquad 2.4.5$$

$$F = M_L \ddot{y} - M_L g \qquad 2.4.6$$

From Section 2.2 we know that the force equation for a motor is

$$F = K_I \left(\frac{V_a - K_b \frac{\dot{y}}{r_H}}{R_a} \right) \qquad 2.4.7$$

Combining (2.4.6) and (2.4.7) the equation for the hoist dynamics is

$$K_I\left(\frac{V_a - K_b\frac{\dot{y}}{r_H}}{R_a}\right) = M_L\ddot{y} - M_L g \qquad 2.4.8$$

The states of the hoisting system are defined as follows

x_5 = rope length = y

x_6 = rope velocity = $\dot{y} = \dot{x}_5$

u = the applied motor voltage = Va

By rearranging (2.4.8) it can be expressed in terms of the states as follows

$$\dot{x}_6 = -\left(\frac{\frac{K_I}{R_a}\frac{K_b}{r_H}}{M_L}\right)x_6 + \left(\frac{\frac{K_I}{R_a}}{M_L}\right)u + g \qquad 2.4.9$$

The state space representation of the hoist model is now given as

$$\begin{bmatrix}\dot{x}_5\\ \dot{x}_6\end{bmatrix} = \begin{bmatrix}0 & 1\\ 0 & \frac{-f\,h}{M_L}\end{bmatrix}\begin{bmatrix}x_5\\ x_6\end{bmatrix} + \begin{bmatrix}0\\ \frac{f}{M_L}\end{bmatrix}u + \begin{bmatrix}0\\ g\end{bmatrix} \qquad 2.4.10$$

$$y = \begin{bmatrix}1 & 0\end{bmatrix}\begin{bmatrix}x_5\\ x_6\end{bmatrix}$$

where

$f = K_I / Ra$

$h = K_b / r_H$

2.5 CONCLUSION

In this chapter the model of the gantry crane system was developed by making the fundamental assumption that the rope length appears as a variable in the coupling terms between the hoist dynamics and the cart and swing dynamics. This assumption was made to establish the differences between a complete model of the crane (appendix A) and the loosely coupled model. The question is which one of the models gives a more accurate representation of the real-time system ?

To answer this question one must have some knowledge of the real-time system. If the equations of motion are observed from both derivation methods i.e.(2.3.7) and (A.46), it is noted that equations of motion are different. The difference occurs because in the development of the complete model a frictionless model was assumed which allows the goods to fall freely. Where as in (2.3.7) (which is a component of the loosely coupled model) the rope length can be fixed.

If the rope length is fixed, then as the goods swing the cart moves as well. This occurs because as the goods swing there is a change in the centre of gravity of the goods. Since the rope length is fixed the only way that the system can compensate for the change in the centre of gravity is to move the cart.

If we consider the equations of motion which pertain to the acceleration of the cart and thus the position of the cart in (A.46), it can be seen that as the goods swing the cart does not move. This occurs because there is no friction between the rope and the drum, which means that there is no force to stop the goods falling. Therefore, in this instance as the goods swing and a change in the centre of gravity occurs, the goods pull on the rope and the rope length changes.

In observing the real-time system it was noted that the cart moves as the load swings. This occurs due to the frictional components between the rope and the drum. The model developed in this chapter highlights this action even though a frictionless model is assumed. Thus, the cart's equations of motion in (2.3.7) provides a more accurate representation of the real-time system.

If we consider the angular acceleration of the load, both models show that it is influenced not only by the input force, but also by gravity and the length of the rope. Once again one must consider the dynamics of the real-time system in order to determine which mathematical model is a more accurate representation.

It was noted in the real-time system that the angular acceleration was also related to the mass of the load as well as gravity and the length of the rope. The complete model (A.46) does not relate the angular acceleration to the mass of the load , while the model developed in this chapter (2.3.7) does show this relationship. Thus, once again the model developed in this chapter is a more realistic.

The equations of motion which pertain to the hoist dynamics are similar for both the complete model and the loosely coupled model. Thus, there is no need to justify a more accurate model.

From the observations made of the real-time system and the justifications presented above, it is concluded that for this thesis the loosely coupled model (which is developed in this chapter) provides a more accurate representation of the real-time system then the complete mathematical model. The loosely coupled model will be used throughout this thesis.

CHAPTER 3 MODEL VERIFICATION

From Sections 2.3 and 2.4 the linearised mathematical model of the system was derived. This next section details all parameter measurements and calculations. The masses of the cart (M_c) and goods (M_L) were measured whilst all other parameters that needed to be calculated were determined by experiments.

3.1 THE MOMENT OF INERTIA OF THE CART

The moment of inertia term J ($kg\,m^2$) is determined from the significant rotating parts of the system. In this case the moment of inertia is not a dominating factor in the system's overall performance. In fact, the moment of inertia can be described as having a second order affect on the system's performance. Thus, the calculation of moment of inertia will only be an approximation. The assumption for the approximation that was made is that the system is a rigid body rotating about an axis.

The moment of inertia is calculated using the formula

$$J = \sum mr^2 \qquad 3.1.1$$

where r = the radius of rotation.

m = the mass of the rigid body. Strictly, m is a mass at a point.

The radius is a function of the linear distance (x metres) that is travelled by the cart and the angular rotation of the motors shaft (θ radians).
Thus, the effective radius of the cart is $r_C = x / \theta$ and it was found to be 0.00417 m.

Now to calculate the moment of inertia

$$M = M_C + M_L \qquad 3.1.2$$

where

$M_C = 6.5$ kg $\qquad M_L = 1.5$ kg

Thus

$$J_C = 8 \times (0.00417)^2 \qquad 3.1.3$$

$$J_C = 0.000139\ (kg\,m^2) \qquad 3.1.4$$

3.2 MOTOR CONSTANTS OF CART

The armature resistance of the motor was determined by plotting the applied voltage to the motor and the current that was required to stop the motor shaft from turning. This is illustrated by the table below.

Applied Voltage (V)	**Current (A)**
5 (V)	0.35 (A)
10 (V)	0.7 (A)
15 (V)	1.1 (A)
20 (V)	1.5 (A)

From the above table R_a was calculated to be 14.3 (Ω). The armature resistance for most DC motors is within the range of 0 - 20 (Ω). Thus, the armature resistance calculated for this motor falls neatly within this range.

The motor constants K_I and K_b were determined by taking step responses of the system with various input voltages. These step responses will give the time taken to travel a certain distance with a constant motor voltage. Figure 3.2.1 - 3.2.6 illustrate the crane's step response with different applied voltages.

From Figure 3.2.1 it can be seen that when a 1.6 V step is applied to the crane, it takes the crane approximately 6 sec. to reach 1.2 m. From Figure 3.2.3 it can be seen that when a 2.9 V step is applied to the crane, it takes the crane approximately 3.4 sec. to reach 1.2 m. From Figure 3.2.5 it can be seen that when a 4.2 V step is applied to the crane, it takes the crane approximately 2.4 sec. to reach 1.2 m.

These figures illustrate the motor's step response in relation to an applied voltage from the PC. This is not the actual voltage that is applied onto the motor. This is because the motor itself has a dead band of 1 V for moving the cart from left to right. The actual applied voltage to the motor is the PC voltage plus 1 V the dead band compensation. Thus, for a 1.6 V step the motor is actually being applied with 2.6 V.

Cart position step response with 1.6 V step

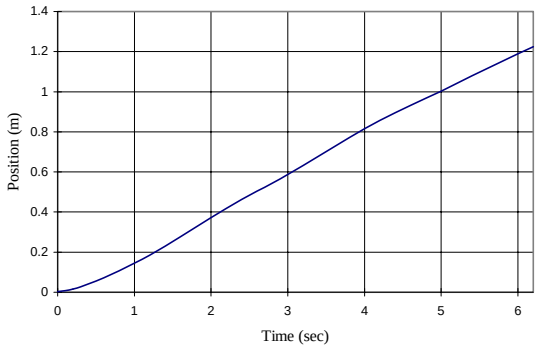

Figure 3.2.1

Swing angle step response with 1.6 V step

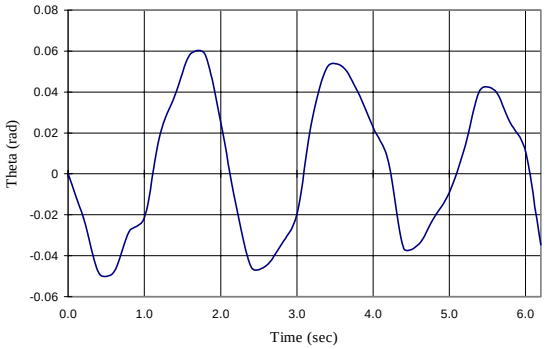

Figure 3.2.2

Cart position step response with 2.9 V step

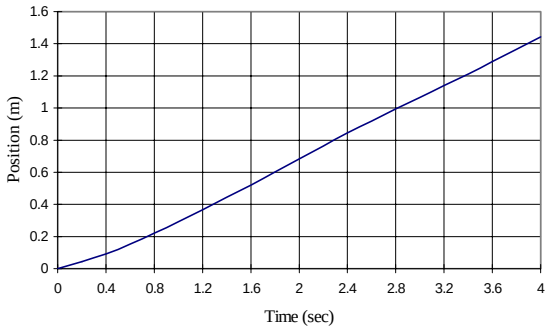

Figure 3.2.3

Swing angle step response with 2.9 V step

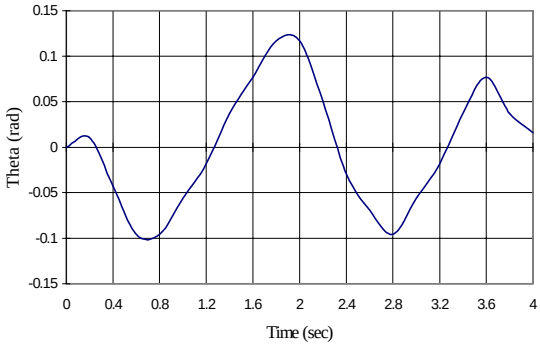

Figure 3.2.4

Cart position step response with 4.2 V step

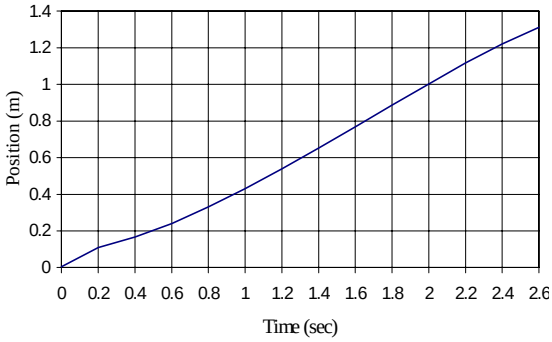

Figure 3.2.5

Swing angle step response with 4.2 V step

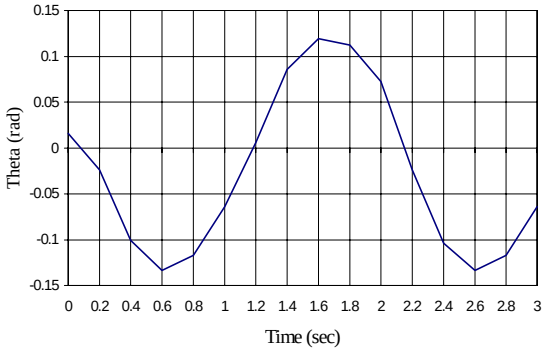

Figure 3.2.6

The values of K_I and K_b can be determined using Figures 3.2.3 and 3.2.5 in conjunction with (2.3.3). In using (2.3.3) it is assumed (only to make the calculation of K_I and K_b easier) that the swing of the system is 0 rad. Thus, its effect is neglected.

Neglecting the effects of the swing angle reduces (2.3.3) to

$$K_I\left(\frac{V_a(s) - K_b\frac{\dot{x}}{r_C}}{R_a}\right) = M_C\ddot{x} + M_L\ddot{x} + J_C\frac{\ddot{x}}{r_C{}^2} \qquad 3.2.1$$

It is known that the cart will travel a distance x (metres) in a time of t (seconds) when a voltage of v (volts) is applied to the motor of the cart Thus, rearranging (3.2.1) gives

$$K_I\left(\frac{v_1 - \frac{K_b}{r_C}\frac{x}{t_1}}{R_a}\right) = M\frac{x}{(t_1)^2} \qquad 3.2.2$$

$$K_I\left(\frac{v_2 - \frac{K_b}{r_C}\frac{x}{t_2}}{R_a}\right) = M\frac{x}{(t_2)^2} \qquad 3.2.3$$

where $M = M_C + M_L + \frac{J_C}{r_C{}^2}$

From Figure 3.2.3

$v_1 = Va = 2.9$ V $t_1 = 3.4$ sec. $x = 1.2$ m

From Figure 3.2.5

$v_2 = Va = 4.2$ V $t_2 = 2.4$ sec. $x = 1.2$ m

From the previous section it was determined that

$J_C = 0.000139\ (\text{kg m}^2)$ $R_a = 14.3\ (\Omega)$. $r_C = 0.00417$ m

By weighing the cart and the load, their masses were found to be

$M_C = 6.5$ kg $M_L = 1.5$ kg

The two unknowns K_I and $K_{b.}$ can now be determined by using (3.2.2) and (3.2.3)

$K_I = 152.8800\ (\text{Kg m}^2\text{s}^{-2}\text{A}^{-1})$ $K_b = 0.0324\ (\text{V m}^{-1}\text{s})$

3.3 SIMULATION OF CART AND SWING DYNAMICS

The state space model of the cart and swing dynamics was simulated using Matlab's Simulink in order to verify the constants that were determined previously.

$M_C = 6.5$ kg $M_L = 1.5$ kg

$K_I = 152.8800\ (\text{kg m}^2\text{s}^{-2}\text{A}^{-1})$ $K_b = 0.0324\ (\text{V m}^{-1}\text{s})$

$J_C = 0.000139\ (\text{kg m}^2)$ $r_C = 0.00417$m

$R_a = 14.3\Omega$

$a = K_I / R_a$ $b = K_b / r_C$

$c = g(M_C + M_L + J_C / r_C^2)$ $d = (M_C + J_C / r_C^2)$

$e = M_L\, g$

$$\begin{bmatrix} \dot{x}_1 \\ \dot{x}_2 \\ \dot{x}_3 \\ \dot{x}_4 \end{bmatrix} = \begin{bmatrix} 0 & 1 & 0 & 0 \\ 0 & \frac{-ab}{d} & \frac{e}{d} & 0 \\ 0 & 0 & 0 & 1 \\ 0 & \frac{ab}{d\ell} & \frac{-c}{d\ell} & 0 \end{bmatrix} \begin{bmatrix} x_1 \\ x_2 \\ x_3 \\ x_4 \end{bmatrix} + \begin{bmatrix} 0 \\ \frac{a}{d} \\ 0 \\ \frac{-a}{d\ell} \end{bmatrix} u \qquad 3.3.1$$

$$\begin{bmatrix} \dot{x}_1 \\ \dot{x}_2 \\ \dot{x}_3 \\ \dot{x}_4 \end{bmatrix} = \begin{bmatrix} 0 & 1 & 0 & 0 \\ 0 & -5.73 & 1.014 & 0 \\ 0 & 0 & 0 & 1 \\ 0 & \frac{5.73}{\ell} & \frac{-10.81}{\ell} & 0 \end{bmatrix} \begin{bmatrix} x_1 \\ x_2 \\ x_3 \\ x_4 \end{bmatrix} + \begin{bmatrix} 0 \\ 0.7376 \\ 0 \\ \frac{-0.7376}{\ell} \end{bmatrix} u \qquad 3.3.2$$

Figures 3.3.1–3.3.6 represent the step response of the simulated system. These responses are similar to those of the real-time system (Figures (3.2.1 - 3.2.6)). It is therefore reasonable to conclude that the model derived in Chapters 2 and 3 is a sufficiently accurate representation of the system for controller design.

Cart position step response with 1.6 V step

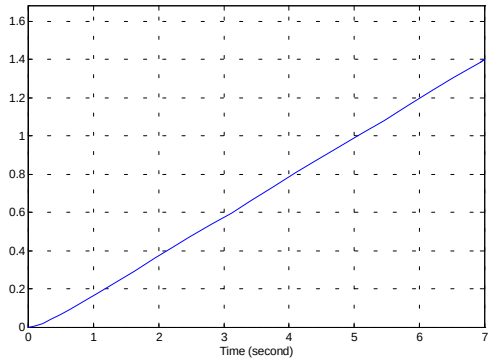

Figure 3.3.1

Swing angle step response with 1.6 V step

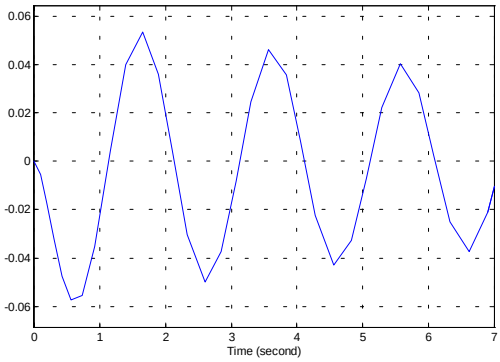

Figure 3.3.2

Cart position step response with 2.9 V step

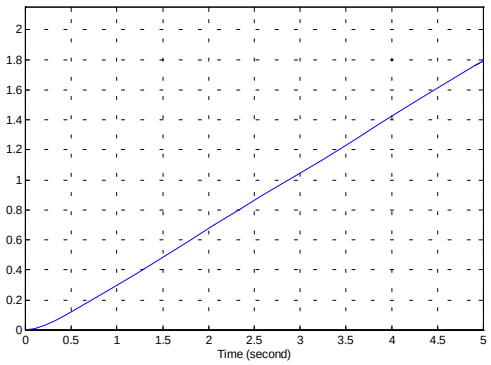

Figure 3.3.3

Swing angle step response with 2.9V step

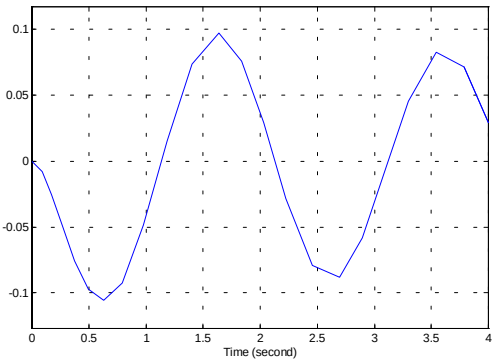

Figure 3.3.4

Cart position step response with 4.2 V step

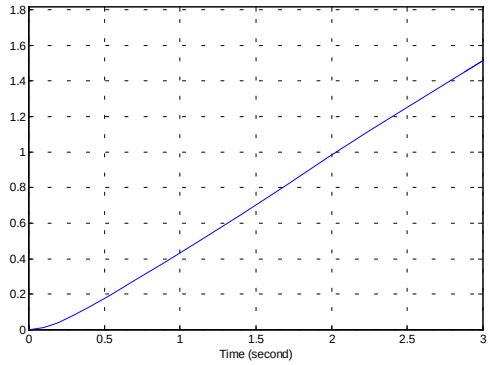

Figure 3.3.5

Swing angle step response with 4.2 V step

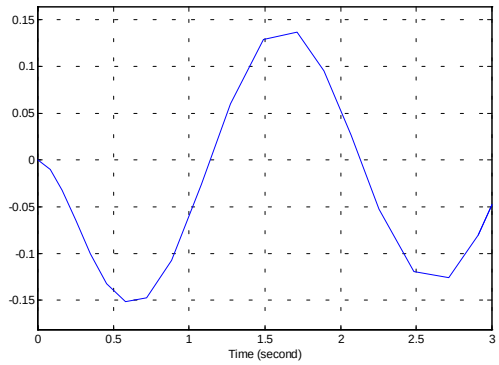

Figure 3.3.6

3.4 MOTOR CONSTANTS OF HOIST

The armature resistance of the hoisting motor was determined to be 14.3 (Ω).The armature resistance calculated for the hoisting motor also falls neatly within this range of 0 - 20 (Ω).

The motor constants K_I and K_b were determined by taken step responses of the system and various input voltages. From these step responses the time taken to travel a certain distance with a constant motor voltage can be determined. The graphs below illustrate the step response of the hoisting motor with different applied voltages.

Note: The graphs illustrate the motors step response in relation to an applied voltage from the PC. This is not the actual voltage that is applied to the motor. This is because the motor itself has a dead band of 2 V for lifting. The actual applied voltage to the motor is the PC voltage plus 2 V for the dead band compensation.

Figure 3.4.1 - 3.4.3 illustrate the time taken to displace the goods a distance of 0.9 m with different voltage steps. In Figure 3.4.1 it can be seen that when a 1.9 V step is applied to the hoisting motor, it takes the hoisting motor approximately 9.8 sec. to raise the goods a height of 0.9 m. Figure 3.4.2 illustrates that when a 3.2 V step is applied to the hoisting motor, it takes the hoisting motor approximately 6.1 sec. to raise the goods a height of 0.9 m. And Figure 3.4.3 illustrates that when a 8.2 V step is applied to the

hoisting motor, it takes the hoist approximately 2.6 sec. to raise the goods a height of 0.9 m.

Rope length step response with 1.9 V step

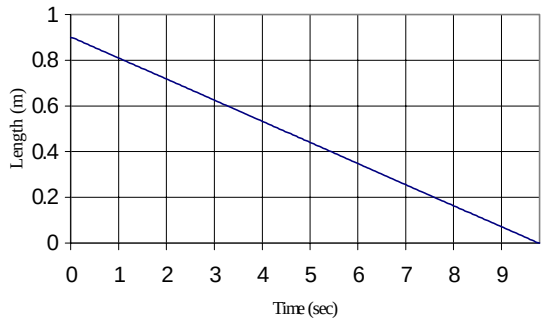

Figure 3.4.1

Rope length step response with 3.2 V step

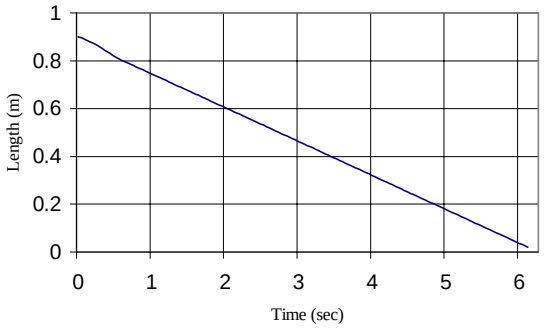

Figure 3.4.2

Rope length step response with 8.2 V step

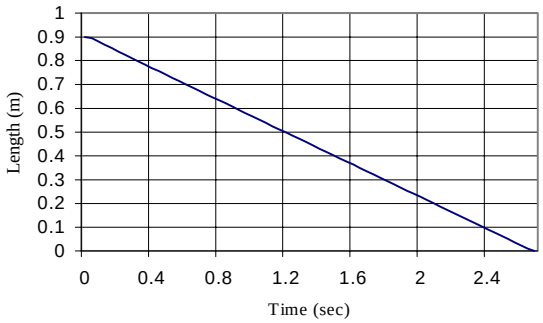

Figure 3.4.3

The values of K_I and K_b can be determined using Figures 3.4.2 and 3.4.3 in conjunction with (2.4.10). It is noted that the last matrix in (2.4.10) is a disturbance matrix that comprises of the effect due to gravity. Thus, a voltage has to be applied to the motor in order to keep the goods from falling. When a step response is taken from one steady state condition to another the disturbance matrix disappears. This will be discussed in Section 3.5.

The disappearance of the disturbance matrix produces the following equation

$$K_I\left(\frac{V_a - K_b\frac{\dot{y}}{r_H}}{R_a}\right) = M_L\ddot{y} \qquad 3.4.1$$

It is known that the goods will travel a distance y (metres) in a time of t (seconds) when a voltage of v (volts) is applied to the motor of the hoist Thus, rearranging (3.4.1) gives

$$K_I\left(\frac{v_1 - \frac{K_b}{r_H}\frac{y}{t_1}}{R_a}\right) = M_L\frac{y}{(t_1)^2} \qquad 3.4.2$$

$$K_I\left(\frac{v_2 - \frac{K_b}{r_H}\frac{y}{t_2}}{R_a}\right) = M_L\frac{y}{(t_2)^2} \qquad 3.4.3$$

From Figure 3.4.2 let

$v_1 = Va = 8.2$ V $t_1 = 2.6$ sec. $y = 0.9$ m

From Figure 3.4.3 let

$v_2 = Va = 3.2$ V $t_2 = 6.1$ sec. $y = 0.9$ m

The values of the load mass, armature resistance and the effective radius of the hoist were determined to be

$M_L = 1.5$ kg Ra = 14.3 (Ω). $r_H = 0.09$ m

The two unknowns K_I and K_b can be solved by using (3.4.2) and (3.4.3)

$K_I = 2.3668\ (\text{kg m}^2\text{s}^{-2}\text{A}^{-1})$

$K_b = 0.032\ (\text{V m}^{-1}\text{s})$

3.5 SIMULATION OF HOIST DYNAMICS

Using Matlab the state space model of the cart and swing dynamics was simulated in order to verify the constants that were determined previously.

$f = K_I / Ra$

$h = K_b / r$

$$\begin{bmatrix} \dot{x}_5 \\ \dot{x}_6 \end{bmatrix} = \begin{bmatrix} 0 & 1 \\ 0 & \frac{-fh}{M_L} \end{bmatrix} \begin{bmatrix} x_5 \\ x_6 \end{bmatrix} + \begin{bmatrix} 0 \\ \frac{f}{M_L} \end{bmatrix} u + \begin{bmatrix} 0 \\ g \end{bmatrix} \qquad 3.5.1$$

$$\begin{bmatrix} \dot{x}_5 \\ \dot{x}_6 \end{bmatrix} = \begin{bmatrix} 0 & 1 \\ 0 & -2.229 \end{bmatrix} \begin{bmatrix} x_5 \\ x_6 \end{bmatrix} + \begin{bmatrix} 0 \\ 0.11 \end{bmatrix} u + \begin{bmatrix} 0 \\ g \end{bmatrix} \qquad 3.5.2$$

As stated previously, the last matrix in (3.5.1) is a disturbance matrix which contributes the effects due to gravity. This matrix was earlier neglected because a definition of the system dynamics as it is moved from one steady state condition to another is required. During this movement this matrix disappears because it is a constant dc offset. However, at steady state the goods will fall because of this disturbance matrix. If the goods are required to remain stationary at steady state (i.e. not fall) then when simulating (3.5.1) a value of 9.88/0.111 must be added to the applied motor voltage.

Since an objective of this thesis is to derive a realistic model of the gantry crane system, then the dynamics of the real-time system must be considered. From observation of the real-time system it is noted that the goods do not fall freely at steady state. Thus, there are some other external disturbances which negate the effects due to gravity. These are possibly attributed to friction in the system. Another justification for neglecting the disturbance matrix (since it is a constant dc offset), is that in the design of the rope length controller, integral action will be introduced, and the integrator should take care of any dc offsets that are in the system.

Linearisation techniques are another method of removing constant terms (like gravitational forces) from a model. This will cause any constant terms to go to zero when the partial differential is taken of the system equations about the operating point.

Therefore there is reason to conclude that a more realistic model to simulate is given by

$$\begin{bmatrix} \dot{x}_5 \\ \dot{x}_6 \end{bmatrix} = \begin{bmatrix} 0 & 1 \\ 0 & -2.229 \end{bmatrix} \begin{bmatrix} x_5 \\ x_6 \end{bmatrix} + \begin{bmatrix} 0 \\ 0.11 \end{bmatrix} u \qquad 3.5.3$$

An alternative method for deriving the model of the system is to use system identification techniques. In using system identification techniques, the system that is derived consists only of an A, B, C and D matrix. Usually system identification is performed with differences, so constant terms are eliminated. Thus, the dc offset disappears when the system is moved from one steady state condition to another. To verify this , a quick system identification was performed using Matlab's ARX routine. This produced system matrices which were very similar to (3.5.3).

As can be seen Figure 3.5.1 - 3.5.3 represent the step response of the real-time system quite accurately. The figure below illustrates the hoisting motor displacing the goods a distance of 0.9 m in the same time frame as the real-time system for the similar applied motor voltage. Thus, it is concluded that the model derived in Chapters 2 and 3 is an accurate representation of the system for which the controller will be designed.

Rope length step response with 1.9 V step

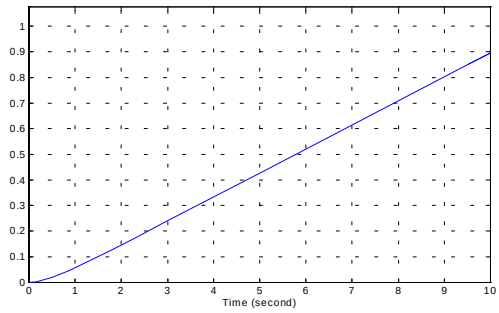

Figure 3.5.1

Rope length step response with 3.2 V step

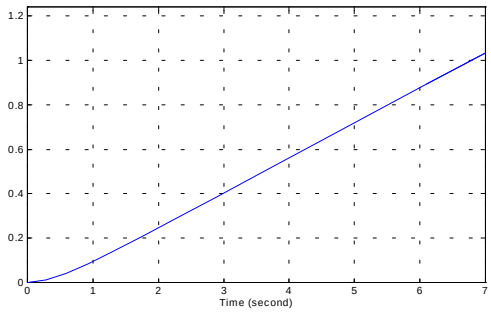

Figure 3.5.2

Rope length step response with 8.2 V step

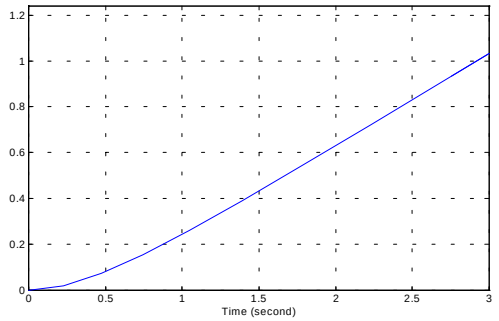

Figure 3.5.3

CHAPTER 4 SLIDING MODE CONTROL

In this chapter an overview of the sliding mode control theory that was published by Utkin [1] is given. There have been numerous papers published in relation to Utkin's work and the use of sliding mode controllers [2], [3], [4] and [5]. De Carlo [2] has written a tutorial in the use of sliding mode control and the various different forms that the sliding mode controller can be expressed. In this chapter only one form of the sliding mode controller (which consists of a switching surface and the equivalent control dynamics) is discussed. This form of the controller is discussed, as it will be the controller that will eventually be implemented on the real-time system. Alternative approaches to the controller are discussed in [1] and [2].

Control engineers always aim to design systems that are insensitive to system uncertainties. All industrial processes are subject to parameter fluctuations and disturbances that result from such things as measurement noise, mechanical stresses and friction. Also in the design of controllers a mathematical model of the process is required. In deriving a model of a process one may need to linearise the model to make calculations easier, thus leading to unknown controller performance outside the linearised region. The use of sliding mode control allows engineers to overcome some of these difficulties.

The theory of sliding mode control is characterised by the ability to drive the system to a predefined switching surface or sliding surface and then once on the sliding surface to move the representative point of the system along the switching surface in state space for all subsequent time. The sliding mode operation occurs once the system states are on the sliding surface and there are no disturbances.

The sliding mode controller consists of two parts. The first part of the controller is the equivalent control dynamics, which give the closed loop dynamics of the system once on the sliding surface.

The second part is a discontinuous or switched control law, which drives the system towards the sliding surface and maintains the system on the sliding surface. This part of the controller also controls the remaining state of the system. The discontinuous control action is necessary because of the different control paths that are required depending on whether the system states are above or below the switching surface. This part of the controller will push / pull the system states back onto the sliding surface, thus switching the control law across the sliding surface.

One disadvantage of such a controller is its switching nature. The pushing of the system on to the sliding surface (i.e. switching across the sliding surface), coupled with the high gain elements of the controller induces high frequency switching, or chattering which may not be practical for some industrial applications.

4.1 THE SLIDING SURFACE

Consider the system

$$\dot{x}(t) = A(x,t)x(t) + B(x,t)u(t,x) + D(x,t)f(t) \qquad 4.1.1$$

where $x \in R^n$ $u \in R^m$ $f \in R^L$ represent the state, control and disturbance vectors respectively. The sliding or switching surface is defined as

$$s_i = k_i^T x = 0 \qquad i= 1,\ldots,m \qquad 4.1.2$$

Now assembling the vectors k_i^T into full rank matrix $K \in R^{m \times n}$

$$s = Kx = 0 \text{ where K is the sliding matrix} \qquad 4.1.3$$

A sliding mode (De Carlo *et. al*. 1988) 'will exist for a system if in the vicinity of the switching surface, the state velocity vector (the derivative of the state vector) is directed towards the surface. Once the state trajectory intercepts the surface and remains on the surface for all subsequent time'.

From [1], [2], [13] and [14] it is given that the sliding motion will occur on the i^{th} switching surface if the condition below is met.

$$\lim_{s_i \to 0^+} S_i < 0 \quad \text{and} \quad \lim_{s_i \to 0^-} S_i > 0 \qquad 4.1.4$$

or equivalently

$$s_i \dot{s}_i < 0 \qquad 4.1.5$$

Thus in sliding mode the system will satisfy the following equations

$$s_i(x) = 0 \qquad 4.1.6$$

$$\dot{s}_i(x) = 0 \qquad 4.1.7$$

From the definition of (4.1.2) it can be seen that the sliding surface is defined as $s(x) = 0$. Thus the magnitude of the switching surface in (4.1.2) is actually the distance the system is away from the sliding surface.

4.2 EQUIVALENT CONTROL

In a similar manner to De Carlo [2] a description of equivalent control is given. A basic method for dealing with multi-input systems known as the method of equivalent control was described by Utkin [1]. This method will give an understanding of the system's performance once it is on the sliding surface. The equivalent control portion of the sliding mode controller is the low frequency component of the control structure. When the system is working in an ideal manner the equivalent control has no effect. i.e. it does not control anything. The equivalent control has 2 functions:

1) Analysis: It enables the determination of the closed loop dynamics on the sliding surface.
2) Simplification: It removes unnecessary terms from the determination of the non-linear switching control.

The equivalent control system equation can be made asymptotically stable upon choosing a suitable sliding gain matrix such that the existence of the sliding (4.1.6) - (4.1.7) will be met.

Proof

Consider the system described by (4.1.1) without external disturbances. Using the property that $\dot{s}_i(x) = 0$ and the chain rule the following equations are established.

$$\dot{s} = K\dot{x} = 0 \qquad 4.2.1$$

Substituting (4.1.1) into (4.2.1)

$$K\dot{x} = K[Ax + Bu_{eq}] = 0 \qquad 4.2.2$$

$$u_{eq} = (-K * B)^{-1} * (KAx) \qquad 4.2.3$$

now substituting (4.2.3) into (4.1.1) gives

$$\dot{x} = [I - B(K * B)^{-1}K]Ax \qquad 4.2.4$$

with the constraint that $(K * B)^{-1}$ is nonsingular

The structure of (4.2.4) can now be exploited in the design of the sliding surface. The motion of the system on the sliding surface can be determined by using a reduced order set of equations. The order reduction is only made possible because of the property $s(x) = 0$ (i.e. the "equivalent control assumption").

4.3 REDUCED ORDER

The reduced order will enable the design of a sliding mode controller by using linear control techniques. The reduced order system's main property is that it uses one state of the system as an input to drive the other states. With proper transformation of the system matrices, a linear controller can be designed to have the property of one state acting as an input into the other states.

In order to give a better understanding of how this can be achieved, a system that is in regular form will be used to illustrate this property.

The regular form of a system is given as:

$$\begin{bmatrix} \dot{x}_1 \\ \dot{x}_2 \end{bmatrix} = \begin{bmatrix} A_{11} & A_{12} \\ A_{21} & A_{22} \end{bmatrix} \begin{bmatrix} x_1 \\ x_2 \end{bmatrix} + \begin{bmatrix} 0 \\ B_2 \end{bmatrix} u \qquad 4.3.1$$

$$\dot{x}_1 = A_{11} x_1 + A_{12} x_2$$

$$\dot{x}_2 = A_{21} x_1 + A_{12} x_2 + B_2 u$$

In order to compute the reduced order dynamics a linear sliding surface is assumed. This sliding surface has the equation given below

$$s = \begin{bmatrix} K_1 & K_2 \end{bmatrix} \begin{bmatrix} x_1 \\ x_2 \end{bmatrix} = 0 \qquad 4.3.2$$

with the constraint that K_2 is non-singular. This means that the system $K(sI-A)^{-1}B$ has relative degree 1.

Thus

$$x_2 = -K_1 K_2^{-1} x_1 \qquad 4.3.3$$

Substituting (4.3.3) into (4.3.1) gives

$$\dot{x}_1 = (A_{11} - A_{12} K_1 K_2^{-1}) x_1 \qquad 4.3.4$$

Thus it can be seen that (4.3.4) has the feedback structure of a system whose input is $u = -K_1 K_2^{-1}$. Since the A and B matrices are controllable, the pair A_{11} and A_{12} are controllable. Therefore classical feedback control techniques can be used to control the pair A_{11} and A_{12}. It also should be noted that A_{11} now becomes the new system matrix and A_{12} is the new input matrix.

Since the control action of $K_1 K_2^{-1}$ will produce a linear controller which stabilises the system, then from (4.3.3) the sliding surface s can be found.

$$s = \begin{bmatrix} K_1 K_2^{-1} & I \end{bmatrix} \begin{bmatrix} x_1 \\ x_2 \end{bmatrix} = 0 \qquad \text{where I is the identity matrix} \qquad 4.3.5$$

Thus it is shown that a system which is of the regular form can be used in a reduced order form to design a linear switching surface.

4.4 TRANSFORMATION MATRIX

The example given in Section 4.3 describes a system that is already in regular form. The question is how does one transform a linear system that is not in regular form into the regular form, such that a linear controller can be designed using reduced order dynamics of the system. By using a transformation matrix a linear system can be transformed into the regular form. The non-linear problem is similar, but far more complicated.

Consider the example outlined in Section 4.3, except that the A and B matrices are of higher order and they are compatibly dimensioned. It is assumed that the matrix B has full rank *m.* Thus there exists a transformation matrix T such that

$$TB = \begin{bmatrix} 0 \\ B_2 \end{bmatrix} \qquad 4.4.1$$

where matrix T is an *n x n* transformation matrix and B_2 is *m x m* and non singular.

Now on the assumption that (4.4.1) is true a transformation can be defined such that

$$z = Tx \qquad 4.4.2$$

Substituting (4.4.2) into (4.3.1) gives

$$\dot{z} = \tilde{A}z + \tilde{B}u \qquad 4.4.3$$

where

$$\tilde{A} = \begin{bmatrix} \tilde{A}_{11} & \tilde{A}_{12} \\ \tilde{A}_{21} & \tilde{A}_{22} \end{bmatrix} = TAT^{-1} \qquad \tilde{B} = \begin{bmatrix} 0 \\ \tilde{B} \end{bmatrix} = TB$$

Now the system which was not initially in regular form has now been transformed into the regular form. By now placing the system into the reduced order form a linear sliding surface can be designed.

The sliding surface is now a function of the transformed states.

$$s = Kz = 0 \qquad 4.4.4$$

Once the sliding surface has been determined a reverse transformation must take place in order to make the sliding surface a function of the original states. Thus the sliding surface as a function of the original states is:

$$s = KTx = 0 \qquad 4.4.5$$

4.5 CONTROLLER DESIGN

The sections above have dealt with the existence of sliding mode, and the dynamics of the system once on the sliding surface. The next problem is how to reach the sliding surface. This is a reachability problem. This problem occurs because of any initial conditions or external disturbances that will cause the system to stray off the sliding surface. It should be noted that the sliding surface merely prescribes the nominal performance during the existence of the sliding mode.

Thus, the sliding mode condition described by (4.1.5) will be attained if the reachability problem is solved. To solve the reachability problem the following condition must apply.

$$s_i \dot{s}_i < 0 \qquad i = 1 \ldots\ldots m \qquad 4.5.1$$

This is a Lyapunov stability condition, ensuring that $s \rightarrow 0$.

The condition (4.5.1) will ensure that the direction of motion of the representative point of the system (state trajectory) is not away from the sliding surface.

In general the sliding mode controller consists of two parts. The first is a linear controller and the second is a discontinuous (i.e. switched) controller, which solves the reachability problem. There are numerous solutions outlined in the literature [1], [2] and [3] that detail the solutions to the reachability problem.

Thus, the input to the system is formed from these two sections and is described as follows:

$$U = u_{eq} + u_n \qquad 4.5.2$$

where u_{eq} is the linear control action which is associated with the movement on the sliding surface.

u_n is the discontinuous control action which is used to reach the sliding surface.

A suitable solution to the reachability problem is to make u_n a relay controller with constant gains.

$$u_n = \begin{cases} \alpha \, \mathrm{sgn}(s) & s \neq 0 \quad \alpha > 0 \\ 0 & s = 0 \end{cases} \qquad 4.5.3$$

The u_n component of the controller is the high frequency component where the sign function performs the high frequency switching action. The value of α merely dictates the amplitude of the frequency component or the rate at which the system will be thrust towards the sliding surface. Under closed loop analysis the system and the equivalent control dynamics reduce to a simple integrator (this is discussed in Section 4.7). Therefore the value of α has to only compensate for a pole at the origin. This means that the value of α can be large, which will stabilise the pole and provides a means for fast convergence towards the sliding surface. Thus, greater stability in the presence of disturbances can be achieved.

Note, the sign of the parameter α is in some literature given as positive and others negative. The sign of the parameter α must ensure negative feedback. In some instances negative feedback is assumed in the design of the switching surface (through the transformation matrix), thus α is positive. Other literature does not assume this, thus α is negative. Therefore one must consider where negative feedback is introduced in the choice of the sign for α.

Consider the following standard example.

$$\begin{aligned} \dot{x}_1(t) &= x_2(t) \\ \dot{x}_2(t) &= a_1(t)\, x_2(t) + a_2(t)\ x_2(t) + bu(t) \end{aligned} \qquad 4.5.4$$

where b is known and $a_1(t)$ and $a_2(t)$ are unknown but bounded by

$$|\, a_1(t)\,| \le M_1, \quad |\, a_2(t)| \le M_2 \qquad 4.5.5$$

Now consider the control law

$$u(t) = -\frac{M+k}{b}\left[x_1(t) + x_2(t)\right] \qquad 4.5.6$$

where $k > 0$ and $M = \max\{M_2 + 1, M_1\}$

The closed loop system is

$$\begin{aligned} \dot{x}_1(t) &= x_2(t) \\ \dot{x}_2(t) &= a_1(t)\, x_2(t) + a_2(t)\ x_2(t) - (M+K)[x_1(t) + x_2(t)] \end{aligned} \qquad 4.5.7$$

With the introduction of the sliding surface

$$s(t) = x_1(t) + x_2(t) \qquad 4.5.8$$

note that

$$\begin{aligned} Ms^2(t) &\ge s(t)\{a_1(t)x_1(t) + (a_2 + 1)(t)\, x_2(t)\} \\ \dot{s}(t) &= \dot{x}_1(t) + \dot{x}_2(t) \\ \dot{s}(t) &= a_1(t)x_1(t) + (\, a_2(t) + 1)x_2(t) - (M+K)s(t) \end{aligned} \qquad 4.5.9$$

It follows that

$$s(t)\dot{s}(t) \le -k\, s^2(t) < 0 \qquad 4.5.10$$

This is the convergent condition which ensures that s(t) converges to zero. Which implies that the control law (4.5.6) forces s(t) =0. Note: one should consider all possible sign conditions of $s(t)$ and $\dot{s}(t)$.

4.6 ROBUST CONTROL (DEALING WITH UNCERTAINTY)

It is always possible to consider uncertainty as an unknown external signal that perturbs the process away from the trajectory predicted during the design process. As outlined previously, using sliding mode control enables disturbances to be rejected under certain conditions. Thus, the trajectory is not effected.

Consider the system given by (4.5.4) with a bounded matched external disturbance signal v(t):

$$\begin{aligned} \dot{x}_1(t) &= x_2(t) \\ \dot{x}_2(t) &= a_1(t)\, x_2(t) + a_2(t)\ x_2(t) + bu(t) + v(t) \end{aligned} \qquad 4.6.1$$

v(t) is a “matched disturbance” which impacts directly on only those states which are also directly affected by the control law u(t).

With the control law defined by (4.5.6) the closed loop system is

$$\begin{aligned} \dot{x}_1(t) &= x_2(t) \\ \dot{x}_2(t) &= -[Ms(t) - a_1(t)\, x_1(t) - a_2\, x_2(t)] - [ks(t) - v(t)] \end{aligned} \qquad 4.6.2$$

When s(t) is small, we have $|v(t)| > k|s(t)|$. Thus, the convergent condition 4.5.10 is not satisfied and s(t) may not converge to zero. To satisfy the convergent condition, we have to modify the choice of control law

$$u(t) = -\frac{M}{b}s(t) - \frac{k\, s(t)}{b\,|s(t)|} \qquad k > |v(t)| \qquad 4.6.3$$

This is a standard sliding mode controller and the signal

$$\mathrm{sgn}(s(t)) = \frac{s(t)}{|s(t)|} \qquad 4.6.4$$

Thus this discontinuous function encourages switching across the sliding surface, and negates the matched disturbances that may cause the system states to stray away from the sliding surface.

However in practice it is sometimes not feasible to implement a sign function as this switching may cause severe wear and tear on equipment. A continuous approximation to the sign function is to use the saturation function. The use of the saturation function may have the draw back of incurring steady state error. Thus in order to compensate for the steady state error, integral action must be introduced.

A practical sliding mode controller may be

$$U=u_{eq}+\alpha\int \text{sat}(s)\, dt \qquad 4.6.5$$

where α is a gain which ensures negative feedback and causes (4.5.1) to hold.

Note that the sliding mode controller given by (4.6.5) is not used in this thesis because initial investigations lead to instability issues with the introduction of the integrator. It was found that only certain values of α would produce a stable system. This is because under closed loop analysis the system and the equivalent control dynamics reduce to a simple integrator (as will be shown in Section 4.7) and therefore the feedback gain α may not be able to compensate for the introduction of another pole at the origin. Thus, further investigation is needed to determine under what conditions α in (4.5.6) will produce a stable system. This work is beyond the scope of this thesis.

The sliding mode controller used in this thesis is the standard sliding mode controller given by (4.6.3).

4.7 CLOSED LOOP ANALYSIS

The basic sliding mode controller is one which reduces the controller design to a first order control problem. This occurs because of the reduced order system design. In performing a reduced order system design, a controller is being designed to control the n-1 poles of the system. Under closed loop analysis it can be seen that there are (n-1) poles that are stable and one pole is left to be controlled, which lies at the origin. This occurs because the equivalent control dynamics are determined by (4.2.1) and the feedback gains are determined for a reduced order system. Thus, an integrator is all that

remains to be controlled (this will be shown later). The control of the integrator is performed by a simple feedback gain. This gain is the α parameter given in (4.5.3).

Consider the system below

$$\begin{bmatrix} \dot{x}_1 \\ \dot{x}_2 \end{bmatrix} = \begin{bmatrix} 1 & -1 \\ 1 & 1 \end{bmatrix} \begin{bmatrix} x_1 \\ x_2 \end{bmatrix} + \begin{bmatrix} 0 \\ 1 \end{bmatrix} u \qquad 4.7.1$$

Thus the poles of the system are

1.0000 + 1.0000i

1.0000 - 1.0000i

Now using the reduced order method described by (4.3.1) - (4.3.5) a sliding surface can be designed such that

$$S = K x = 0 \qquad 4.7.2$$

Using the LQR method (with Q=1 and R=1) to design a set of feedback gains gives

$$K = [\ -2.4142 \quad 1] \qquad 4.7.3$$

Thus the equivalent control which is given by (4.2.3) which is also the control input becomes

$$U = u_{eq} = [\ 1.4142 \quad -3.4142]\ x(t)$$

Considering the closed loop system ($A + B*u_{eq}$). Note that negative feedback has already been taken into consideration in the design of the equivalent control dynamics.

Thus the poles for the closed loop system are

$P_1 = 0$

$P_2 = -1.4142$

Now the only pole left to control is P_1, which can be achieved by a simple state feedback gain and adding the robustness capability of the sgn function. In this case α must be chosen to be negative to ensure stability.

It can be seen from the closed loop poles that the system is broken up into a n-1 control problem, which is taken care of in the design of the equivalent control dynamics and a first order control problem, which is controlled by the αsgn(s) controller.

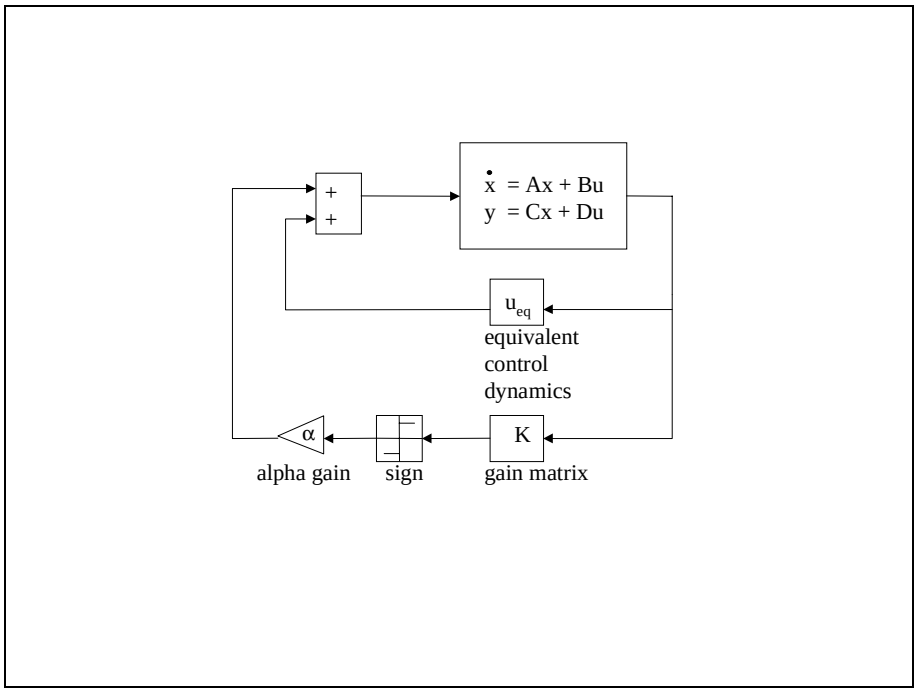

Figure 4.7.1 Block diagram of sliding mode controller

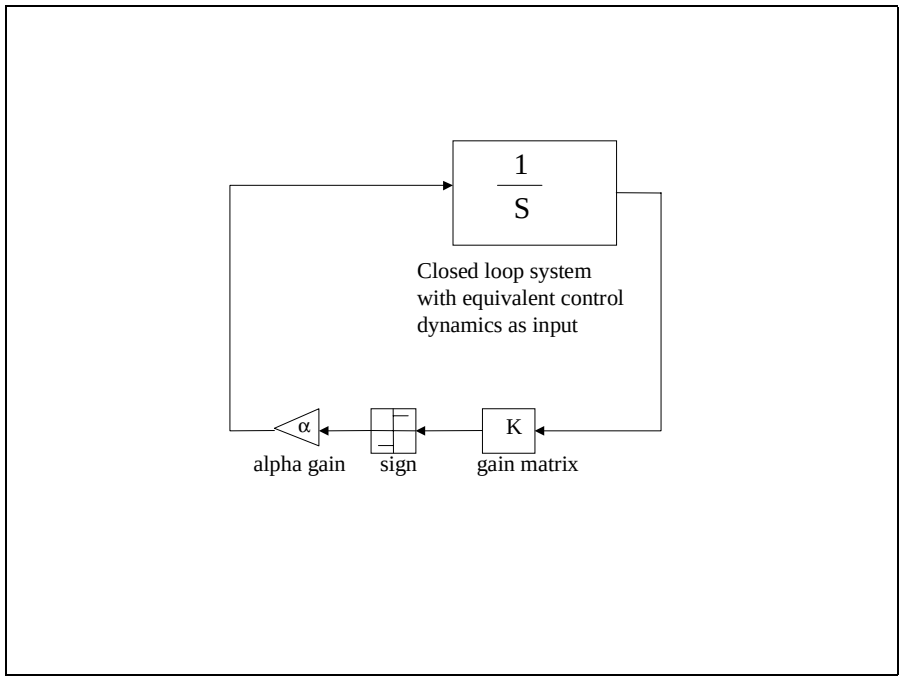

Figure 4.7.2 A simplification of the sliding mode controller

CHAPTER 5 CONTROLLER DESIGN

In this chapter the design of the sliding mode controller (as described in Chapter 4) to control the cart position and the swing dynamics of the gantry crane system is discussed. The controller designed in this chapter uses the state space model that was derived in Chapter 3. Since the sliding mode controller is comprised of the equivalent control dynamics and the sliding surface, the derivation of each of these components is given in this chapter.

In the subsequent chapters, a discussion of the real-time implementation for a controller which achieves cart setpoint control and swing cancellation will be given. Then in Chapter 8 a discussion of the controller's performance will be given when rope length control will is incorporated into the controller's structure.

The gantry crane system as modelled in Chapter 2 is basically a type 1 system. But there are non-linearities that are known to exist and have not been accounted for such as friction and a dead band region. The crane was assumed to be linear, clearly it is not. Even though there already exists an integrator in the model, in considering all these non-linearities, the gantry crane system can be thought of as a type 0 system. (i.e. no integrator in the forward path of the plant). Even with dead band compensation (which will be discussed latter) the cart may not always move to the desired position, as the dead band region is not linear. Thus to keep the error signal gradually increasing in order to make the cart move, an integrator must be added.

The key aspect of this chapter is the use of pole placement in the derivation of the sliding mode controller. Since the swing angle is a function of the rope length, using pole placement, a set of feedback gains can be easily designed which are also a function of the rope length. Thus, the rope length is the scheduling parameter. If optimal control techniques were used, such as LQR, there is no known method to suitably manipulate the systems matrices that will produce a set of feedback gains which are a function of the rope length. As the rope length changes so does the system's dynamics. Thus, the cart and swing controller must be a function of the rope length, so that the closed system

has the same performance characteristics (i.e. closed loop poles) with a varying rope length.

5.1 CART POSITIONING CONTROL

The first step to achieve both cart position control and swing control is to add an integrator in the forward path between the error comparator and the plant. Introducing the integrator converts the system into a type 1 system. This is needed in order to achieve positional control of the cart, and changing the system to track a desired setpoint.

Thus, the system now has five states, each of which will be controlled about the operating point of zero. From Chapter 3 the state space presentation of the system is

$$\begin{bmatrix} \dot{x}_1 \\ \dot{x}_2 \\ \dot{x}_3 \\ \dot{x}_4 \end{bmatrix} = \begin{bmatrix} 0 & 1 & 0 & 0 \\ 0 & \frac{-ab}{d} & \frac{e}{d} & 0 \\ 0 & 0 & 0 & 1 \\ 0 & \frac{ab}{d\ell} & \frac{-c}{d\ell} & 0 \end{bmatrix} \begin{bmatrix} x_1 \\ x_2 \\ x_3 \\ x_4 \end{bmatrix} + \begin{bmatrix} 0 \\ \frac{a}{d} \\ 0 \\ \frac{-a}{d\ell} \end{bmatrix} u \qquad 5.1.1$$

$$y = \begin{bmatrix} 1 & 0 & 0 & 0 \\ 0 & 0 & 1 & 0 \end{bmatrix} \begin{bmatrix} x_1 \\ x_2 \\ x_3 \\ x_4 \end{bmatrix}$$

where x1 = cart position

x2 = cart velocity

x3 = swing angle

x4 = swing velocity

An integral state is introduced for setpoint tracking such that

$$\dot{\xi} = r - y = r - Cx \qquad 5.1.2$$

where

r = the reference input signal (step function, scalar quantity)

ξ = output of the integrator (state variable of system, scalar quantity)

The state space representation of the system now becomes

$$\dot{\hat{x}} = \hat{A}\hat{x} + \hat{B}u + Dr \qquad 5.1.3$$

where

$$\dot{\hat{x}} = \begin{bmatrix} \dot{x} \\ \dot{\xi} \end{bmatrix} \quad \hat{x} = \begin{bmatrix} x \\ \xi \end{bmatrix} \quad \hat{A} = \begin{bmatrix} A & 0 \\ -C & 0 \end{bmatrix} \quad \hat{B} = \begin{bmatrix} B \\ 0 \end{bmatrix} \quad D = \begin{bmatrix} 0 \\ 1 \end{bmatrix}$$

The above can now be expanded to incorporate the system matrix described above and the integrator to give the following state space matrix of the system.

$$\begin{bmatrix} \dot{x}_1 \\ \dot{x}_2 \\ \dot{x}_3 \\ \dot{x}_4 \\ \dot{\xi} \end{bmatrix} = \begin{bmatrix} 0 & 1 & 0 & 0 & 0 \\ 0 & \frac{-ab}{d} & \frac{e}{d} & 0 & 0 \\ 0 & 0 & 0 & 1 & 0 \\ 0 & \frac{ab}{d\ell} & \frac{-c}{d\ell} & 0 & 0 \\ -1 & 0 & 0 & 0 & 0 \end{bmatrix} \begin{bmatrix} x_1 \\ x_2 \\ x_3 \\ x_4 \\ \xi \end{bmatrix} + \begin{bmatrix} 0 \\ \frac{a}{d} \\ 0 \\ \frac{-a}{d\ell} \\ 0 \end{bmatrix} u + \begin{bmatrix} 0 \\ 0 \\ 0 \\ 0 \\ 1 \end{bmatrix} r \qquad 5.1.4$$

Since the system matrices have been modified to incorporate cart positional control, the sliding mode controller will be designed based on the above system matrices and on the technique outlined in the previous chapter.

5.2 DERIVATION OF SWITCHING SURFACE

In this section a discussion of the steps used in the design of the sliding mode controller which achieves cart setpoint control and swing cancellation is given. These steps are those described in Chapter 4. Taking the system matrices as described by (5.1.4) and substituting for the numerical values gives the system matrices as follows:

$$\begin{bmatrix} \dot{x}_1 \\ \dot{x}_2 \\ \dot{x}_3 \\ \dot{x}_4 \\ \dot{\xi} \end{bmatrix} = \begin{bmatrix} 0 & 1 & 0 & 0 & 0 \\ 0 & -5.7312 & 1.0142 & 0 & 0 \\ 0 & 0 & 0 & 1 & 0 \\ 0 & \frac{5.7312}{\ell} & \frac{-10.8412}{\ell} & 0 & 0 \\ -1 & 0 & 0 & 0 & 0 \end{bmatrix} \begin{bmatrix} x_1 \\ x_2 \\ x_3 \\ x_4 \\ \end{bmatrix} + \begin{bmatrix} 0 \\ 0.7376 \\ 0 \\ \frac{-0.7376}{\ell} \\ 0 \end{bmatrix} u + \begin{bmatrix} 0 \\ 0 \\ 0 \\ 0 \\ 1 \end{bmatrix} r \qquad 5.2.1$$

$$y = \begin{bmatrix} 1 & 0 & 0 & 0 & 0 \\ 0 & 0 & 1 & 0 & 0 \end{bmatrix} \begin{bmatrix} x_1 \\ x_2 \\ x_3 \\ x_4 \\ \end{bmatrix}$$

The first step in designing the controller is to define a transformation matrix such that

$$T\hat{B} = \begin{bmatrix} B1 \\ 0 \end{bmatrix} \qquad 5.2.2$$

It would be ideal to define T to be orthogonal as this would ease the design process, but it is not completely necessary.

Let T be defined as

$$T = \begin{bmatrix} 0 & \frac{-d}{a} & 0 & \frac{d\ell}{a} & 0 \\ \frac{-d}{a} & \frac{1}{\ell} & 0 & 1 & 0 \\ 0 & 0 & 1 & 0 & 0 \\ \frac{d\ell}{a} & 1 & 0 & \ell & 0 \\ 0 & 0 & 0 & 0 & 1 \end{bmatrix} \qquad 5.2.3$$

The transformed state space representation of the system described by (5.2.1) can now be determined. The transformed state variable matrix is given by

$$\hat{z} = T\hat{x} \tag{5.2.4}$$

Substituting (5.1.3) into (5.2.4) gives

$$T^{-1}\dot{\hat{z}} = \hat{A}T^{-1}\hat{z} + \hat{B}u + \begin{bmatrix}0\\1\end{bmatrix}r \tag{5.2.5}$$

$$\dot{\hat{z}} = T\hat{A}T^{-1}\hat{z} + T\hat{B}u + T\begin{bmatrix}0\\1\end{bmatrix}r \tag{5.2.6}$$

Now let

$$\tilde{A} = T\hat{A}T^{-1} = \left[\begin{array}{c|c} * & * \\ \hline \bar{B} & \bar{A} \end{array}\right] = \left[\begin{array}{c|cccc} \frac{-ab}{d} & \frac{b\ell}{2} & \frac{-e-c}{a} & \frac{1}{2b} & 0 \\ \hline \frac{1}{2} & \frac{d\ell}{4a} & \frac{e-c}{d\ell} & \frac{d}{4a} & 0 \\ \frac{a}{2d\ell} & \frac{1}{4} & 0 & \frac{1}{4\ell} & 0 \\ -\frac{\ell}{2} & \frac{d\ell^2}{4a} & \frac{e-c}{d} & \frac{d\ell}{4a} & 0 \\ 0 & \frac{a}{2d} & 0 & -\frac{a}{2d\ell} & 0 \end{array}\right] \tag{5.2.7}$$

From the previous chapter it can been seen that $\tilde{A}$ contains a new input matrix $\bar{B}$ and a new system matrix called $\bar{A}$, these are given respectively as follows:

$$\bar{A} = \begin{bmatrix} \frac{d\ell}{4a} & \frac{e-c}{d\ell} & \frac{d}{4a} & 0 \\ \frac{1}{4} & 0 & \frac{1}{4\ell} & 0 \\ \frac{d\ell^2}{4a} & \frac{e-c}{d} & \frac{d\ell}{4a} & 0 \\ \frac{a}{2d} & 0 & -\frac{a}{2d\ell} & 0 \end{bmatrix} \tag{5.2.8}$$

$$\bar{B} = \begin{bmatrix} \frac{1}{2} \\ \frac{a}{2d\ell} \\ -\frac{\ell}{2} \\ 0 \end{bmatrix} \qquad 5.2.9$$

Now a simple state feedback controller can be designed.

Before any poles can be placed, it is necessary to define the performance criteria. The cart and swing should be bought under control in approximately 5 sec. It is required, that at best, the cart's step response be critically damped. But, to have a fast step response for the cart's position a damping ratio of 0.7 is acceptable, as this will produce little overshoot, and still achieve a fast settling time.

The two dominant poles for the state feedback controller will be chosen to have a settling time of 3 sec. with a damping ratio of 0.7. This does not necessarily mean that the system will settle in 3 sec., since there are three other poles that must be placed and they will also influence the settling time. This is the fundamental limitation of pole placement design techniques, in that for systems which are greater than second order, there is no clear method for determining the closed loop characteristics. Thus, one must look at the closed loop step response and determine if the settling time displayed is satisfactory.

Taking the 2% criterion

$$t_s = \frac{4}{\zeta\omega_n} \qquad 5.2.10$$

$$\omega_n = \frac{4}{0.7*3} = 1.9 \text{rads}^{-1} \qquad 5.2.11$$

poles are located at

$$p = -\zeta\omega_n \pm j\omega_n\sqrt{1-\zeta^2} \qquad 5.2.12$$

Substituting the values for ω_n and ζ from (5.2.10) and (5.2.11) into (5.2.12) gives the following poles

$$p = -1.33 \pm 1.35j \qquad 5.2.13$$

Since the system matrix is fourth order there are four poles that must be placed. The poles that are given by (5.2.13) will be the dominant poles and two other poles will be introduced to satisfy the pole placement technique. Since the motor has a maximum input voltage of ±13v and dead band region of 4.7v, then maximum voltage that can be applied to the motor is approximately ± 8v. Therefore the choice of these two poles must ensure that the controller's control effort will not exceed this limit. Thus, the poles will be located at -3.0 and -3.1.

The complete pole placement set is

$$p = -1.33 \pm 1.35j, -3.0, -3.1 \qquad 5.2.14$$

Using standard pole placement techniques the feedback gains can be calculated. The feedback gain matrix for the reduced order system is defined as

$$\bar{K} = \begin{bmatrix} \bar{K}_1 & \bar{K}_2 & \bar{K}_3 & \bar{K}_4 \end{bmatrix} \qquad 5.2.15$$

Therefore the characteristic equation that needs to be solved is given as

$$(s + 1.3 - 1.35j)*(s + 1.3 + 1.35j)*(s + 3.0)*(s + 3.1) = \det(SI - (\bar{A} - \bar{B}\bar{K})) \qquad 5.2.16$$

The equation above will derive the feedback gains for the reduced order system. Now it is required to convert the reduced order gains into the full order feedback gains. The full order feedback gain will also define the switching surface. This is given as

$$\tilde{K} = [1 \ \bar{K}] \qquad 5.2.17$$

Thus in order to achieve the correct gains a reverse transformation must take place

$$\hat{K} = \bar{K}T \qquad 5.2.18$$

Since the length of the rope ℓ (i.e. the distance that the goods are displaced from the cart) is a variable in the system matrices, the feedback gains (and thus the switching surface and equivalent control dynamics) are defined as a function of the rope length ℓ.

The feedback gain as a function of the rope length are:

$$\hat{K}^T = \begin{bmatrix} -12.62\ell \\ 0.92\ell^2 - 7.9\ell - 0.1*10^{-8} \\ -12.62\ell^2 + 23.59\ell \\ 0.92\ell^3 - 7.9\ell^2 + 2.7\ell \\ 9.04\ell \end{bmatrix} \qquad 5.2.19$$

Another method to determine the closed loop poles is to use LQR techniques to derive a set of feedback gains that will give the desired step response. Once a satisfactory step response is achieved, the closed loop poles can be determined.

For the system described by (5.2.8) and (5.2.9) and choosing $Q = \begin{bmatrix} 10 & 0 & 0 & 0 \\ 0 & 1 & 0 & 0 \\ 0 & 0 & 100 & 0 \\ 0 & 0 & 0 & 100 \end{bmatrix}$ $R = 1$

a similar step response to the one that is produced by using the feedback gains described by (5.2.19) is achieved. The closed loop poles produced by the LQR technique are:

P_1 = -1.2146 + 1.3435i

P_2 = -1.2146 - 1.3435i

P_3 = -2.7041 + 1.9252i

P_4 = -2.7041 - 1.9252i

which can be seen are very similar to those chosen in (5.2.14).

5.3 DERIVATION OF EQUIVALENT CONTROL DYNAMICS

The equivalent control dynamics are used to establish the performance of the controller under closed loop conditions. The equivalent control dynamics are determined when the derivative of the sliding surface equals 0.

Thus

$\dot{s} = 0$ (where s is the switching surface) 5.3.1

$s = \hat{K}\hat{x}$ 5.3.2

$\dot{s} = \hat{K}\dot{\hat{x}} + \dot{\hat{K}}\hat{x}$ where $\dot{\hat{K}} = 0$ 5.3.3

$$\dot{\hat{x}} = \hat{K}(\hat{A}\hat{x} + \hat{B}u_{eq} + Dr) = 0 \qquad 5.3.4$$

Substituting (5.3.4) into (5.3.3) and solving for u_{eq}

$$u_{eq} = -\frac{1}{\hat{K}\hat{B}}(\hat{K}\hat{A}\hat{x} + \hat{K}Dr) \qquad 5.3.5$$

$$u_{eq} = \frac{-9.038\ell \mathbf{x}1}{1.99 + 0.11*10^{-8}\ell} + \frac{(-12.618\ell + 0.243*10^{-10}\ell^2 + 15.539)\mathbf{x}2}{1.99 + 0.11*10^{-8}\ell} + \frac{(-29.321 - 9.038\ell^2 + 77.742\ell)\mathbf{x}3}{1.99 + 0.11*10^{-8}\ell} +$$

$$\frac{-0.286*10^{-6}\ell(-0.824*10^{8} + 0.441*10^{8}\ell)x4}{1.99 + 0.11*10^{-8}\ell} - \frac{-9.038\ell \mathbf{r}}{1.99 + 0.11*10^{-8}\ell} \qquad 5.3.6$$

Making the assumption of a constant rope length of 1 m

$$u_{eq} = 1.46x_2 + 19.69x_3 + 5.48x_4 + 4.52(r - x_1) \qquad 5.3.7$$

As in Section 4.7 the closed loop system of the equivalent control dynamics should be stable for all poles except for one. The poles should be located where they were placed and one at the origin.

Thus the closed loop poles are

P1 = 0

P2 = -3.1000

P3 = -3.0000

P4 = -1.3000 + 1.3500i

P5 = -1.3000 - 1.3500I

As was stated in Section 4.7 the remaining pole is made stable by use of a feedback gain. This feedback gain and the discontinuous function ensure that the Lyapunov stability criterion is met.

5.4 COMPLETE CONTROL STRUCTURE

In order for the controller to fully maintain its sliding mode nature, the system states must be maintained on the sliding surface. If there exist external disturbances which cause the system states to deviate from the sliding surface, then the controller must push the system states towards the sliding surface. As was stated earlier in Chapter 4, the complete control structure consists of the equivalent control section plus a discontinuous section that copes with disturbances and system uncertainties. From (4.5.2) the complete controller structure is as follows:

$U = u_{eq} + \alpha sat(s)$ where s is the sliding surface 5.4.1

The only parameter now left to determine is α. There is no known mathematical method for determining α, thus it must be determined from simulation.

After many simulations the best value for the parameter α was found to be 1. Note also that the value of α is positive and not negative. This is because the transformation matrix took care of negative feedback. One must be careful in choosing the sign for α as positive feedback can be easily introduced.

Now the complete controller structure for a fixed rope length of 1 m is:

$$U = u_{eq} + sat(-12.62x_1 - 7.01x_2 + 10.97x_3 - 4.299x_4 + 9.038x_5) \quad 5.4.2$$

where

$$u_{eq} = 1.46x_2 + 19.69x_3 + 5.48x_4 + 4.52(r - x_1) \quad 5.4.3$$

CHAPTER 6 SIMULATION AND IMPLEMENTATION OF CART AND SWING CONTROLLER

In this chapter discussion of the simulation and implementation of the sliding mode controller is given. The chapter contains a discussion on the problems that were encountered in the real-time implementation of the sliding mode controller.

The controller is solely designed for swing control and cart positioning control. The rope length control system will be discussed in a later chapter. The sliding mode controller implemented is that as described in Chapter 5 for a fixed rope length of 1 m.

This chapter will include both simulations and real-time implementation data for both controller implementations. The program Maple was used to perform most of the matrix manipulations. Simulation data was obtained by using Matlab to simulate the controllers. The program RTShell was used in implementing the real-time controller.

The simulation and real-times implementation of the sliding mode controller should behave according to the design specifications, that is, a settling time of approximately 5 sec. with damping ratio between 1 and 0.7.

Figure 6.1 is a block diagram representation of the sliding mode controller. The block labelled Equivalent control dynamics, consists of the Ueq equation and the sliding surface is represented by the block labelled K Matrix which is multiplied by the states to give the sliding surface. The system model block only represents the cart and swing dynamics. There is a variable L that represents the rope length.

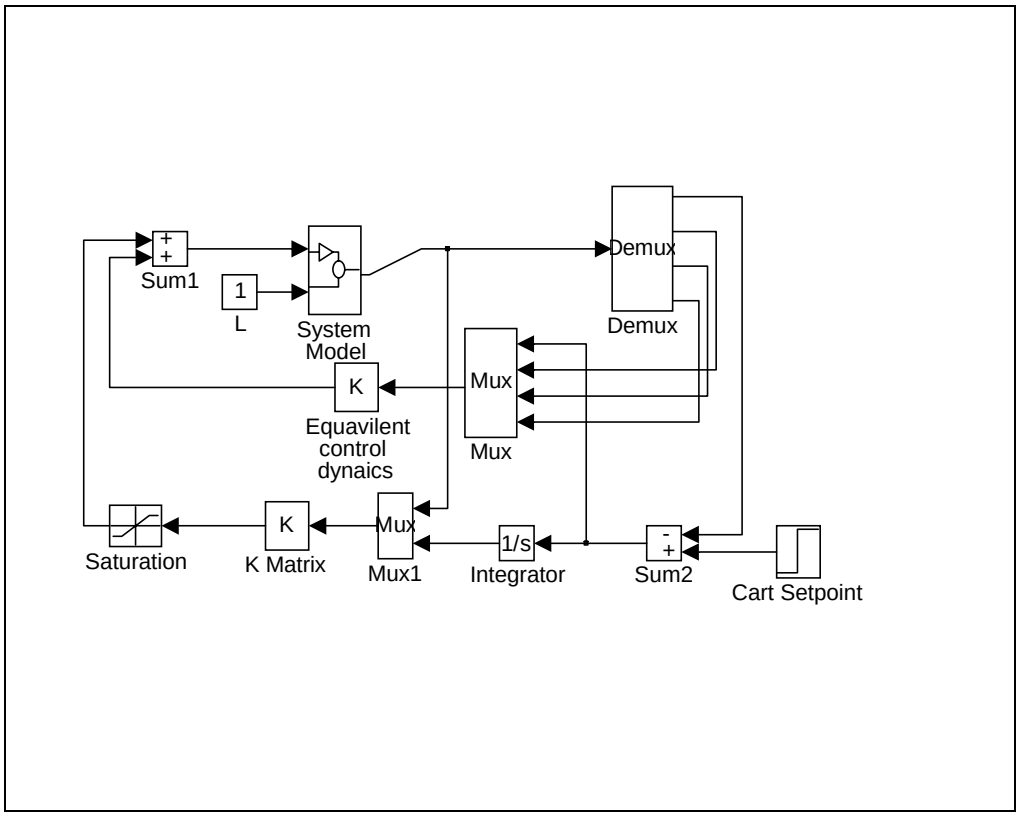

Figure 6.1 Block diagram of sliding mode controller

6.1 SIMULATION OF SLIDING MODE CONTROLLER

6.1.1 CART RESPONSE

The controller simulated in this section should behave according to the design specifications. This is because the controller has been designed based on the simulated system which assumes that the rope length is 1 m.

Figure 6.1.1 represents the step response of the cart with a setpoint of 1 m. The figures illustrates that the cart's response meets all the design criteria. The controller was designed to have a fast settling time and a damping ratio of 0.7 i.e. to have an underdamped response. The figure shows that at the 3 second mark (i.e. time = 3 sec.) the cart has reached the setpoint and now will remain within the 2% tolerance limit, but the cart does not reach perfect setpoint until 5 sec. This is because of the influence of the other three poles that were also placed.

In this application the settling time of 5 sec. is a quick enough settling time for the task at hand. Figure 6.1.3 illustrates the control effort. For practical reasons that will be discussed later it is not desired that the simulated control effort far exceed 5 V. Thus this also influences the settling time.

6.1.2 SWING ANGLE

It can be seen in the Figure 6.1.2 that the swing angle is bought under control in 6 sec. The swing has not completely settled in 5 sec. as designed because the cart itself is still slightly moving, which can be seen from the control effort. Since the values of the swing angle and the cart position are small, they do have an influence in an idealistic simulation. However, in practice these small numbers are assumed to be zero and thus, it can be said that the swing is bought under control in 5 sec.

6.1.3 CONTROL EFFORT

A well designed controller will have a smooth control action or control effort. Figure 6.1.3 illustrates that the sliding mode controller designed in Chapter 5 has a smooth control effort. This will be the applied voltage to the motor driving the cart on the real-time system.

The control effort also allows us to examine the controller’s behaviour in catching the swing and achieving setpoint control. From Figure 6.1.3 it can be seen that the cart is initially instructed to move towards the setpoint, thus causing the goods to swing in the opposite direction of motion. As the goods swing back in the same direction of motion, the cart's velocity is dropped to allow the goods to catch up with the motion of the cart. Once the goods pass 0 rad and swing towards a positive angle, the velocity of the cart is increased to catch the swinging goods. Then as the angular velocity of the goods decreases and the vicinity of the setpoint is near, the velocity of the cart is lessened until setpoint is reached.

6.1.4 SWITCHING SURFACE

The switching surface provides a means for determining what type of action the controller will take. Since it is known that the system is on the sliding surface when $s = kx = 0$, then the magnitude of the switching surface can be viewed as the distance the system is from being in the sliding mode condition.

As can be seen by Figure 6.1.4 the distance from the switching surface is very small. This is due to Matlab's inability to place initial conditions on transfer functions. Thus, when the simulation is started all initial conditions are assumed to be 0. This means that the system is already on the sliding surface. The waveform shown arises from 'rounding off' errors in Matlab. Because the system is already on the sliding surface in simulation, the switching surface does not play a significant roll in the control action. Thus, the controller's performance in this simulation is determined by the equivalent control dynamics.

To ensure that the controller is robust in the presence of external disturbances, the system should always converge to the sliding surface. In order to ensure that convergence to the sliding surface occurs, an external disturbance of 0.1 rad is applied to the swing angle at the 2 second mark (i.e. time = 2 sec.). Figure 6.1.7 illustrates that the system does converge to the sliding surface in the presence of the external disturbance. The magnitude of the sliding surface in Figure 6.1.7 is far greater then Figure 6.1.4. This is because the system has been pushed off the sliding surface and the controller is attempting to bring the system back onto the sliding surface, as was not the case in Figure 6.1.4 which is explained above. It can be seen from Figures 6.1.5 and 6.1.6 that the system still settles in the same time frame as Figures 6.1.1 - 6.1.4. Thus, the controller is shown to be robust in the presence of external disturbances and the performance criteria will always be met.

6.1.5 SIMULATION WITH NOISE

For completeness a simulation with noise is conducted, since it is known that the real-time system is subjected to noise. Figure 6.1 8 - 6.1.11 illustrate the cart's response, swing angle response, control effort and switching surface response when noise is introduced into the simulation.

In order to keep the simulation as realistic as possible it is known that the only directly measurable states on the real-time system are the cart position and the swing angle. Thus, noise will only be added on to these states in simulation. The respective velocity states are influenced by noise since they are direct derivatives of the states that will have noise introduced. Noise is introduced by using a random number generator where the random number is bound by upper and lower limits. For the cart position the noise level is between ±0.05 m and the swing angle noise level is between ±0.02 rad. These limits were determined from observing the noise level on the real-time system.

Figures 6.1.8 - 6.1.10 illustrate that the basic envelope waveform of the cart position, swing angle, and control effort are the same as in the clean (i.e. no noise) system illustrated by Figures 6.1.1 - 6.1.3. It can be seen from Figures 6.1.8 - 6.1.11 that the system never really settles, and this is due to the introduction of noise. But even with the introduction of noise, it can be seen that both the cart position and swing angle reach setpoint in the same time frame as in Figures 6.1.1 - 6.1.2, and from then on, hover about their respective setpoint.

Figure 6.1.11 illustrates the switching surface. It is clearly seen that the system never really converges to the switching (sliding) surface, because noise is continually pushing the system off the switching surface. What is clearly evident is that the system hovers about the switching surface, which means that the system is constantly crossing the sliding surface. It is also noted that noise dramatically increases the magnitude of the value 's', which is the distance the system is away from the sliding.

Overall the controller is shown to be robust in the presence of noise, and if the envelope waveforms are taken of the cart position and swing angle, it can be seen that the controller meets all the performance criteria.

Cart position step response setpoint 1 m

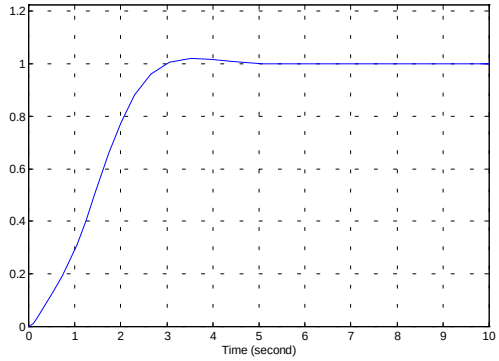

Figure 6.1.1

Swing angle step response

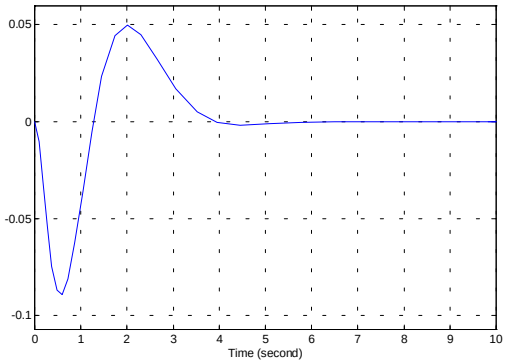

Figure 6.1.2

Control effort of cart and swing controller

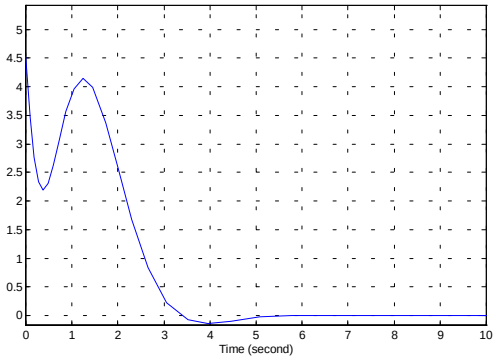

Figure 6.1.3

Switching surface

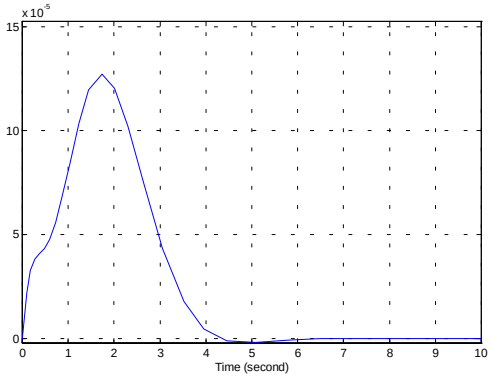

Figure 6.1.4

Cart position step response with external disturbance on swing angle

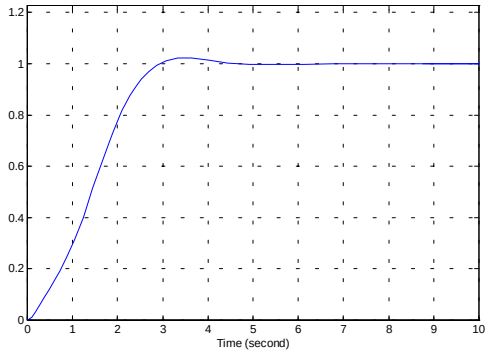

Figure 6.1.5

Swing angle step response with external disturbance

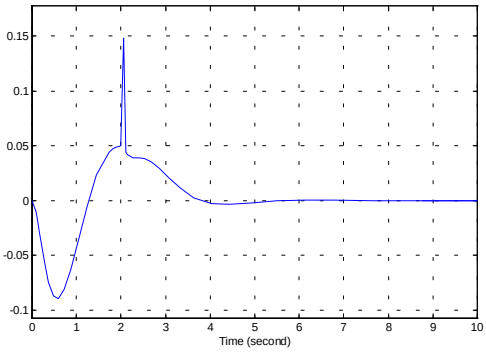

Figure 6.1.6

Switching surface with external disturbance

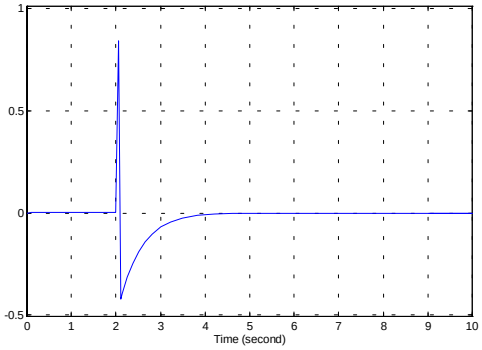

Figure 6.1.7

Cart position step response with noise, setpoint 1 m

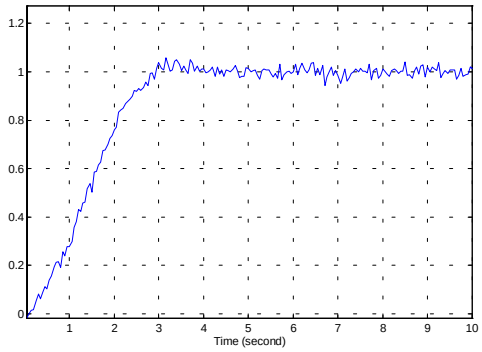

Figure 6.1.8

Swing angle step response with noise

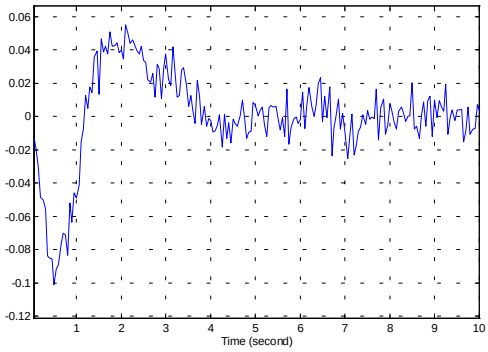

Figure 6.1.9

Control effort of cart and swing controller with noise

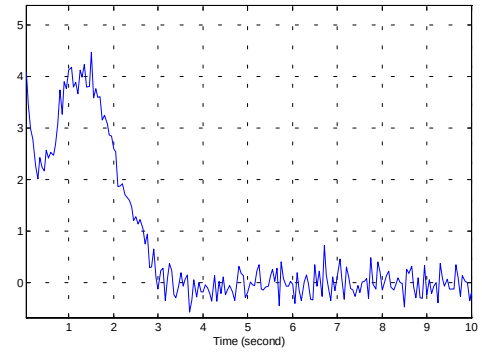

Figure 6.1.10

Switching surface with noise

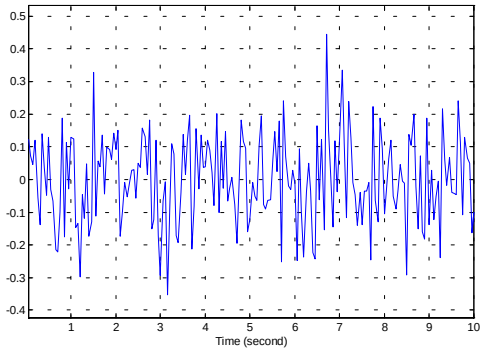

Figure 6.1.11

6.2 REAL-TIME IMPLEMENTATION

A discussion of the differences between the simulated model and the real-time system, as well as, the issues related to the real-time implementation of the sliding mode controller is given in this section. The sliding mode controller implemented on the real-time system is the controller designed in Chapter 5.

6.2.1 FRICTION

The real-time system was assumed to be frictionless. This is not the case in the real-time system. In fact, friction plays a significant role in the model's performance. The friction in the real-time system occurs from two components. The first component is the wheels of the cart. The cart's wheels were knurled to add traction to prevent the wheels from slipping and thus giving false positional readings. The second frictional component is the four guides attached to the cart which attempt to keep the cart moving in a straight line. These guides rub on the side of the rails thus keeping the cart straight.

6.2.2 UNBALANCED SYSTEM MASS

The simulated model assumes that the mass of the cart is a point mass, but this is not the case in the real-time system. The real-time system has the carts mass unevenly distributed. The system was designed in this way to add mass to the drive shaft of the cart to prevent slippage. Thus the cart is significantly heavier at one end then the other. Also, the simulated model assumes that the cart's mass lies directly above the pivot point of the goods. The real-time system has the pivot point of the goods in the middle of the cart, and the weight is distributed at both ends of the cart.

6.2.3 DEAD BAND

The motor that drives the cart has a dead band region. In modelling the motor dynamics, the dead band region was accounted for by means of adding a voltage to the applied motor voltage, which would overcome the dead band region. The dead band region is due to two factors:

1. The friction component of the cart.
2. The lack of torque that the motor produces for small applied voltages. That is the motor does not produce enough torque when a small voltage is applied to move the cart.

The motor dead band region was also found to be uneven. In the positive direction a voltage of 1 V was added to the control action and in the negative direction a voltage of -4.5 V was added.

Even though an integrator has been added to achieve better positional control of the cart, because of the large dead band region these voltages were still required to be added to the applied motor voltage. The reason for this is that the integrator would take time before it actually reached a voltage that would make the cart move. These sudden and large “bangs” to the cart are not desired. Rather, a smooth gradually applied voltage would be better.

Thus the combination of the integrator plus the addition of these voltages should give a quick reacting and smooth control voltage to the cart’s motor.

6.2.4 NOISE

Noise is the most unmodelled element in any application of control. Obviously the noise component was not modelled in the simulated model. Noise can be added to the simulated model to observe its effect. The noise in the real-time system mainly occurs from the potentiometer which measures the swing angle. The optical encoder which measures the cart’s position also is influenced by white noise, but not to the same extent as the swing angle measurement.

6.2.5 ESTIMATION OF STATES

The simulated system assumes that all states are directly accessible, in the real-time system this is not the case. The only states directly measured from the system are the cart position and the swing angle. The other two states (i.e. the cart velocity and the swing velocity) are estimated. Since the cart position and the swing angle are influenced by noise, derivatives of each of the states were not used, in an attempt to minimise the effects of the noise on the derivative states.

The alpha-beta filter as described by Skolnick [38] was used to estimate the respective velocities. The alpha-beta filter is used as a radar-tracking filter, and its function is to make a smooth estimate of a target's present position and predicted velocity.

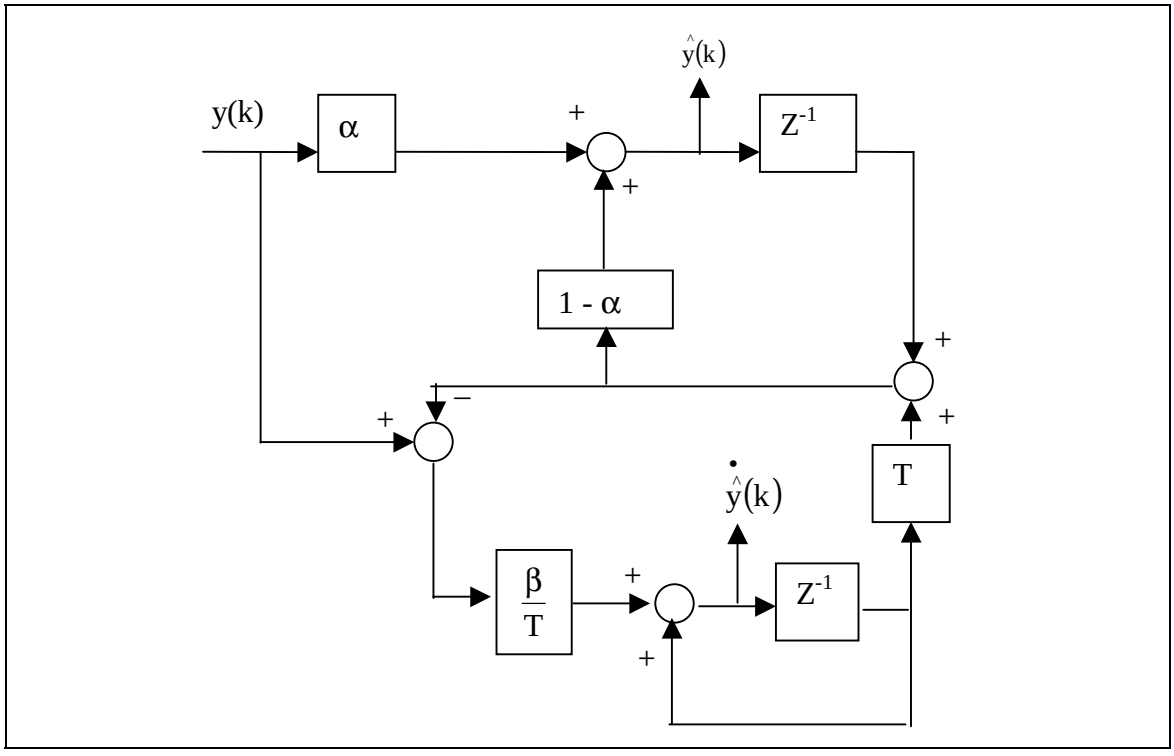

Figure 6.2.1 Block diagram of the alpha-beta filter

The alpha-beta filter tracking equations are:

$$\hat{y}(k) = \alpha y(k) + (1-\alpha)[\hat{y}(k-1) + T\dot{\hat{y}}(k-1)] \qquad 6.2.1$$

$$\dot{\hat{y}}(k) = \dot{\hat{y}}(k-1) + \frac{\beta}{T}[y(k) + \hat{y}(k-1) + T\dot{\hat{y}}(k-1)] \qquad 6.2.2$$

$$\beta = \frac{\alpha^2}{(2-\alpha)} \qquad 6.2.3$$

where

$y(k)$ = measured position signal $\quad \hat{y}(k)$ = predicted smoothed position

$\dot{\hat{y}}(k)$ = predicted smoothed velocity $\quad \alpha$ = position smoothing parameter

β = velocity smoothing parameter

The difference (6.2.1) and (6.2.2) can be easily programmed into a computer. This will give a smooth predicted velocity, while at the same time smoothing out the input signal.

The values of α and β are related be (6.2.3). The values of $\alpha = 0.3$ and $\beta = 0.053$ were determined experimentally and were found to be acceptable.

Figure 6.2.2 illustrates the actual swing angle and Figure 6.2.3 illustrates the estimated swing angle as given by the alpha-beta filter. It can be seen that if the two figures were superimposed, then the alpha-beta filter provides an accurate and filtered estimate of the swing angle.

The swing angle itself is not completely sinusoidal, because these figures represent the swing angles motion with the implementation of the sliding mode controller. Thus some of the noise on the swing angle is white noise, and other is quick changes of direction of the cart as the controller attempts to compensate for the noise of the angle signal and the angular velocity signal. Thus there exists a dilemma, if the controller compensates for a fluctuation swing angle, it will produce a fluctuation control signal, which will in turn produce a fluctuation swing angle. Thus the filter will attempt to filter anything that it considers as noise to provide a nice clean signal.

Figure 6.2.4 illustrates the estimated angular velocity and derivative (with respect to time) of the swing angle signal. Note that the swing angle signal is sinusoidal in motion, thus the velocity should also be sinusoidal. But as can be seen by Figure 6.2.4 the derivative signal is extremely noisy, and a very poor resemblance to a sinusoid.

The estimated angular velocity on the other hand is a lot cleaner and tends to exhibit a sinusoidal motion, but it too is still noisy. The alpha-beta filter is only a simple algorithm for estimation, but for this application it will suffice.

The Bode plots for the alpha-beta filter are shown in Figures 6.2.6 and 6.2.7. These figure illustrate that the alpha-beta filter is a low pass filter with a good phase margin. The break frequencies for the predicated smoothed position signal $\hat{y}(k)$ and the predicated smoothed velocity signal $\dot{\hat{y}}(k)$ are 250hz and 30hz respectively. This means that $\dot{\hat{y}}(k)$ is approximately an order of magnitude slower then $\hat{y}(k)$. This is due to the fact that the calculation of $\dot{\hat{y}}(k)$ depends on calculation $\hat{y}(k)$, and therefore $\dot{\hat{y}}(k)$ must wait until $\hat{y}(k)$ is calculated before it can be calculated. This is observed in (6.2.2).

The sampling rate of the computer was set to 25 Hz because it is known that for the fastest system dynamics this sampling rate would be acceptable. Figure 6.2.6 and 6.2.7 clearly illustrate that the filter has a faster response than the sampling rate, therefore the derived $\hat{y}(k)$ and $\dot{\hat{y}}(k)$ signals should be acceptable.

Actual swing angle

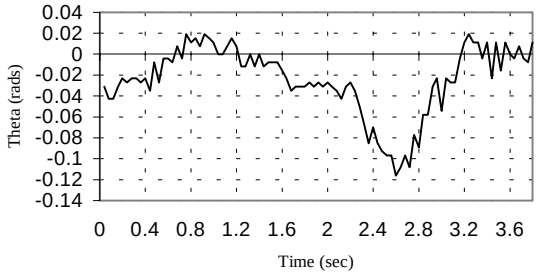

Figure 6.2.2

Estimated swing angle

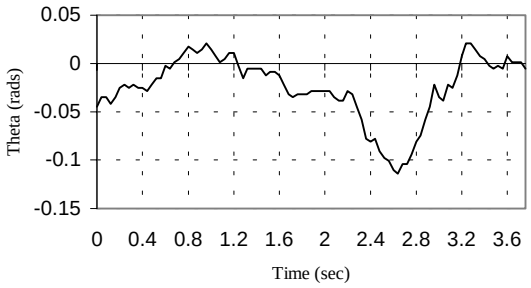

Figure 6.2.3

Angular velocity using differentiation

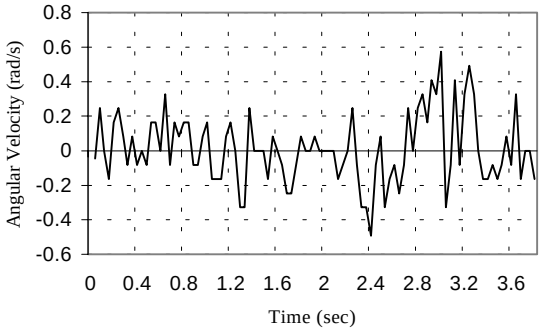

Figure 6.2.4

Estimated angular velocity

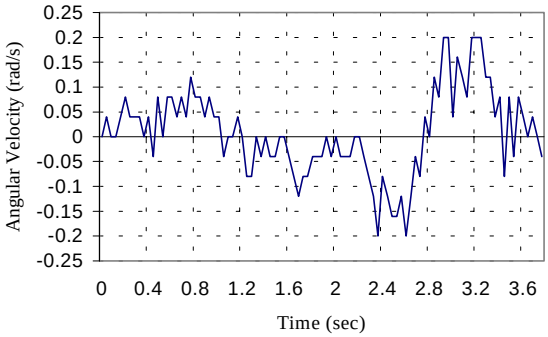

Figure 6.2.5

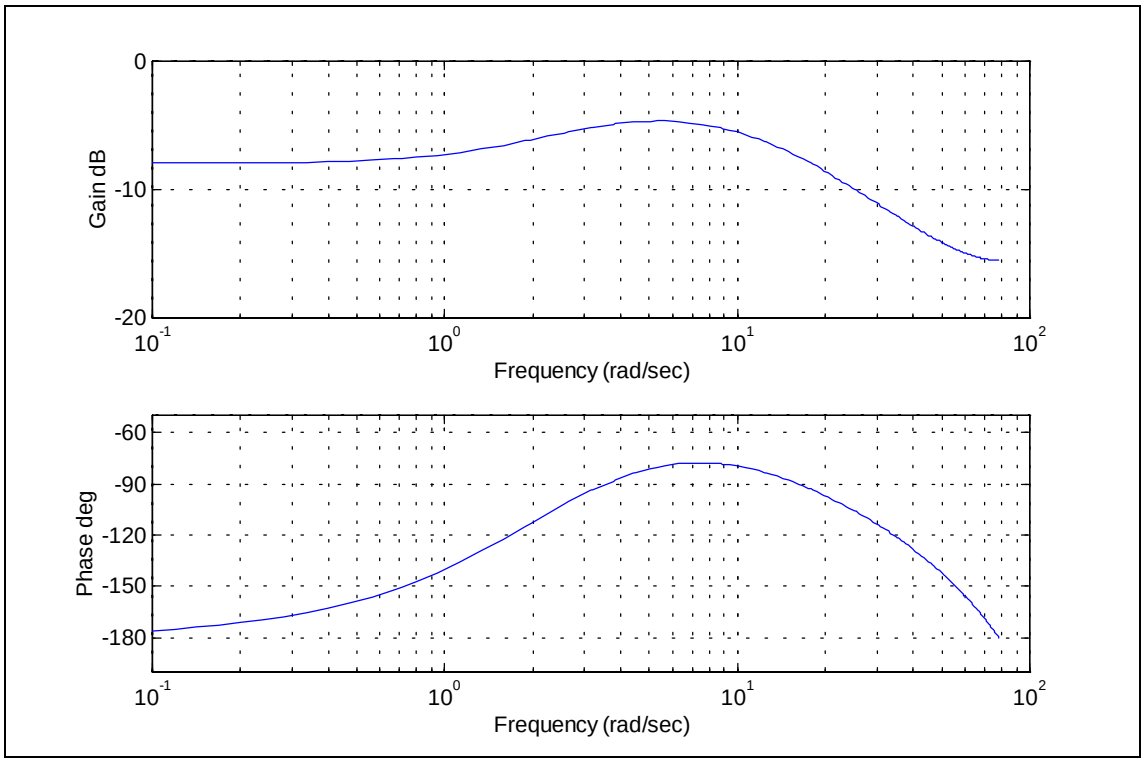

Figure 6.2.6 Bode plot for predicted smoothed position ($\hat{y}(k)$)

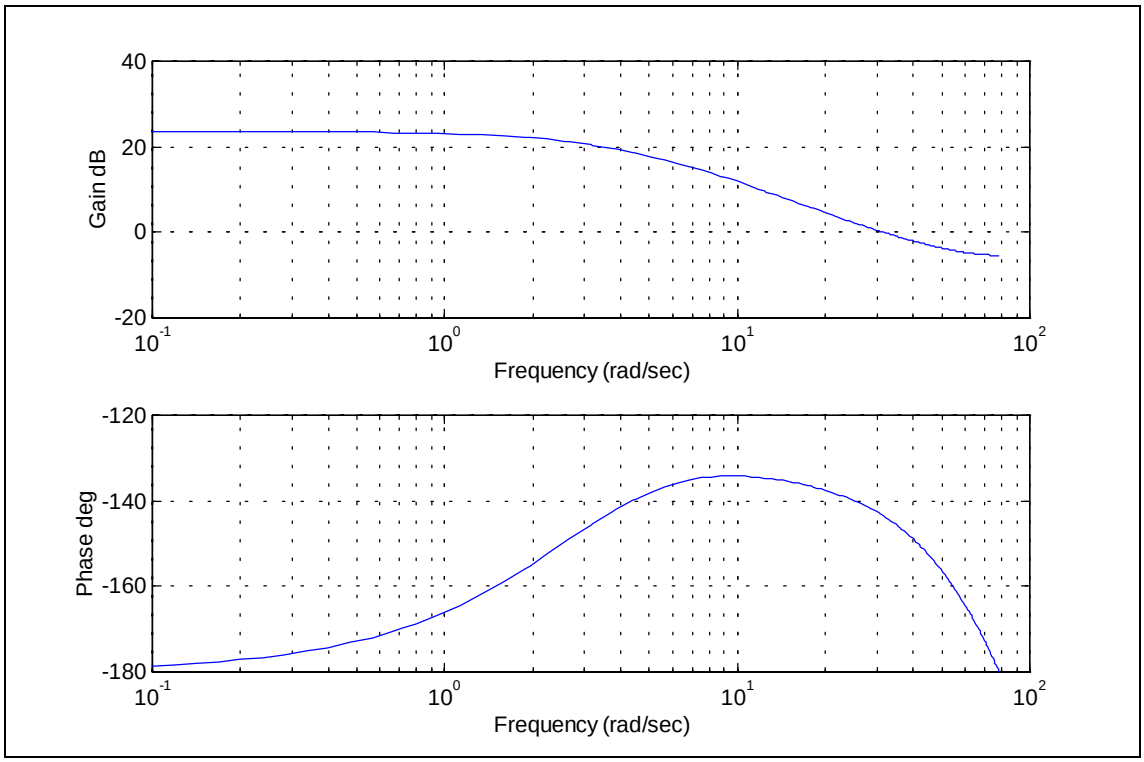

Figure 6.2.7 Bode plot for predicted smoothed velocity ($\dot{\hat{y}}(k)$)

6.3 REAL-TIME RESULTS

This section contains the real-time results of the implementation of the sliding mode controller on the real-time system. As can be seen the real-time results virtually mimic the simulated system , even though the real-time system has non-linearities and external disturbances such as noise and friction which the simulated model does not have.

6.3.1 CART RESPONSE

Figure 6.3.1 illustrated the real-time step response of the cart. The cart's step response has the same shape as the simulated step response. The real-time system crosses the setpoint at approximately 4 sec., which is 1 sec. slower then the simulated system. This is due to the friction and the dead-band region in the cart's motor which is not allowing the cart to accelerate as quickly as the simulated system.

The percentage of overshoot is identical to that simulated, but the most significant difference is the time taken to reach the exact setpoint. For the simulated system, the cart reached setpoint in 5 sec., but the real-time system reaches exact setpoint in approximately 7.8 sec., which is 2.8 sec. slower then the simulated system. The reason for this is once again friction and the dead-band. The motor at low voltage does not have enough torque to over come the frictional component. Thus, the motor must wait until the integrator has wound up enough to produce a voltage which will substantially over come the friction component. Even though there is dead band compensation, it is only useful if the applied voltage to the motor is maintained for a long enough period to allow the cart to move.

In the case of the real-time system there is also the noise component, and looking at the controller structure it can be seen that the dominating factor is the gain which is related to the swing angle. Since the angle measurement is noisy it will produce (only for short instances in time) an undesired control voltage to the cart motor. This causes the cart to move in a jerky action instead of a smooth action.
Once the cart does move and approximately reaches setpoint, the controller exhibits the phenomenon known as hunting. This can be best seen from Figure 6.3.3 and will be discussed in Section 6.3.3.

Even with all these external disturbances it can be seen from Figure 6.3.1 that the cart's response approximately meets the design requirement. That is, to have a settling time of 5 sec. with a damping ratio between 1 and 0.7. Figure 6.3.1 clearly illustrates that these design requirements are closely adhered to, with the exception of an increase in the settling time by 1 sec.

6.3.2 SWING ANGLE

The swing angle measurement poses the greatest influence on the controller's action. In both the equivalent control dynamics and the switching surface the gain associated with the swing angle has the largest effect on the controller's action. Thus any noise induced on the swing angle measurement will effect the controller's performance. The alpha-beta filter is a very simple filter and a more sophisticated filter should be used, but nevertheless it will test the robustness of the sliding mode controller.

Figure 6.3.2 illustrates the swing of the goods. As can be seen there is a substantial noise component of the measurement signal even after filtering has taken place. The response of the swing angle is very similar to the simulated results. It has a peak of -0.1 rad at 0.5 sec. which compares favourable to Figure 6.1.2 which has a peak of 0.08 rad at 0.5 sec. . Both then rise to 0.6 rad at 2 sec. If noise is neglected the envelope waveform of Figure 6.3.2 is as in Figure 6.1.2.

Since the directly measurable states are influenced by noise, and the fact that the real-time implementation is similar to the simulation, then there is good reason to conclude that the controller is robust in the presence of noise.

6.3.3 CONTROL EFFORT

The study of the control effort is very import to view the controller's overall performance. Figure 6.3.4 illustrates the control effort of the real-time system. The most significant detail that is revealed by the control effort is that the controller is exhibiting hunting.

Hunting occurs when the system is attempting to reach setpoint, but for some reason, (in this case friction and noise on the directly measurable states) the system overshoots and then undershoots setpoint. What causes hunting to occur is the integrator that is placed in the forward path to eliminate steady state error.

As the cart's position is not exactly equal to the setpoint, the integrator's value is constantly changing thus, applying a voltage to the motor. When the voltage is large enough to overcome friction, the cart moves, but the controller does not apply the exact voltage required to stop the cart from moving slightly beyond the setpoint. Thus, the hunting cycle is started again. This can be seen in Figure 6.3.1.

In Figure 6.3.3 the voltage being applied to the motor can be easily seen. Notice that there are large changes in the applied voltage after 5 sec. This is when the controller is hunting for the exact setpoint. Nevertheless, if dead-band compensation is taken away from Figure 6.3.3, (i.e. 1 V added in the positive direction and -4.5 V added in the negative direction) it would closely resemble Figure 6.1.3. Both figures show an initial voltage of 4.3 V, then there is a decrease in the applied voltage. At approximately 0.5 sec. the voltage rises to a value of just over 4 V, then tapers off to 0 V. Hunting starts to occur after 5 sec. in the real-time implementation, where as in simulation, since the system is not influenced by noise it is brought under control within 5 sec. and hunting does not occur.

Thus, the basic envelope of the control effort in Figure 6.3.3 is very similar to the simulated system. The control effort in the real-time system is not as smooth as the simulation because there is noise on the directly measurable states which are then used to produce the control effort.

6.3.4 SWITCHING SURFACE

As has been established in the previous sections, noise is very apparent in the real-time system and the function which can greatly emphasise the effects of noise is the switching surface. In designing the controller, noise was not accounted for. The simulation of the switching surface in Figure 6.1.4 assumed cleanliness of all signals. This simulation and the noise simulation Figure 6.1.11 assumed initial conditions of 0.

The switching surface for the simulate (both with and without noise) and the real-time system are different in terms magnitude and waveform. This is due to two major reasons,

1) The initial conditions.
2) The magnitude and frequency of the noise component.

Examining the switching surface for both the simulated system where noise was introduced and the real-time system demonstrates that if any of the states are influenced by noise, then magnitude and waveform of the switching surface is greatly affected. This is clearly illustrated by Figure 6.4.4.

It is clear by observing Figure 6.4.4 that the system never really converges to the sliding surface, but does continually cross the switching surface. This factor was also observed in the noise simulation. The reason that the real-time system is continually crossing the switching surface is the same as for the simulation, in that the controller pulls the systems towards the sliding surface and noise keeps pushing it off the sliding surface. Thus, it is concluded that the behaviour of the controller in real-time is similar to the simulation.

Cart position step response setpoint 1 m

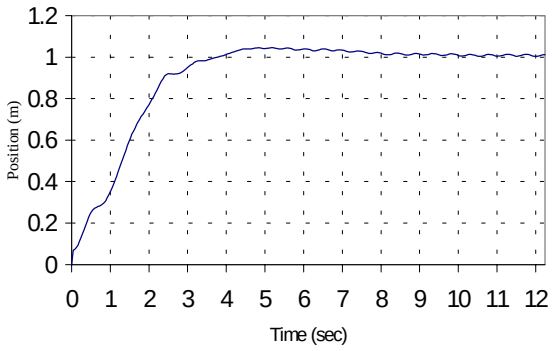

Figure 6.3.1

Swing angle step response

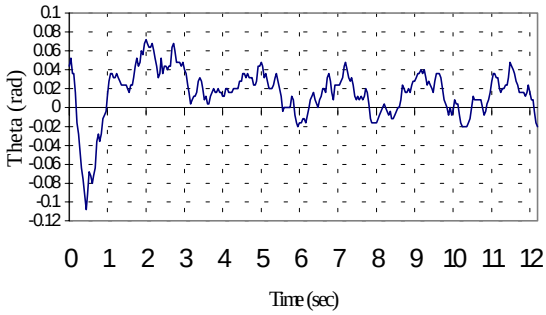

Figure 6.3.2

Control effort of cart and swing controller

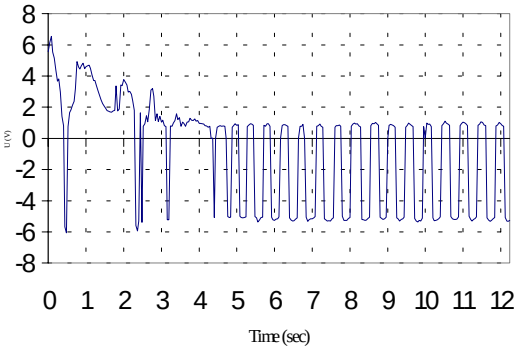

Figure 6.3.3

Switching Surface

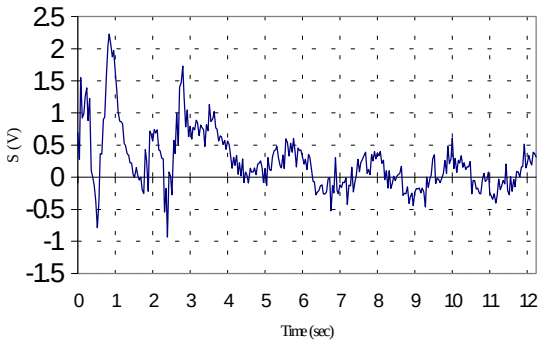

Figure 6.4.4

6.4 HUNTING COMPENSATION

The effects of hunting compensation when added into the controller structure are discussed in this section. Sophisticated control to eliminate hunting as described in Toshiaki [39] was not used. Instead a simple conditional statement that applies 0 V to the drive motor if all the hunting compensation conditions are satisfied. The conditions are as follows:

1. Cart position = ±2% of setpoint
2. Cart velocity = ±0.05 m s^{-1}
3. Swing angle = ±0.02 rad
4. Swing velocity = ±0.05 rad s^{-1}

If all these conditions were met then the controller is turned off to eliminate integral wind up, and 0 V is applied to the motor.

6.4.1 CART RESPONSE

Figure 6.4.1 illustrates the step response of the cart. As can be seen the cart reaches setpoint at 3.9 sec., which is similar to the time taken by the controller without hunting compensation. The most noticeable difference is that there is no overshoot. This is because as all the above conditions are met and 0 V is applied to the motor, friction takes over and stops the cart at a position which is very close to the setpoint.

6.4.2 SWING ANGLE

Figure 6.4.2 illustrates that the swing angle has also been bought under control. The most interesting aspect is still the level of noise on the swing angle signal. To allow the controller to behave more smoothly and lessen the effects of noise, a dead band region on the swing angle was introduced. This region lies between ±0.02 rad or ±1.2 degrees. The introduction of this dead band region has not hindered to performance of the controller, as Figures 6.3.2 and 6.4.2 have the same characteristics and the design criteria is met.

6.4.3 CONTROL EFFORT

The reasons to include hunting compensation in the controller are:

1) To eliminate wear and tear on the system due to a fluctuating control effort.
2) Practically, the goods must be bought to a stationary position when they are placed on to a truck or ship.

Figure 6.4.3 illustrated how the control effort is turned off with the aid of hunting compensation. Once again Figure 6.4.3 illustrates that hunting compensation does not effect the controller's performance, as this figure is similar to Figure 6.3.3.

6.4.4 SWITCHING SURFACE

The most dramatic effect that such a simple solution to the hunting problem has can be seen by examining the switching surface. As can be seen from Figure 6.4.4, the basic envelope waveform of the switching surface is similar to the simulated system (Figure 6.1.4), but once again the numerical values of the switching surface are not. The most interesting aspect is that unlike Figure 6.3.4, where the switching surface hovers about the 0 V, in this instance the switching surface does not reach 0 V. This is due to the tolerance limits (dead band) introduced for each state to compensate for hunting. Examining the switching surface function

$$s = -12.62x_1 - 7.01x_2 + 10.97x_3 - 4.299x_4 + 9.038x_5$$

indicates that all the states must cancel each other in order for the switching surface function to be zero. When the system states are within the specified tolerance limits, the controller is turned off and the swing angle, swing angular velocity and cart's velocity are all set to zero. When this occurs, the switching surface equation becomes:

$$s = -12.62x_1 + 9.038x_5$$

If the system states all fall within the tolerance limits then there is no guarantee that the value of the integrator x_5 will offset the value of the cart's position x_1. Thus it is always possible for the switching surface not to be equal to zero.

Cart position step response setpoint 1 m

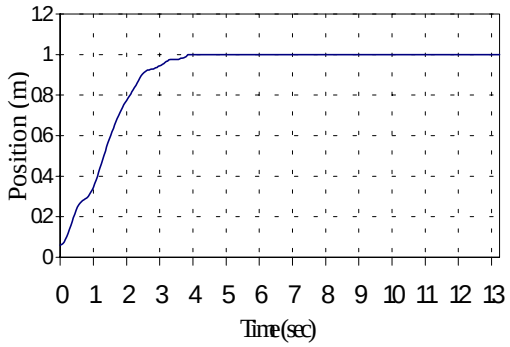

Figure 6.4.1

Swing angle step response

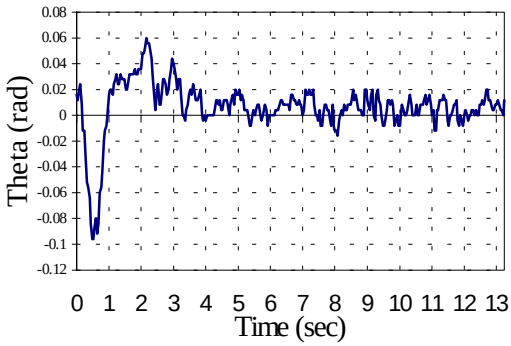

Figure 6.4.2

Control effort of cart and swing controller

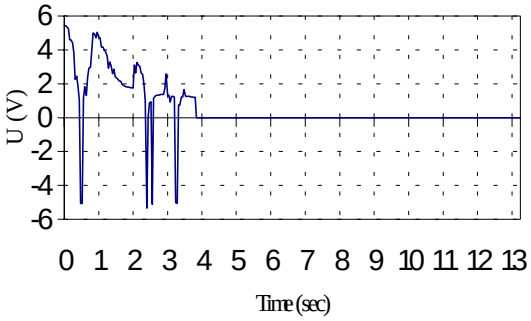

Figure 6.4.3

Switching surface

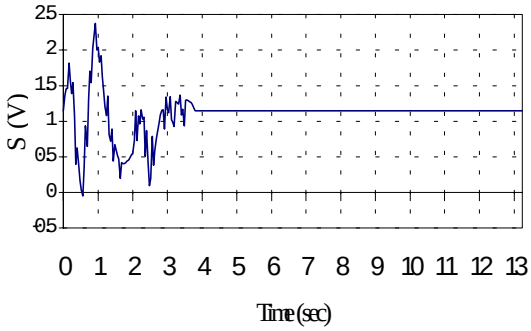

Figure 6.4.4

6.5 CONCLUSION

In this chapter a discussion of the simulation and implementation of the sliding mode controller for cart positioning and swing cancellation was given. From the simulation results Figures 6.1.1 – 6.1.11 it can be seen that the controller moves the cart to the desired location and stops the goods from swinging. The criterion of having the system exhibit a damping ratio of between 1 and 0.7 has been met, and a settling time of 5 sec. is satisfactory.

In implementing the controller on the real-time system, it is noted that the real-time system has a dead band region that is non-linear, and the model itself is not totally linear as was assumed in the modelling. This is clearly evident when observing Figure 6.3.3 and 6.4.3. It can be seen by these control signals that the sliding mode controller is robust against parameter uncertainties. Note that in these two figures at approximately the 2 second mark (i.e. time = 2 sec.), the cart's velocity is too great and the controller is signalling the cart to slow down by applying a reverse voltage. Thus there exists a slight parameter variation that has not been taken into the modelling, but the controller is still performing well.

The swing angle on the real-time system is influenced by noise. This coupled with the fact that both the cart's and swing velocity had to estimated, results in a jagged control signal. The controller produces a noisy control signal because it is attempting to control the system with these disturbances affecting the system.

In the real-time implementation of the sliding mode controller no on line tuning was performed, that is the results that were given by Matlab were directly implemented on the real-time system. As can be seen, the real-time results and the simulated results are very similar, thus it is concluded that:

1) The controller is quite robust to uncertainties and disturbance.
2) The model developed is an adequately accurate model for this particular system.

CHAPTER 7 ROPE LENGTH CONTROLLER DESIGN, SIMULATION AND IMPLEMENTATION

Throughout this thesis, different control techniques are used to control different aspects of the gantry crane system. In previous chapters a sliding mode controller was used to control the cart and swing dynamics, and in subsequent chapters a LQR is implemented as an output feedback model following controller. The controller for the rope length will be designed using pole placement by the state variable feedback technique.

In Chapter 5 the closed loop poles were determined by a set formula which encompassed the settling time and the damping ratio, but this method can only be used for second order systems. Since the hoisting system is increased to a third order system with the addition of integral action, using the method in Chapter 5 may not give the desired control response as the location of each pole has an effect on the system's closed loop performance. In this chapter an alternative method for the selection of the closed loop poles is described. By observing the system's performance under closed loop conditions, a method of experimentation is used to determine the feedback gains for the rope length controller.

7.1 ROPE LENGTH CONTROL

In order to achieve rope length control (i.e. place the goods at a pre-specified height) with no steady state error, integral action must be incorporated into the system in a similar manner as in Chapter 5.

Now with the introduction of the integrator, the system is

$$\begin{aligned} \dot{x} &= Ax + Bu \\ y &= Cx + Du \\ \dot{\xi} &= r - y = r - Cx \end{aligned} \qquad 7.1.1$$

where r = the reference input signal (step function, scalar quantity)

ξ = output of the integrator (state variable of system, scalar).

And so

$$\dot{\hat{x}} = \hat{A}\hat{x} + \hat{B}u + Dr$$

where

$$\dot{\hat{x}} = \begin{bmatrix} \dot{x} \\ \dot{\xi} \end{bmatrix} \quad \hat{x} = \begin{bmatrix} x \\ \xi \end{bmatrix} \quad \hat{A} = \begin{bmatrix} A & 0 \\ -C & 0 \end{bmatrix} \quad \hat{B} = \begin{bmatrix} B \\ 0 \end{bmatrix} \quad D = \begin{bmatrix} 0 \\ 1 \end{bmatrix}$$

Expanded to incorporate the system matrix and the integrator gives the state space system

$$\begin{bmatrix} \dot{x}_5 \\ \dot{x}_6 \\ \dot{\xi} \end{bmatrix} = \begin{bmatrix} 0 & 1 & 0 \\ 0 & -2.229 & 0 \\ -1 & 0 & 0 \end{bmatrix} \begin{bmatrix} x_5 \\ x_6 \\ \xi \end{bmatrix} + \begin{bmatrix} 0 \\ 0.11 \\ 0 \end{bmatrix} u + \begin{bmatrix} 0 \\ 0 \\ 1 \end{bmatrix} r \qquad 7.1.2$$

7.2 SELECTION OF THE CLOSED LOOP POLES

The desired closed loop pole locations are acquired by pole placement to determine the gain matrix K. Noting that the control effort has to be taken into account, pole locations should be selected to give a satisfactory system performance with small control effort.

Several different closed loop poles will be examined, and after computer simulation the gain matrix K will be chosen which provides the “best overall” system performance. The system equations used in the simulation are those that are described by (7.1.2), which includes the integral action for the rope length positioning.

7.3 SIMULATION OF THE ROPE LENGTH CONTROLLER

The simulation of the controller will be achieved by using the Matlab package. The use of the PLACE command in the Matlab package basically solves the characteristic equation for the desired closed loop poles.

In order to determine the “best overall” performance by experimentation of different pole locations three major factors were considered.

1. The applied voltage to the hoisting motor could not exceed ±13 V.
2. A settling time of approximately 5 sec. would be desirable as cart positioning is achieved in approximately 5 sec. (as it is desired to settle the cart and the rope length in the same time frame).
3. A damping ratio of 1 (i.e. a critically damped response) would also be desirable, as a commercial gantry crane driver would not want the height if the goods to overshoot as it may have some dangerous side effects. For example, if the crane is used to place goods on a truck, then the truck could be crushed by the overshoot.

For the purpose of this experimentation to illustrate the choice of the closed loop poles, three different pole locations are simulated and their closed loop characteristics discussed.

The figure below illustrates the block diagram of state variable feedback controller. Gain 1 is the feedback gain associated with the hoist position, gain 2 is the feedback gain associated with the hoist velocity and gain 3 is the feedback gain associated with the integral error signal between the setpoint of the rope length and the actual rope length.

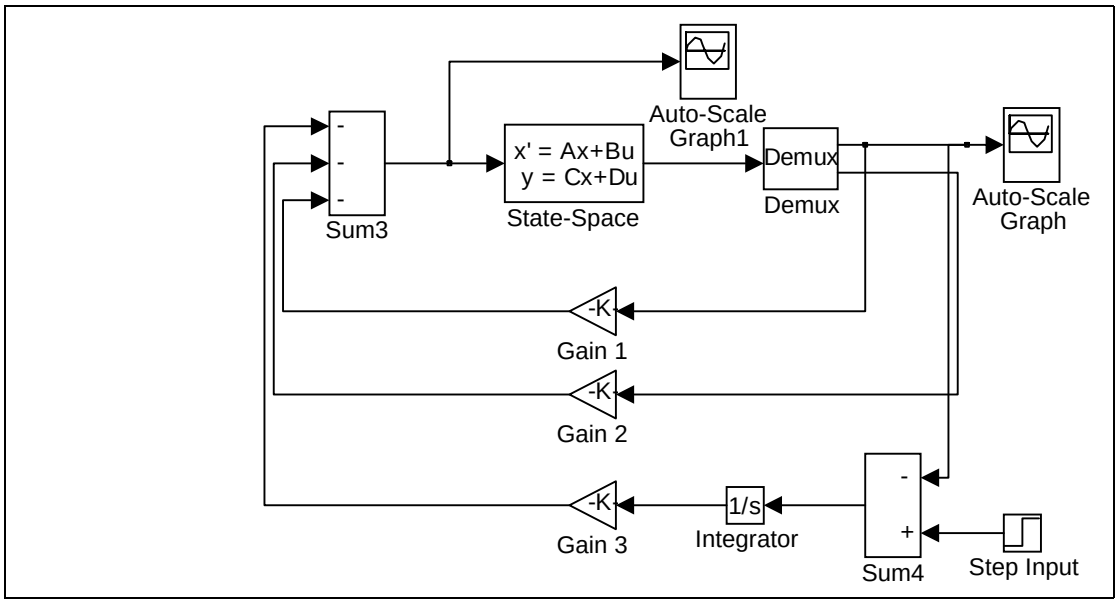

Figure 7.3.1 Block diagram of state variable feed back controller

7.3.1 CLOSED LOOP POLES SET #1

The first set of closed loop poles are placed at:

$P_1 = -1.5+0.5j$ $P_2 = -1.5-0.5j$ $P_3 = -5$

P_1 and P_2 are the dominant poles and are placed to counter balance the effects of the dominant poles of the hoisting system. P_3 is associated with the integrator and is placed far to the left, so as not to have a dramatic influence on the system. Note that this pole affects the speed of the controller, and if it is placed too far to the left, then the control effort will exceed the motor's maximum allowable applied voltage.

Using these poles, the feedback gains are

$K_1 = 159.0909$ Position gain (gain 1)

$K_2 = 52.4636$ Velocity gain (gain 2)

$K_3 = -113.6364$ Integral gain (gain 3)

Figure 7.3.2 illustrates the system's step response with a setpoint of 0.5 m. Note that the response illustrates a damping ratio of 1 and it's settling time is approximately 5 sec. Thus, requirements 1) to 3) are met.

Figure 7.3.3 illustrates the control effort. The control effort peaks at approximately 8 V. It was noted that the system has a dead band of 2 V, thus in implementing the real-time controller, the actual applied voltage to the motor will be 10 V, which does not exceed the motor maximum allowable applied voltage. Thus these pole locations satisfy all of our specified requirements.

Another set of poles could be chosen, which will apply the maximum allowable voltage to the motor. This is not a good idea, because in a real-time implementation running motors at their maximum levels induces heat, and could cause the winding of the motor to burn out. Also in the real-time system is influenced by noise, thus effecting the control effort. If there is a significant level of noise, this could cause the control effort to exceed the maximum level, and thus, the controller would not perform as expected.

7.3.2 CLOSED LOOP POLES SET #2

The second set of closed loop poles are placed at:

P_1 = -2.5+0.5j P_2 = -2.5-0.5j P_3 =-5

This set of poles given above produces the system's performance as illustrated by Figure 7.3.4 and 7.3.5. Placing the above poles produces the feedback gains.

K_1 = 286.3636 Position gain (gain 1)

K_2 = 70.6455 Velocity gain (gain 2)

K_3 = -295.4545 Integral gain (gain 3)

These poles satisfy requirements 2) and 3) of the specified requirements, viz., the system does has a settling time of less then 4 sec., and the system produces a critically damped response. Note that moving the poles slightly further to the left decreases the system's settling time. These poles do not meet the first requirement. These poles produce a control effort greater then the allowable maximum motor applied voltage. This is illustrated by Figure 7.3.5.

7.3.3 CLOSED LOOP POLES SET #3

The third set of closed loop poles are placed at:

$P_1 = -2.5+2.5j$ $P_2 = -2.5-2.5j$ $P_3 = -5$

This set of poles given above produces the performance illustrated by Figure 7.3.6. and 7.3.7. Placing the above poles produces the feedback gains

$K_1 = 213.6364$ Position gain (gain 1)

$K_2 = 52.4636$ Velocity gain (gain 2)

$K_3 = -386.3636$ Integral gain (gain 3)

These poles do not meet two of the specified criteria. Figure 7.3.6 illustrates that the system will overshoot, which in a real life application can be potentially dangerous, but it does have a settling time of 4 sec. Also the control effort as illustrated by Figure 7.3.7 is greater then the maximum allowable applied motor voltage.

Analysing all three pole locations with respect to the system's performance, I choose to use the first set of poles in the real-time controller implementation.

Rope length step response for poles (-1.5±0.5j, -5)

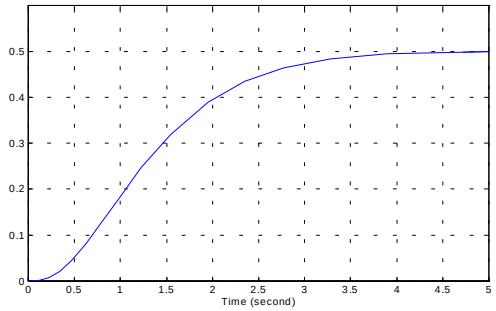

Figure 7.3.2

Control effort of rope length controller for poles (-1.5±0.5j, -5)

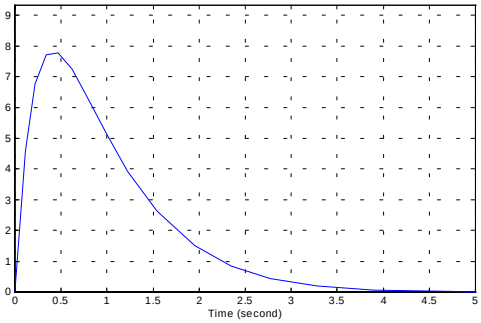

Figure 7.3.3

Rope length step response for poles (-2.5±0.5j, -5)

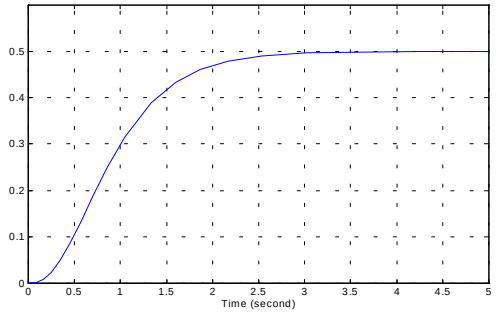

Figure 7.3.4

Control effort of rope length controller for poles (-2.5±0.5j, -5)

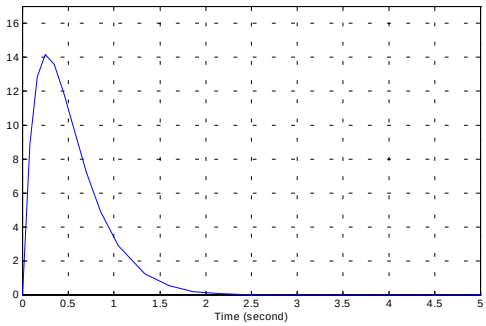

Figure 7.3.5

Rope length step response for poles (-2.5±2.5j, -5)

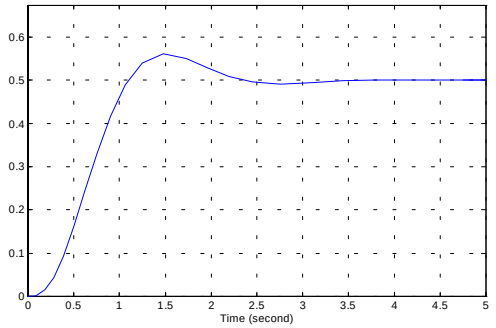

Figure 7.3.6

Control effort of rope length controller for poles (-2.5±2.5j, -5)

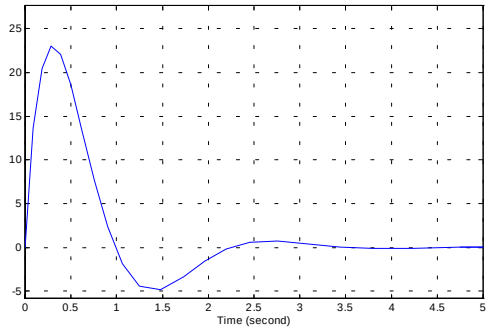

Figure 7.3.7

7.4 REAL-TIME IMPLEMENTATION OF THE ROPE LENGTH CONTROLLER

In implementing the controller, the rope length velocity must be estimated or observed as it is not directly available. The only signal that is directly available in the real-time system is the rope length. Thus, as described in Chapter 6, to estimate the rope length's velocity, an alpha-beta filter is used.

The feedback gains that will be used are those which are derived from placing the poles at $P_1 = -1.5+0.5j$ $P_2 = -1.5-0.5j$ $P_3 = -5$

Using these poles, the feedback gains are

$K_1 = 159.0909$	Position gain (gain 1)
$K_2 = 52.4636$	Velocity gain (gain 2)
$K_3 = -113.6364$	Integral gain (gain 3)

From Figure 7.4.1 and 7.4.2 it can be seen that the rope length controller performs similarly to the simulation (Figures 7.3.2 and 7.3.3) for the same feedback gains. The implemented rope length controller has a settling time of approximately 4.2 sec. which corresponds to the simulated system of approximately 4.8 sec., and both exhibit a critically damped response. Note that the real time system has a slightly faster settling time. This could be caused by some slight inaccuracy in the initial modelling of the system, but the system's performances is not sufficiently different to warrant any remodelling.

Figure 7.4.2 illustrates the control effort, note that the control effort has the same peak voltage as in Figure 7.3.3. Figure 7.3.3 has a peak voltage of 8 V from a time of 0.4 - 0.5 sec. where as in the real-time system there are two peaks, one at 0.2 sec. and another at 0.8 sec. The reason for the two peaks is that when the motor is initially applied with a voltage large enough to displace the goods, the goods temporarily display a bouncing motion, which causes noise on the position signal and thus on the velocity signal. As soon as the goods move freely the control signal is smoothly applied to the hoisting motor, as can be seen by Figure 7.4.2.

As the hoisting motor does not move with small voltages, dead band compensation had to be introduced, which was to simply add a voltage that would move the goods. The problem with doing this again is that the system would tend to hunt, so a similar solution as described in Chapter 6 was added to the hoisting system.

Overall the real-time system performance, practically mimics the simulated system's performance both for the rope length step response and the control effort. Thus, it can be concluded that the model derived for the hoisting system is quite adequate to design a controller.

Rope length step response setpoint 0.5 m

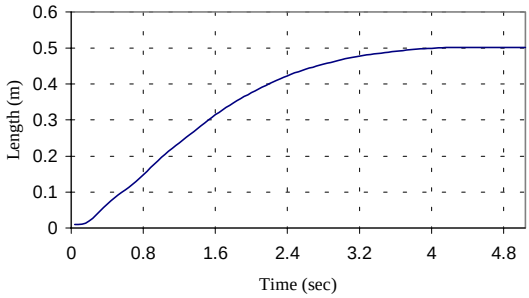

Figure 7.4.1

Control effort of rope length controller

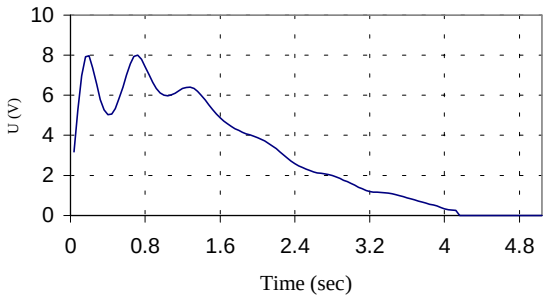

Figure 7.4.2

CHAPTER 8 SIMULATION AND IMPLEMENTATION OF A GAIN SCHEDULED SLIDING MODE CONTROLLER

In this chapter are discussed the effects of a gain scheduled sliding mode controller in order to determine the robustness of the sliding mode controller with a varying rope length. The sliding mode controller is used solely for cart positional control and swing cancellation as described in Chapter 6 and the rope length controller is a state variable feedback controller as described in Chapter 7. Thus all six states of the of the crane system are controlled simultaneously.

The rope length determines the gain scheduling effect of the sliding mode controller at each sample instant. As the rope length changes, the sliding mode controller at each sample time, will have a new switching surface and equivalent control dynamics, as both are functions of the rope length.

The equivalent control dynamics are described by (5.3.6) and the switching surface is described by (5.2.19). Neglecting any small numbers in these two equations gives the controller structure

$$U = u_{eq} + \alpha\, sat(S) \qquad 8.1$$

where

$$\alpha = 1$$

$$u_{eq} = 4.54\ell\,(r - x_1) + (-6.34\ell + 7.81)x_2 + (-14.730 - 5.54\ell^2 + 39.07\ell)x_3 + (11.84\ell - 6.34\ell^2)x_4 \qquad 8.2$$

$$S = \begin{bmatrix} -12.62\ell & (0.92\ell^2 - 7.9\ell) & (-12.62\ell^2 + 23.59\ell) & (0.92\ell^3 - 7.9\ell^2 + 2.7\ell) & 9.04\ell \end{bmatrix} \hat{x} \qquad 8.3$$

$$\hat{x} = \begin{bmatrix} x_1 \\ x_2 \\ x_3 \\ x_4 \\ \xi \end{bmatrix} \qquad \xi = \int r - x_1 \qquad 8.4$$

In order to determine the robustness of the sliding mode controller a comparison between two implementations of the sliding mode controller is given in this chapter. Firstly a gain scheduled sliding mode controller is implemented, in which the controller will be recalculated with respect to the rope length for each sample. Then the effects of designing and implementing a sliding mode controller for a fixed rope length (i.e. non gain scheduled), while the rope length is being varied and controlled is discussed.

The purpose of this comparison is to determine if designing and implementing a fixed rope length controller while varying the rope length behaves effectively the same as a gain scheduled controller, thus determining the robustness of the sliding mode controller. If this experiment is found to be true, then it is easy in the industry to implement a fixed rope length controller without loss of performance.

8.1 SIMULATION OF A GAIN SCHEDULED SLIDING MODE CONTROLLER WITH A VARYING ROPE LENGTH

In this section the simulation of a gain scheduled sliding mode controller (where the gain scheduling effect is due to the change in rope length) is discussed. Theoretically, the gain scheduled sliding mode controller should have a better performance than the controller that is designed for a fixed rope length as the rope length is being varied. This is due to the fact that the sliding mode controller is adapting to the change in rope length.

The diagram below illustrates the block diagram of the gain scheduled sliding mode controller.

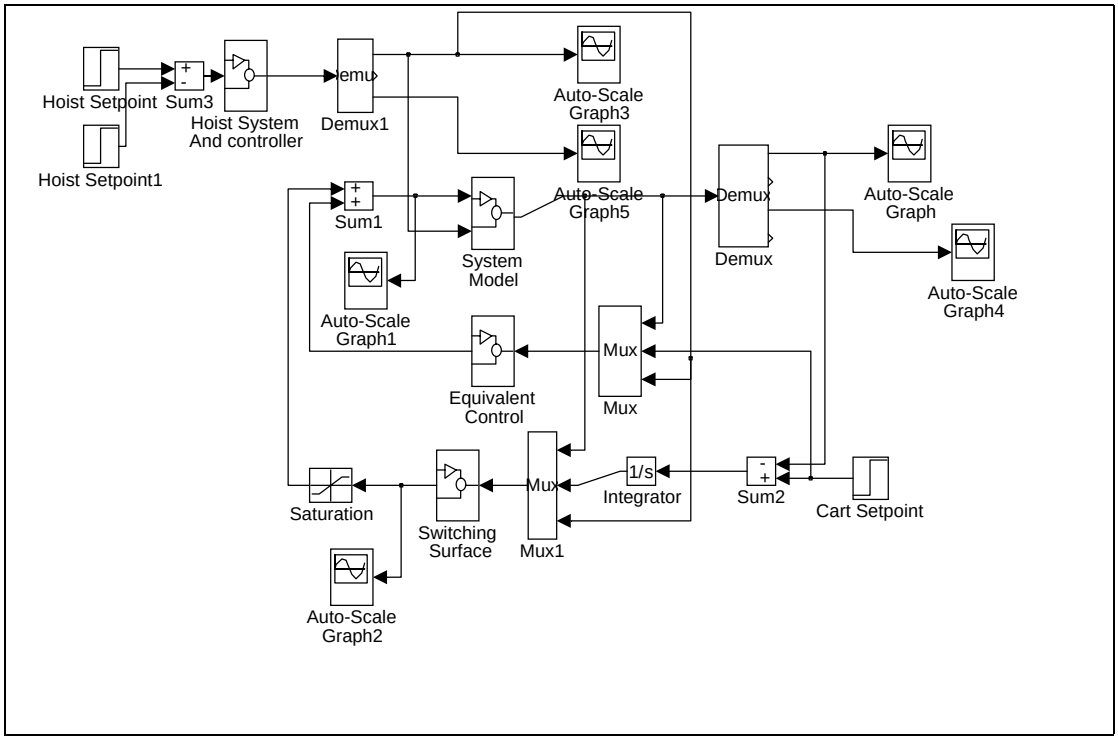

Figure 8.1.1 Gain scheduled sliding mode controller

8.1.1 CART RESPONSE

Figures 8.1.2 - 8.1.7 illustrate the performance of the gain scheduled sliding mode controller as the rope length is positioned from a starting point of 0.8 m, to a final value of 0.4 m. In the initial 5 sec., the rope length is placed to steady state value of 0.8 m (or equivalently an initial condition for the rope length at 5 sec.) and the cart and swing dynamics are not activated. This was done because Matlab produced errors when initial conditions were introduced. The period after 5 sec. is discussed, as the cart and the swing dynamics are activated at this point in time. Thus, all three dynamics are being controlled after the initial 5 sec. period.

As can be seen from Figure 8.1.2 the cart's step response as the rope length is being varied is similar to the step response of Figure 6.1.1, where the cart settles in approximately 5 sec. This is to be expected since at each sample instant the sliding mode controller is adjusting to the rope length.

8.1.2 SWING ANGLE

The Figure 8.1.3 below illustrates the swing angle as the cart is being moved to a setpoint of 1 m and the rope length is being positioned to 0.4 m. It can be seen that the swing angle has the same basic waveform and magnitude as Figure 6.1.2. The swing angle still settles in the same time as Figure 6.1.2. Thus using a gain scheduled sliding mode controller has not greatly affected the performance of the control for the swing angle.

8.1.3 CONTROL EFFORT

Figure 8.1.4 illustrates that the sliding mode controller designed in Chapter 5 has a smooth control effort. Figure 8.1.4 has a similar response to that as in Figure 6.1.3. The control effort illustrated by Figure 8.1.4 shows that in changing the system dynamics the sliding mode controller still behaves as the fixed system dynamics (i.e. controller based on a constant rope length of 1 m). Thus as the rope length is being varied, the sliding mode control is not affected.

8.1.4 SWITCHING SURFACE

The most noticeable effect of the varying rope length can be seen in the switching surface. As can be seen by Figure 8.1.5 and 6.1.4, the two switching surfaces are vastly different. This can be attributed to the change in the system dynamics as the rope length changes. It must be remembered that in simulation the system starts with all initial conditions set to zero, which means that the system is already on the sliding surface.

It is noted that Figure 8.1.5 is the inverse of Figure 6.1.4. All that this means is that the controller is on the other side of the switching surface. Even though the switching surface's magnitude is not large enough to have a dramatic effect on the overall performance of the controller in simulation, it does give an indication as to which side of the switching surface the system lies.

8.1.5 ROPE LENGTH POSITION STEP RESPONSE

The Figures 8.1.6 and 8.1.7 illustrate the rope length controller's performance. It has been stated that the hoist dynamics are not influenced directly by the cart and swing dynamics. Thus even with a gain scheduled implementation of the sliding mode controller the rope length controller should have the same characteristics. This is clearly illustrated by Figures 8.1.6 and 8.1.7, as they are the same as Figures 7.3.2 and 7.3.3.

Cart position step response setpoint 1 m

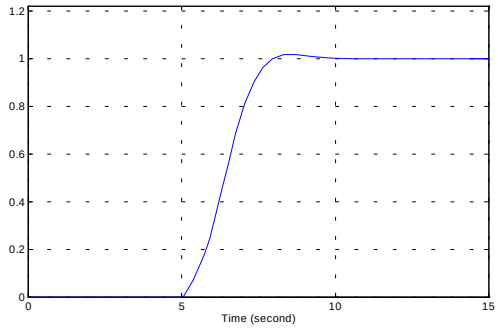

Figure 8.1.2

Swing angle step response

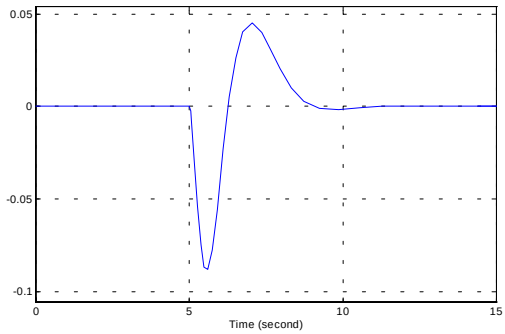

Figure 8.1.3

Control effort of cart and swing controller

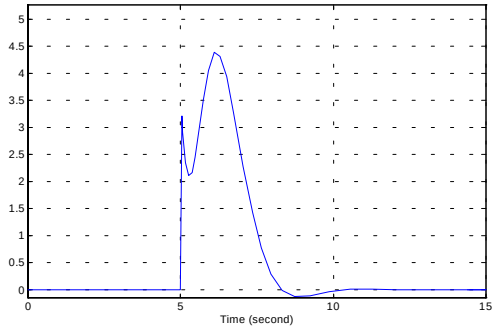

Figure 8.1.4

Switching surface

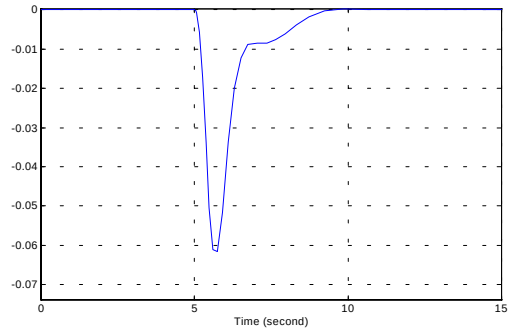

Figure 8.1.5

Rope length step response

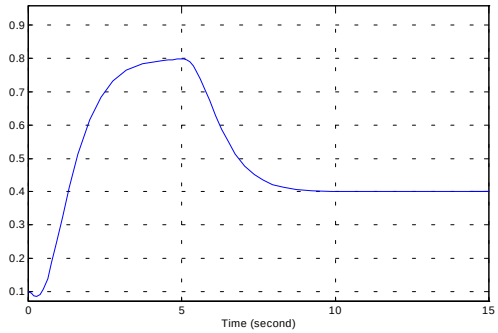

Figure 8.1.6

Control effort of rope length controller

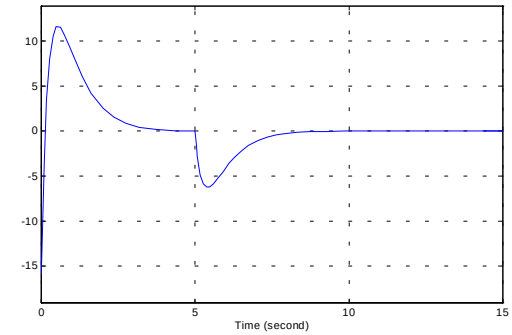

Figure 8.1.7

8.1.6 GAIN SCHEDULED SLIDING MODE CONTROLLER WHILE THE GOODS ARE BEING LOWERED

In this section any differences in the controller's performance as the goods are being lowered is discussed. As can be seen from Figure 8.1.8 - 8.1.13 the gain scheduled sliding mode controller does not exhibit any differences in performance from the raising or lowering of the goods. The only factor that is slightly affected due to the change in direction of motion of the goods is the switching surface.

Figure 8.1.11 illustrates the switching surface as the goods are being lowered. As was discussed previously, the switching surface is a function of all the system state and the rope length. Thus, it is evident that its shape will change with a change in direction of motion of the goods. This is shown by Figure 8.1.11 and Figure 8.1.5.

It is concluded that the gain scheduled sliding mode controller has the same behaviour independent of the direction of motion of the goods. Thus, the gain scheduled sliding mode controller is robust in the presence of a changing rope length since the directions of motion of the goods does not effect the controller's performance.

Cart position step response setpoint 1m

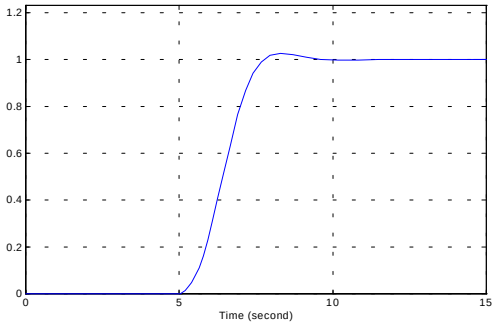

Figure 8.1.8

Swing angle step response

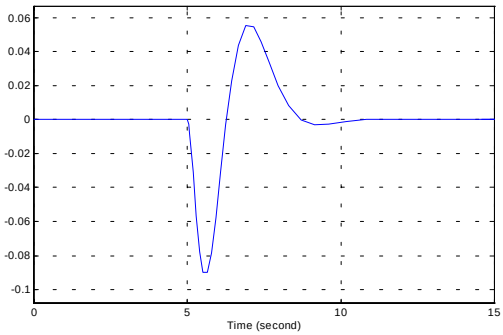

Figure 8.1.9

Control effort of cart and swing controller

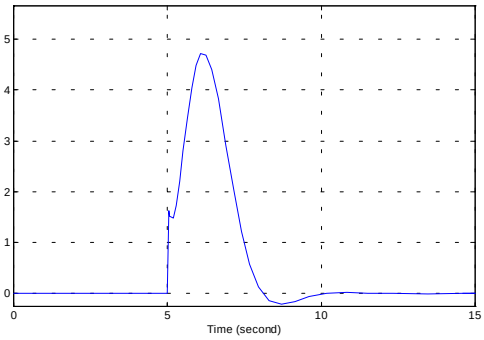

Figure 8.1.10

Switching surface

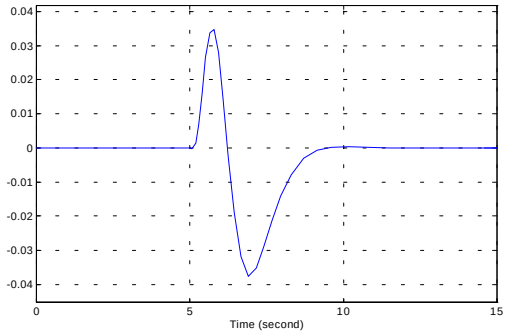

Figure 8.1.11

Rope length step response

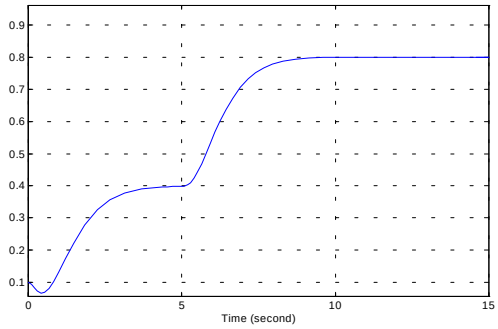

Figure 8.1.12

Control effort of rope length controller

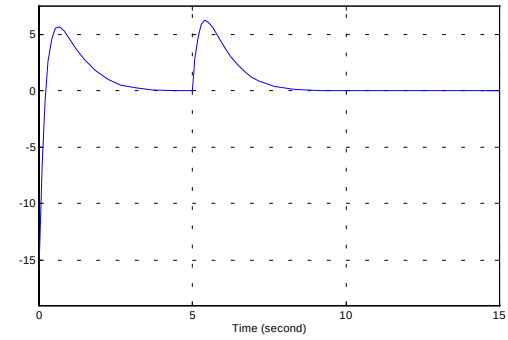

Figure 8.1.13

8.2 REAL-TIME IMPLEMENTATION OF A GAIN SCHEDULED SLIDING MODE CONTROLLER WITH A VARYING ROPE LENGTH

In this section the gain scheduled sliding mode controller's performance when implemented in real-time, is discussed. As can be seen from Chapter 6 and Chapter 7 the simulation and implementation of the previous controllers were almost identical between simulation and real-time implementation. Thus, the real-time implementation of the gain scheduled sliding mode controller should exhibit the same characteristics as the simulated system in Section 8.1.

It was observed in Section 8.1 that using a gain scheduled sliding mode controller produces the same performance as in Chapter 6. This is expected in the real-time system, as the sliding mode controller is adapting to the changes in the rope length.

The real-time implementation of the gain scheduled sliding mode controller will give a better understanding of the robustness of the sliding mode controller. If the real-time implementation behaves as in the simulation then it can be concluded that using a gain scheduled sliding mode controller produces the desired performance.

Note, from previous chapters, the sliding mode controller was robust in the presence of noise, then changing the controller's characteristics online should improve its robustness with respect to changing system dynamics.

8.2.1 CART RESPONSE

The cart's step response that is illustrated by Figure 8.2.1, shows that the gain scheduled sliding mode controller behaves quite reasonably as the rope length is being varied. The cart's step response does appear to be a smooth response

The Figure 8.2.1 also illustrates that the cart's settling time is approximately the same as in Chapter 6. The most noticeable difference is the slight overshoot that has occurred. In the previous chapters overshoot did not occur because of the dead band limit introduced for hunting compensation. Figure 8.2.1 shows overshoot. This is because when the cart is near setpoint, the swing angle is not within the tolerance limit for hunting compensation to turn the controller. This means that the controller is still active and compensating for the swing angle thus causing the overshoot. Once the cart has overshot, the carts control effort as can be seen by Figure 8.2.3 is imitatively being heavily decelerated to bring the cart and the swing angle back to setpoint.

As can be seen by Figure 8.2.7 the overshoot does not always occur, it only tends to occur if the swing angle is not within the tolerance limits set for hunting compensation, which causes the cart to keep moving in a forward motion to catch the swing angle rather then decelerate.

Overall the real-time response of the cart is similar to the simulated system, and has a decreased settling time which was observed with the simulated system. Thus it is concluded that using a gain scheduled sliding mode controller improves the performance of the sliding mode controller. But the performance is not sufficiently improved to warrant implementation of a gain scheduled controller.

It has been observed, that if one cannot design a sliding mode controller using gain scheduling techniques, (i.e. controller is based on a varying system variable) then designing for a fixed or known value of the system variable will suffice and one can still expect reasonable performance from the controller.

8.2.2 SWING ANGLE

Figure 8.2.2 below illustrates the swing angle as the cart is being displaced by 1 m and the rope length is being raised to 0.4 m. It can be seen that the swing angle has the same basic waveform as Figure 8.1.3, but the magnitude of the swing angle is increased, but only slightly. Overall the swing angle performance is similar to that as for Figure 8.1.3. The swing angle still settles in the same time as for a fixed rope length controller. Thus, the varying of the rope length has not greatly affected the performance of the control for the swing angle.

It can be seen from Figure 8.2.2 that the reason for the cart's overshoot is that the swing angle has changed its direction of motion. At the 2.5 second mark (i.e. time = 2.5 sec.) as the cart has reached set point, the controller is still applying a small voltage to the motor. This, plus the inertia affect of the cart is causing the cart to overshoot the swing angle. Thus, the swing angle moved in the opposite direction to which it was and the cart attempts to catch the swing and bring it back under control, thus the overshoot for the cart.

8.2.3 CONTROL EFFORT

The real-time control effort is a lot smoother with a gain scheduled sliding mode controller, because the controller is adapting to the changing system dynamics.

The most interesting characteristic is for the controller to bring the cart quickly back to the set point, which can be seen in Figure 8.2.3. Since the cart has overshoot, between 3.2 and 3.4 sec., the controller produces voltages in the opposite direction in an attempt to bring the cart back under control.

Note that using a gain scheduled approach produces a smother control effort, especially as the cart approaches setpoint. In the other section, it can be seen that the control effort of the cart as it approaches setpoint tends to have a number of kicks in the opposite direction to slow the cart's performance down and thus cause a critically damped response. From Figure 8.2.3 it can be seen that the control effort is decreasing slowly and smoothly as the cart approaches setpoint, and thus not producing severe kicks in the

opposite direction to slow the cart down. Between 3 and 3.6 sec. there is a constant voltage in the opposite direction. This occurs because the cart must be bought back to setpoint since it has overshot the mark.

8.2.4 SWITCHING SURFACE

Figure 8.2.4 below illustrates the switching surface of the real-time system. It can be seen from Figure 8.2.4 that the real-time controller's switching surface is quite different to that of the simulated controller (i.e. Figure 8.1.5). This is once again due to noise, but the interesting fact is that the switching surfaces envelope waveform has remained the same as in Chapter 6. Figure 8.2.4 also illustrates a much smoother switching surface as the controller is adapting to the changing system dynamics

8.2.5 ROPE LENGTH POSITION STEP RESPONSE

The Figures 8.2.5 and 8.2.6 illustrate the rope length controller performance. As discussed earlier the rope length controller is not influenced directly by the cart and swing dynamics.

This is clearly illustrated by Figures 8.2.5 and 8.2.6, as they are the same as Figures 7.4.1 and 7.4.2. As the cart moves the settling time is slightly quicker, about 0.3 sec. faster. This could be due to the fact that at certain points in time, as the goods are swinging there is a counter effect due to gravity and the goods raised slightly faster. Figure 8.2.6 Clearly illustrates, the effect of the hunting compensation. Note that as the rope length position is within the tolerance limits, then the controller is switched off in order to negate the effects of hunting, and integral windup.

Cart position step response setpoint 1 m

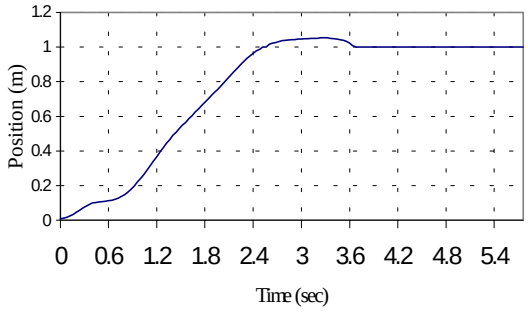

Figure 8.2.1.

Swing angle step response

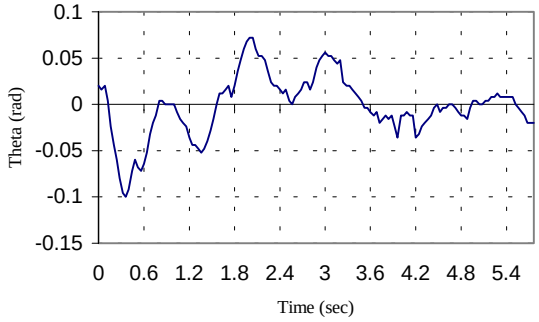

Figure 8.2.2

Control effort of cart and swing controller

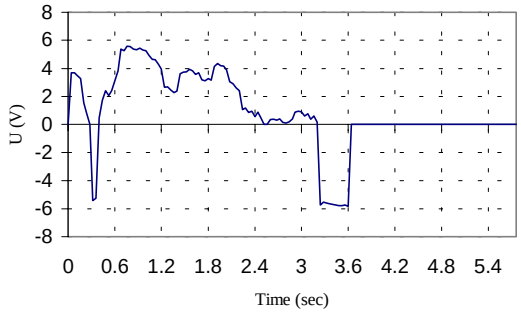

Figure 8.2.3

Switching surface

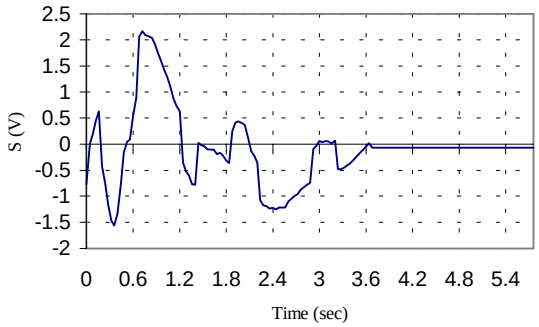

Figure 8.2.4

Rope length step response

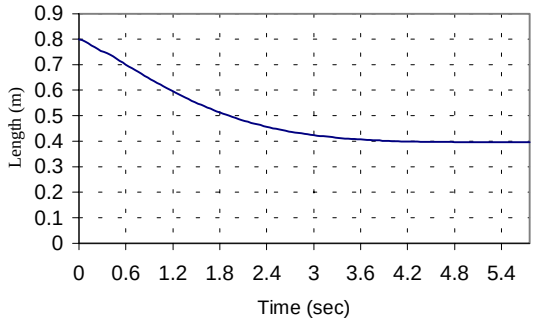

Figure 8.2.5

Control effort of rope length controller

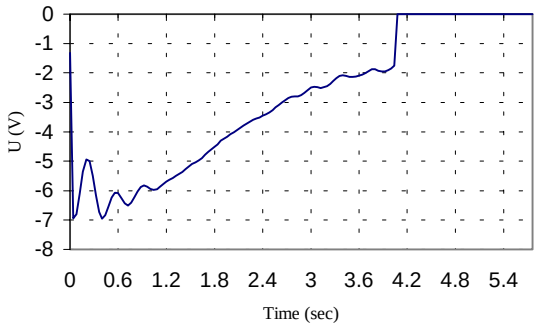

Figure 8.2.6

8.2.6 GAIN SCHEDULED SLIDING MODE CONTROL WHILE THE GOODS ARE BEING LOWERED

In this section any differences in the controller's performance as the goods are being lowered is discussed. Figure 8.2.7 - 8.2.12 illustrate the controller's performance as the goods are being lowered.

As can be seen from Figure 8.2.7 - 8.2.12 the gain scheduled sliding mode controller exhibits no significant difference in performance between raising or lowering of the goods. All nuances with the system still remain the same no matter in which direction the goods are moving (i.e. varying the rope length). It can be seen from Figure 8.2.5 that the cart does not overshoot. This is because the swing angle is not as great and the control effort really is achieving only positional control with swing cancellation. Although, as the cart reaches set point the controller signals the cart to slow down, thus causing the swing angle to move in the opposite direction of motion and causing the cart to slightly move also in the opposite direction. As both the cart's position and the swing angle now do not fall into the dead band region for hunting compensation, the controller is still engaged. Then as the cart reaches setpoint at 3.6 sec. so does the swing angle fall into the dead band region for hunting compensation.

The system still settles in the same time frame, and as can be seen the control is robust enough to factor all matched disturbance. Thus it is concluded that the direction of motion of the goods plays no significant role in the sliding mode controllers performance.

Cart position step response setpoint 1 m

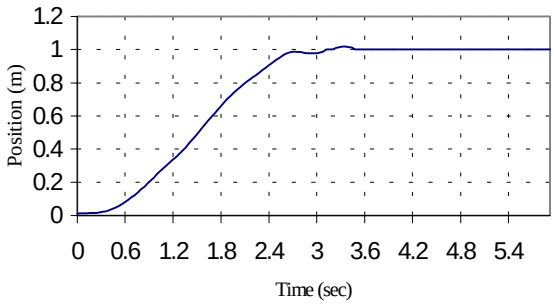

Figure 8.2.7

Swing angle step response

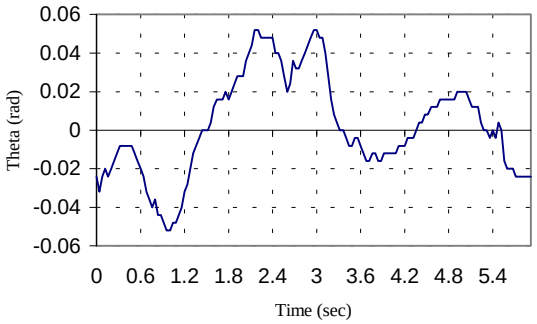

Figure 8.2.8

Control effort of cart and swing controller

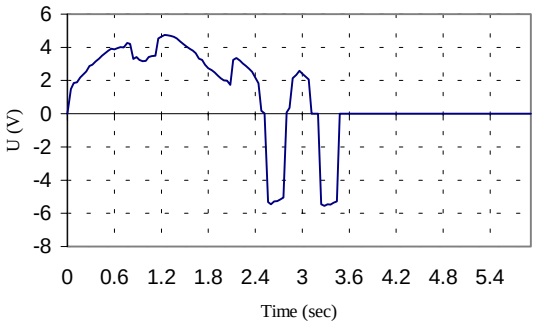

Figure 8.2.9

Switching surface

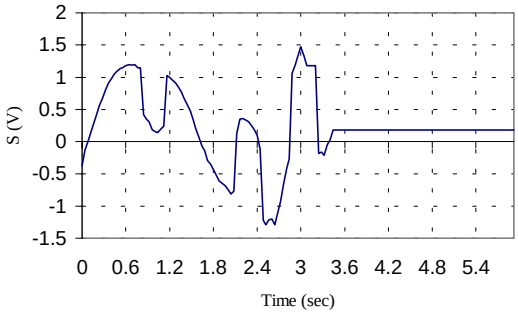

Figure 8.2.10

Rope length step response

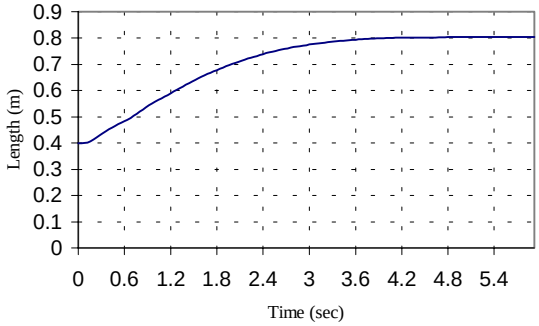

Figure 8.2.11

Control effort of rope length controller

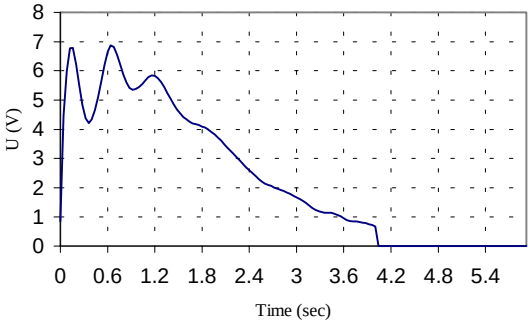

Figure 8.2.12

8.3 SIMULATION OF A CONTROLLER DESIGNED FOR A FIXED ROPE LENGTH WHILE THE ROPE LENGTH IS VARIED

The gantry crane is now controlled by a sliding mode controller which is designed for a fixed rope length of 1 m (described in Chapter 6) and the rope length controller described in Chapter 7. Since the sliding mode controller is robust with respect to external disturbances, it is expected that the cart position, swing angle and the rope length will have the same performance as described in Chapters 6 and 7, even though the sliding mode controller in this section is not changing at each sample instant.

For the purpose of simulation, the rope length is firstly moved from 0 to 0.8 m, then after 5 sec., the cart is displaced to 1m. This is required as the swing dynamics are a function of the rope length. If the rope length is initially 0 m, then a divide by zero error is incurred. Thus, the rope length must initially be non zero. Also the real-time systems rope length initially starts at 0.8 m. The figure below illustrates the block diagram of the complete crane system with a fixed rope length controller

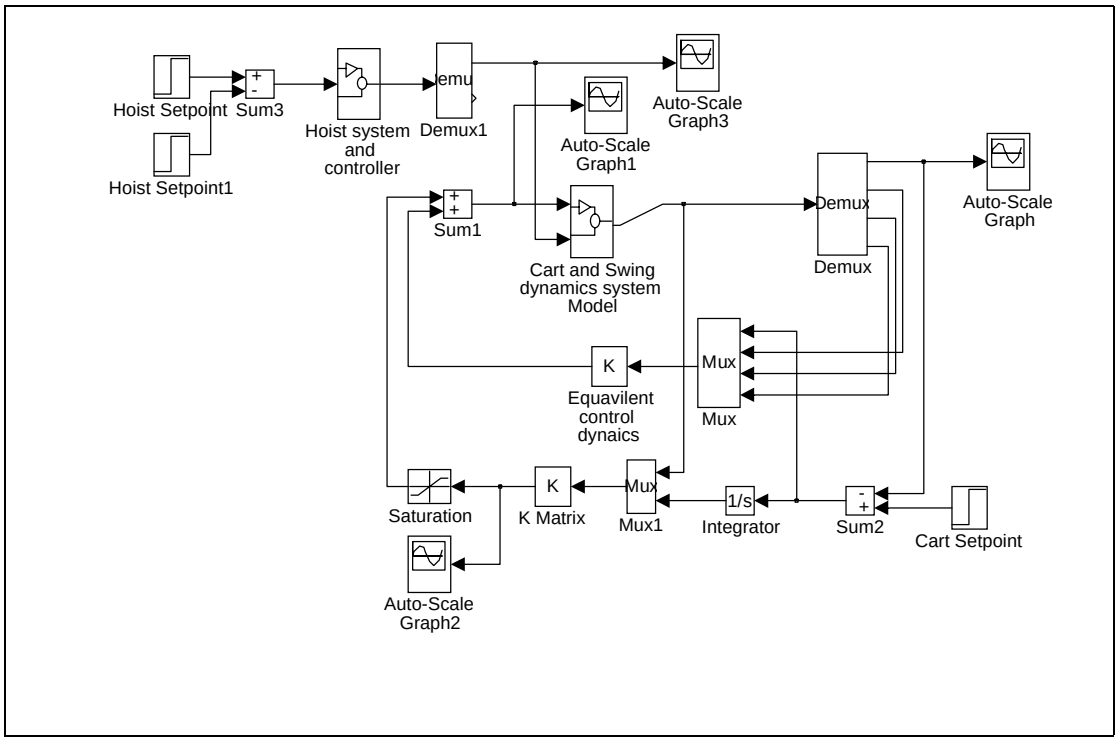

Figure 8.3 The block diagram of the complete crane system with a fixed rope length controller

8.3.1 SIMULATION COMPARISON OF THE TWO CONTROLLERS

A discussion of the simulation differences between the gain scheduled sliding mode controller and the fixed rope length sliding mode controller as the rope length is varied, is given in this section. The sliding mode controller that is designed with a fixed rope length will be known as the non gain scheduled sliding mode controller.

The Figures 8.3.2 - 8.3.7 illustrate the performance of the non gain scheduled sliding mode controller as the rope length is varied from a 0.8 m starting position to a final value of 0.4 m (i.e. goods are being raised). Once again, the controller's performance after the first 5 sec. period is discussed, as the cart and the swing dynamics are activated at this point in time. Thus, all three dynamics are being controlled after the initial 5 sec. period.

As can be seen from Figure 8.3.2, the cart's step response is similar to the step response of Figure 8.1.2 while the goods are being raised. The only difference between the figures is that in Figure 8.3.2 the cart's settling time is increase by 0.5 sec. to 5.5 sec., where as in Figure 8.1.2 the cart settles in 5 sec.

It is known that a change in the rope length will change the system's dynamics. Since the non-gain scheduled sliding mode controller is not adjusted with a change in the rope length, then it can only view a change in the rope length as a modelling uncertainty or parameter fluctuation. Thus, the controllers settling time is slightly increased to cope with the uncertainty caused by the changing rope length.

Figure 8.3.3 illustrates the swing angle as the cart is moving. It can be seen that the swing angle has the same waveform as Figure 8.1.3 with only a slight change in magnitude.

The most noticeable effect of the varying rope length can be seen in the switching surface. As can be seen by Figure 8.3.5 and 8.1.5, the two switching surfaces are vastly different.

This can be attributed to the change in the system dynamics as the rope length is varied. As the switching surface is a function of the system states, it is obvious that the switching surface will change as the system states change due to a change in the rope length.

Overall, considering the changing system dynamics due to the varying rope length and using a controller that was designed for a fixed rope length, the controller's performance is not greatly decreased. In fact, it is virtually identical to the gain scheduled sliding mode controller except for a slight increase in settling time.

Cart position step response setpoint 1 m

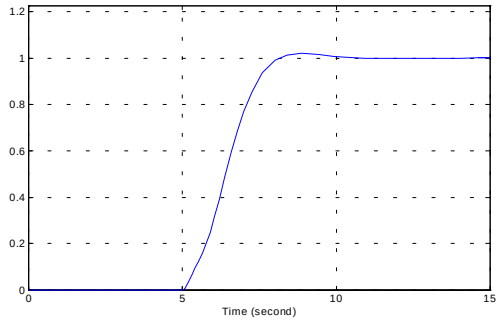

Figure 8.3.2

Swing angle step response

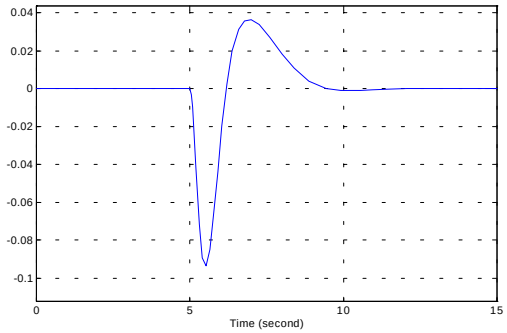

Figure 8.3.3

Control effort of cart and swing controller

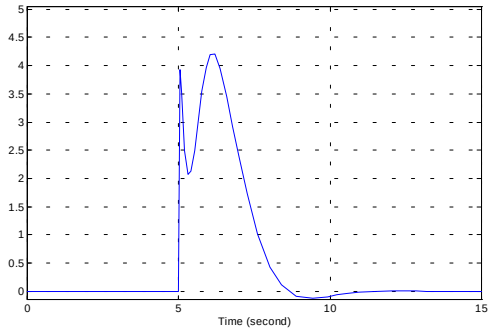

Figure 8.3.4

Switching surface

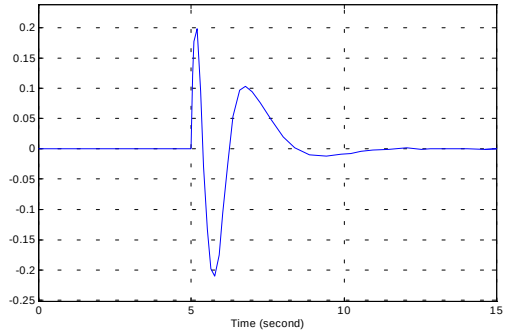

Figure 8.3.5

Rope length step response

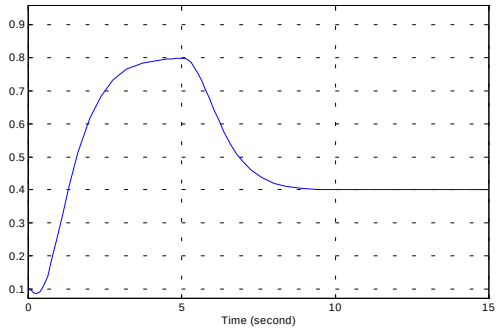

Figure 8.3.6

Control effort of rope length controller

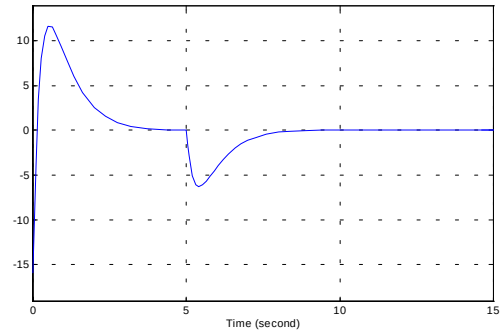

Figure 8.3.7

8.3.2 COMPARISON WITH THE GOODS BEING LOWERED

This section attempts to determine if there is any difference in performance of the non gain scheduled sliding mode controller as the goods are being lowered. As can be seen from Figure 8.3.8 - 8.3.13 the non gain scheduled sliding mode controller exhibits no difference in performance from the raising or lowering of the goods. The only factor that is slightly affected due to the change in direction of motion of the goods is the switching surface.

Figure 8.3.11 illustrates the switching surface as the goods are being lowered. As was discussed previously, the switching surface is a function of all the system states, thus it is evident that it will change its shape with a change in system dynamics which affect the system's states. Overall the switching surface in Figure 8.3.11 has the same basic waveform as in Figure 8.3.5.

Thus it is concluded that the non gain scheduled sliding mode controller has the same behaviour independent of the direction of motion of the goods. Thus, the non gain scheduled sliding mode controller is robust and stable in all directions of motion of the goods (i.e. while the rope length is being varied).

Cart position step response setpoint 1 m

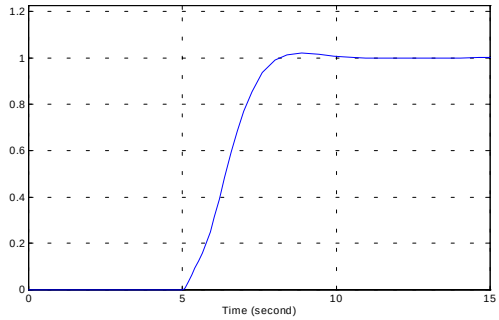

Figure 8.3.8

Swing angle step response

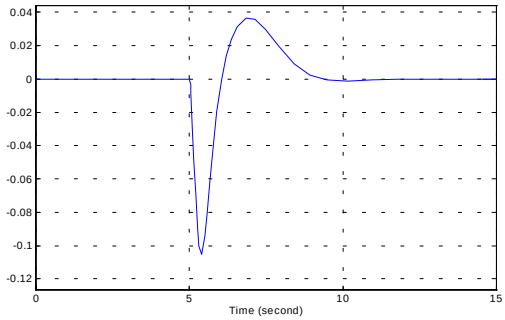

Figure 8.3.9

Control effort of cart and swing controller

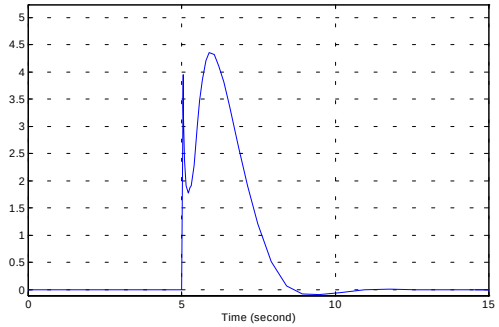

Figure 8.3.10

Switching surface

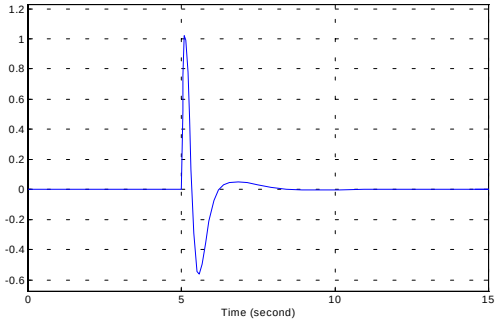

Figure 8.3.11

Rope length step response

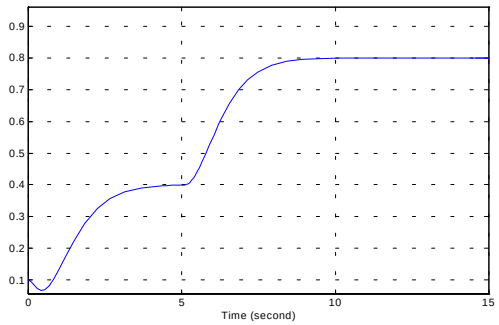

Figure 8.3.12

Control effort of rope length controller

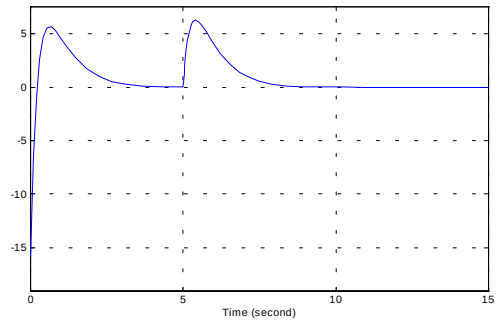

Figure 8.3.13

8.4 REAL-TIME IMPLEMENTATION OF A CONTROLLER DESIGNED FOR A FIXED ROPE LENGTH WHILE THE ROPE LENGTH IS VARIED

A discussion of the real-time implementation of the non-gain scheduled sliding mode controller's performance, while the rope length is changing, is given in the section. It was shown by simulation, that the controller's performance did not greatly deteriorate while one of the major design parameters was changing. Thus, it is expected that the real-time controller should not be greatly effected either.

8.4.1 REAL-TIME IMPLEMENTATION COMPARISON OF THE TWO CONTROLLERS

A discussion of the real-time implementation differences between the gain scheduled sliding mode controller and the non gain scheduled sliding mode controller as the rope length is varied, is given in this section. Figures 8.4.1 - 8.4.12 illustrate the crane's performance. The cart's step response that is illustrated by Figure 8.4.1, shows that the non gain scheduled sliding mode controller behaves quite reasonably as the goods are being raised (i.e. rope length is being varied). The cart's step response does not appear to be as smooth as in Figure 8.2.1, but this is due to a combination of noise and the changing system dynamic. The most noticeable difference is the increase in settling time, because of the lack of adaptation in the control structure. The settling time has once again increased to 4.5 sec. where compared to the gain scheduled sliding mode controller which has a settling time of 4 sec. This was also apparent in the simulation, where the cart has increased it's settling by a factor of 10% to 5.5 sec. Thus, the real-time implementation matches closely with the simulation with respect to a percentage increase in the settling time.

As was stated previously, overshoot does not always occur even though simulation predicts it should. Figure 8.4.1 does not show any overshoot, because all the conditions for hunting compensation have been met and the controller is turned off. Overall, the performance of a non gain scheduled sliding mode controller (i.e. sliding mode

controller designed for a fixed rope length) is very similar to the gain scheduled sliding mode controller.

Cart position step response setpoint 1 m

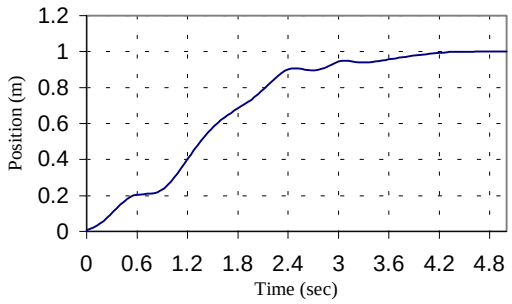

Figure 8.4.1

Swing angle step response

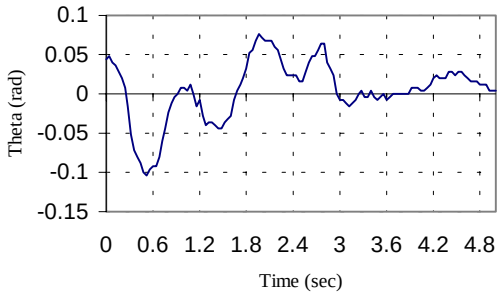

Figure 8.4.2

Control effort of cart and swing controller

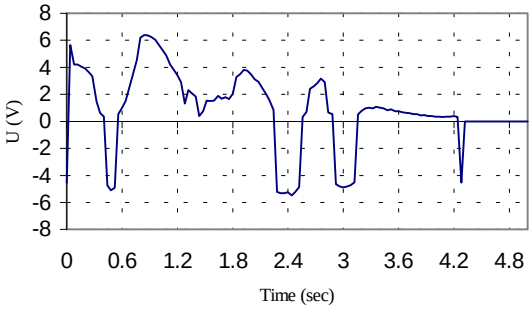

Figure 8.4.3

Switching surface

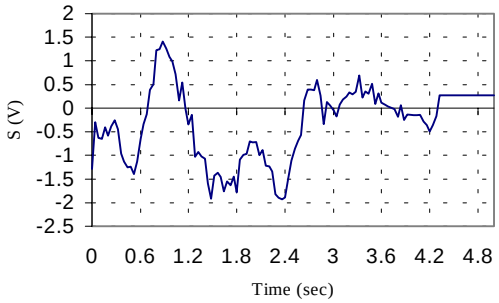

Figure 8.4.4

Rope length step response

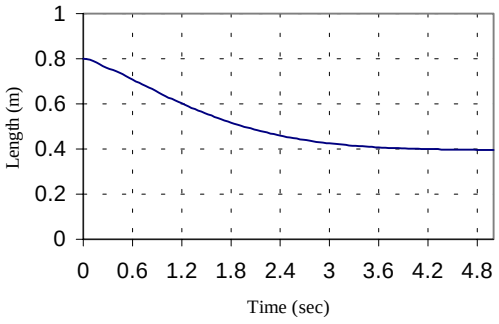

Figure 8.4.5

Control effort of rope length controller

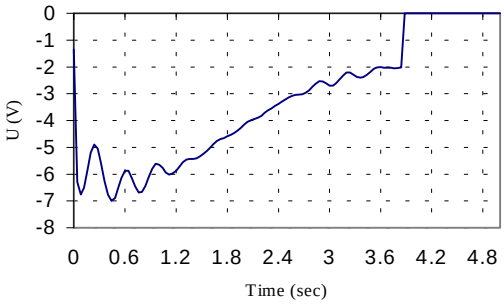

Figure 8.4.6

8.4.2 COMPARISON WITH THE GOODS BEING LOWERED

For completeness we will attempt to determine if there is any difference in non gain scheduled sliding mode controller's performance while the goods are being lowered. Figure 8.4.7 - 8.4.12 illustrate the controller's performance as the goods are being lowered.

As can be seen from Figure 8.4.7 - 8.4.12 raising or lowering of the goods does not effect the non gain scheduled sliding mode controller performance. All characteristics of the system still remain the same no matter in which direction of motion the goods are moving (i.e. direction of motion of the rope length). As can be seen by Figure 8.4.1 and Figure 8.4.2 the cart's response and the swing angle's response are very similar to those in Figures 8.4.2 and Figure 8.4.8. Thus, it is concluded that the direction of motion of the rope length plays no significant role in the non gain scheduled sliding mode controller's performance.

Cart position step response setpoint 1 m

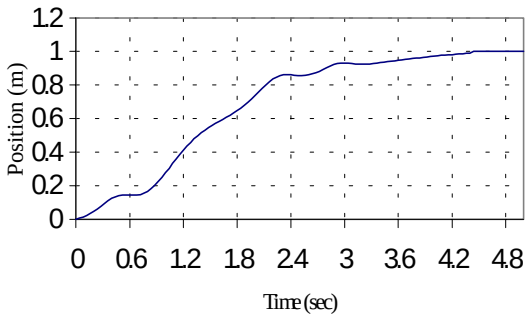

Figure 8.4.7

Swing angle step response

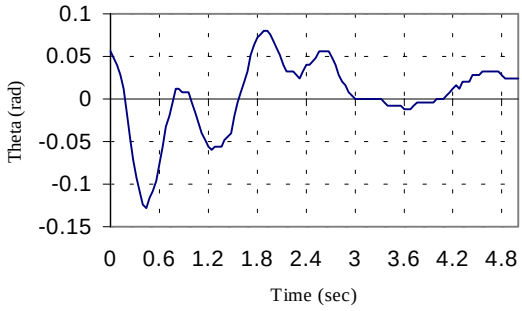

Figure 8.4.8

Control effort of cart and swing controller

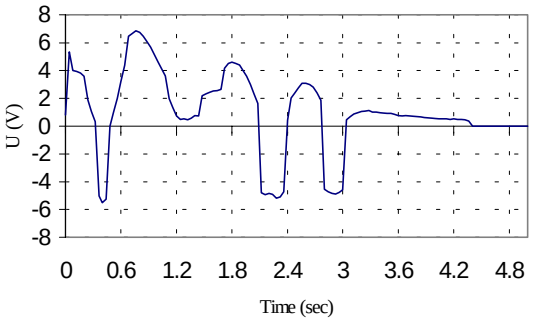

Figure 8.4.9

Switching surface

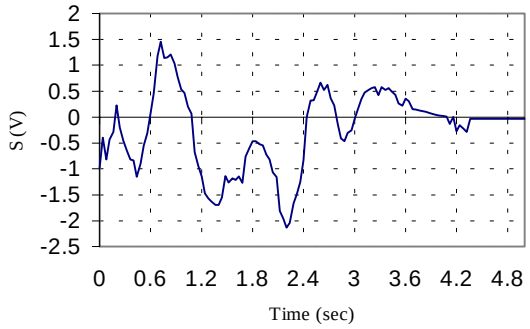

Figure 8.4.10

Rope length step response

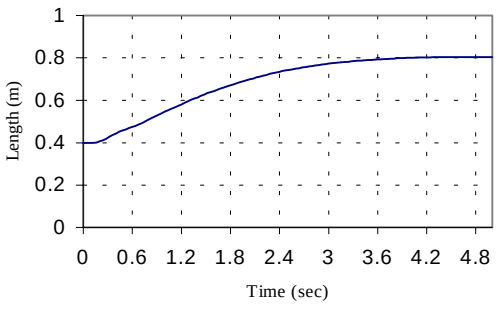

Figure 8.4.11

Control effort of rope length controller

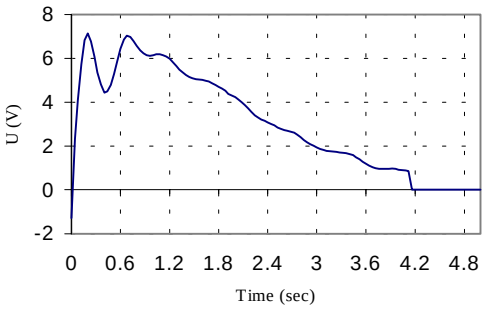

Figure 8.4.12

8.5 CONCLUSION

The aims of this chapter were (1) to develop a gain scheduled sliding mode controller, such that the closed loop poles would not change with the variation in the rope length and (2) to compare the gain scheduled sliding mode controller with a non gain scheduled sliding mode controller while achieving rope length control.

The gain scheduled sliding mode controller was found to be robust while changing the rope length. It was also evident in this chapter that the real-time implementation and the simulation gave very similar results. Thus, the conclusion that the mathematical model is accurate for this system is further strengthened.

The design and implementation of the gain scheduled sliding mode controller was much more difficult than designing for a fixed rope length. Using the gain scheduled sliding mode controller does produce a better and faster system response. However, if the complex nature of this controller is too difficult to design or implement, then one could design and implement a non gain scheduled sliding mode controller without greatly effecting the system's performance while still achieving rope length control. Control of all three dynamics (i.e. cart position, swing angle and the rope length) is thus achieved.

For the non scheduled sliding mode controller while varying the rope length, the robustness of the sliding mode controller (with respect to a changing rope length) can be observed, as the varying rope length can be viewed as a disturbance or an uncertainty. In Section 8.4 this experiment was carried out and it was noted that the controller was robust enough to cope with quickly varying changes in the rope length. This adds further weight to the conclusion that the sliding mode controller is very robust.

In this chapter as with Chapter 6 there was no on-line tuning required of any of the controllers. The real-time controllers implemented are those as in the Matlab results.

CHAPTER 9 MODEL FOLLOWING

Previous work by Athans [34] and Anderson and Moore [31] describes two methods for developing a reference tracking controller, by using the general solution to the LQR problem. Both Athans [34] and Anderson and Moore [31] derive an optimal control law for the tracking problem. They show that the optimal control law is a function of the desired trajectory's future value. Anderson and Moore [31] extend this solution to a special class of the tracking problem, known as the model following problem. They use the dynamics of the model which generates the desired trajectory in the formulation of the control law. These methods impose the constraint that the order of the desired trajectory must be the same as the order of the plant (Perfect Model Matching). Both methods are described in this chapter to give a clearer picture of the limitations of the two methods.

The use of model following techniques tends to lead to a reduction in the control effort and an increase in the speed of response. This occurs because the model itself is taken into consideration in the model design. If a controller is designed as in Chapter 5, where one would like to achieve setpoint control (a specific case of model following) then an initial change in the step size will cause a sharp peak in the control effort as the plant cannot move with the same velocity as the setpoint. It is often the case in practice that the plant under control has a maximum and minimum limit to the allowable control effort. Thus large control efforts will not have the desired effect on the plant, and in some instances may cause the plant to become unstable as the initial design of the controller assumes large control efforts.

The model which the plant is to follow is totally up to the discretion of the designer, but one should take into consideration the rate of change of the plant such that a model is chosen with its rate of change not being greater then the plant's. This will effectively allow the plant to follow the desired model and any changes to the model's input will have no dramatic effects on the control effort and thus will allow the plant to achieve the new reference point.

The plant and the model are combined to form a set of state space equations or transfer functions in terms of the error signal (i.e. $x - x_m$) where x are the states of the plant and x_m are the states of the model. Young [16] first approached the problem of model following using a sliding mode controller to achieve robustness in the control design. Young's two assumptions are:

1) All plant states are known.
2) The order of the model is the same as the order of the plant (Perfect Model Matching).

Hopp and Schmitendorf [17] illustrated a robust design of a linear feedback controller with model following. Their investigation illustrated the relationship between the stability of the model and the plant and how a robust controller may be constructed. But their approach to the problem is limited to the assumption that all the states in both the plant and the model are known. In practice this is not always the case.

The notation of robustness in terms of matched and unmatched dynamics has also been of concern. With the advent of sliding mode control techniques many papers [6] [13] [16] and [18] describe the use of sliding mode control in model following. These papers detail the robustness (with respect to matched disturbances) of such controllers, but Young's assumptions still hold in these publications. Observers have been used to overcome the limitation of knowing all the system states.

Papers have been published on the use of observers [7] [10] and [14]. These observers consist of a high gain which makes them insensitive to external disturbances. This requires a very accurate model of the system to be controlled. Any modelling errors will cause large deviations of the observed states from the actual states due to the high gain component.

Shyu and Liu [15] describe a method to eliminate one of Young's' initial limitations to model following. Their work consisted of imperfect model matching i.e. the order of the model does not have to be the order of the system, but they do assume that all the system states are obtainable by some means. Shyu and Liu [15] describe a method by which a system and model can be mapped to some other arbitrary states. Then by

controlling these arbitrary states the system will follow the model, since these arbitrary states are a relationship between the system states and the model. In fact from an imperfect model matched system, they have produced a perfect model matched system which is then controlled. This is a valid solution to one of the Young's limitations, but the limitation of the availability of all states is still present in their work.

Clearly a more appropriate solution to the problem is to use output feedback control. Bag, Surgeon and Edwards [5] and El – Khazali and De Carlo [12] have written about the asymptotic stability of output feedback control using a sliding mode approach. Clearly using a sliding mode approach to output feedback control will ensure the robustness of the control when the controller is faced with uncertainties, but in both [5] and [12] there is clearly one major draw back to their approach to the solution of the problem of unavailable states. The limitation is that the controller is made up of a set of derivatives of the output state and this is clearly not practical. One method to overcome this problem is to implement the controller as a transfer function. This also requires on line tuning, as the poles of the denominator must be placed far enough on the left-hand side of the root locus plane such that they do degrade the performance of the controller.

An alternative method for the design of an output feedback model following controller is presented in this chapter. This method is used, because it enables a controller to be designed in one single design process such that the resultant controller:

1) Is the exact filter that is needed to smooth out any set point changes. Therefore no additional filter design process is needed.
2) Will give 2 degrees of freedom control since the characteristics of the model is incorporated into the controller structure, instead of a single degree of freedom control which occurs when a step change is used.
3) Does not require the need to have all the states directly measurable or available. Therefore no addition design process is needed to design an estimator for the unavailable states, as was required for the sliding mode controller designed in Chapter 5.

9.1 LINEAR QUADRATIC OPTIMAL CONTROL

In this section a brief description of the linear quadratic controller problem is given. For more detail and discussion the reader is referred to [31], [32], [33], and [34].

Consider the system

$$\dot{x}(t) = A(t)x(t) + B(t)u(t) \qquad 9.1.1$$

defined on the interval $[t_0 , T]$ and the cost function (performance index)

$$J = \int_{t_0}^{T} (x'(t)\, Q\ x(t) + u'(t)\, R\, u(t))\, dt \qquad 9.1.2$$

where both the Q and R matrices are positive definite (or positive semi-definite) real symmetric matrices and x' denotes the transpose of the matrix or vector x.

The control law which minimises (9.1.2) subject to (9.1.1) is

$$u = -Kx = -R^{-1}B'P\,x \qquad 9.1.3$$

where the matrix P satisfies the *Riccati equation*

$$-\dot{P} = PA + A'P - PBR^{-1}B'P + Q, \qquad P(T)=0 \qquad 9.1.4$$

The optimal cost given as

$$J(t_0) = x'(t_0)\, P(t_0)\ x(t_0) \qquad 9.1.5$$

It will be shown that (9.1.3) is the optimal control law by establishing that any other control law is suboptimal. The proof is as follows.

We note that

$$\frac{d}{dt}(x'(t)\, P(t)x(t)) = \dot{x}'\ P\,x + x'\ \dot{P}\ x + x'\ P\,\dot{x} \qquad 9.1.6$$

and so substituting (9.1.1) into (9.1.6) gives

$$\frac{d}{dt}(x'(t)\, P(t)x(t)) = \begin{bmatrix} x' & u' \end{bmatrix} \begin{bmatrix} \dot{P} + PA + A'P & PB \\ B'P & 0 \end{bmatrix} \begin{bmatrix} x \\ u \end{bmatrix} \qquad 9.1.7$$

Integration of (9.1.7) on the interval $[t_0\ T]$ yields

$$x'(T)\,P(T)\,x(T) - x'(t_0)\,P(t_0)\,x(t_0) = \int_{t_0}^{T} \begin{bmatrix} x' & u' \end{bmatrix} \begin{bmatrix} \dot{P} + PA + A'P & PB \\ B'P & 0 \end{bmatrix} \begin{bmatrix} x \\ u \end{bmatrix} dt \qquad 9.1.8$$

and so

$$-x'(t_0)\,P(t_0)\,x(t_0) = \int_{t_0}^{T} \begin{bmatrix} x' & u' \end{bmatrix} \begin{bmatrix} \dot{P} + PA + A'P & PB \\ B'P & 0 \end{bmatrix} \begin{bmatrix} x \\ u \end{bmatrix} dt \qquad 9.1.9$$

with the boundary condition $P(T) = 0$.

From (9.1.2) the cost function can be expressed as

$$J = \int_{t_0}^{T} \begin{bmatrix} x' & u' \end{bmatrix} \begin{bmatrix} Q & 0 \\ 0 & R \end{bmatrix} \begin{bmatrix} x \\ u \end{bmatrix} dt \qquad 9.1.10$$

which, incorporating (9.1.9) gives

$$J = x'(t_0)\,P(t_0)\,x(t_0) + \int_{t_0}^{T} \begin{bmatrix} x' & u' \end{bmatrix} \begin{bmatrix} \dot{P} + PA + A'P + Q & PB \\ B'P & R \end{bmatrix} \begin{bmatrix} x \\ u \end{bmatrix} dt \qquad 9.1.11$$

and so

$$J = x'(t_0)\,P(t_0)\,x(t_0) + \int_{t_0}^{T} \begin{bmatrix} x' & u' \end{bmatrix} \begin{bmatrix} PBR^{-1}B'P & PB \\ B'P & R \end{bmatrix} \begin{bmatrix} x \\ u \end{bmatrix} dt \qquad 9.1.12$$

since $\dot{P} + PA + A'P + Q = PBR^{-1}B'P$.

With

$$u = -Kx + v = -R^{-1}B'Px + v \qquad 9.1.13$$

we have

$$J = x'(t_0)\,P(t_0)\,x(t_0) + \int_{t_0}^{T} v'Rv\,dt \qquad 9.1.14$$

Since R is a real symmetric positive definite matrix, then v =0 minimises (9.1.14).
In using any technique to solve the optimum gain matrix K it should be noted that K will be time varying if the matrices A, B Q and R are constant and the time is finite. This is because the solution matrix P(t) of the matrix Riccati equation will not be constant. For a practical implementation a steady state solution needs to be found., i.e. the optimum gain matrix must converge to a fixed solution.

Thus, the performance integral that must be minimised by the gain matrix K is

$$J = \lim_{T\to\infty} \int_t^T (x' Qx + u' Ru)\ dt \qquad 9.1.15$$

which turns out to be independent of t.

For the infinite solution, the optimum gain matrix K is given by

$$K = R^{-1}B' P \qquad 9.1.16$$

where P satisfies the *Algebraic Riccati Equation (ARE)*

$$0 = PA + A' P - PBR^{-1}B' P + Q \qquad 9.1.17$$

The ARE has a unique, positive definite solution P which minimises J if (A, B) is stabilisable and (A, Q) is detectable. A definition of these conditions is taken from [31].

9.2 MODEL FOLLOWING AND THE LQR

This section will describe the two classical methods for the design of a model following controller by using the general solution to the LQR. The first method is given by Athans [34] and is described in Section 9.2.1 The second method is the one presented by Anderson and Moore [31] and is described in Section 9.2.2. It should be noted that both methods produce a model following controller that is comprised of a feedforward and feedback component.

9.2.1 ATHANS'S APPROACH

Athans [34] gives a solution to the model following problem by constructing error matrices and using the general solution to the LQR to derive a set of gains which makes the controller optimal. One of the advantages of using this approach is that the solution gives a feedforward term and a feedback term. This means that if a predefined trajectory is known, then the feedforward term is used to move the system towards the trajectory and the feedback term takes care of any errors as the system strays from that trajectory.

One disadvantage of Athans's approach is that the optimal control is dependent upon all future knowledge of the model. From a purely theoretical point of view this is clearly a major disadvantage, but practically speaking, in many instances the control engineer knows what trajectory he would like the system to follow.

Athans states that tracking problem reduces to a special case of the LQR problem. The system is required to track the response given by the vector $\tilde{y}(t)$). We assume that the dimensions of $\tilde{y}(t)$ and y(t) are equal and perfect model matching occurs. The object is to optimally control (that is with no excessive expenditure of the control energy) y(t) such that y(t) equals or is 'close enough' to $\tilde{y}(t)$. For this reason the error signal e(t) is defined as

$$e(t) = \tilde{y}(t) - y(t) \qquad 9.2.1$$

The cost function that is required to be minimised is given as

$$J = \int_{t0}^{T} [e'(t)\, Q(t)\, e(t) + u'(t)\, R(t)\, u(t)]\, dt \qquad 9.2.2$$

with the assumptions that Q(t) is positive semidefinite, R(t) is positive definite and T is specified.

Athans [34] demonstrates that the optimal control law is given by

$$u = R^{-1}B'[g - P\,x] = R^{-1}B'g - K\,x \qquad 9.2.3$$

where the matrix P satisfies the *Riccati equation*

$$-\dot{P} = PA + A'P - PBR^{-1}B'P + C'QC, \qquad P(T)=0 \qquad 9.2.4$$

and the vector g is the solution of the linear vector differential equation

$$\dot{g} = -[A - BR^{-1}B'P]'g - C'Q\,\tilde{y}\ , \qquad g(T)=0 \qquad 9.2.5$$

with the optimal cost given as

$$J = x'(t_0)P(t_0)x(t_0) - 2\,x'(t_0)g(t_0) + \Phi(t_0) \qquad 9.2.6$$

where $\Phi(t_0)$ is determined from

$$\dot{\Phi} = -(\tilde{y}'Q\tilde{y} - g'B\,R^{-1}B'g) \qquad \Phi(T) = 0 \qquad 9.2.7$$

It can be seen that Athans's solution to the tracking problem is the same as the solution to the LQR problem together with the feedforward term $v = R^{-1}B'g$.

In a manner similar to that adopted in Section 9.1, it may be shown that the optimal control law to the tracking problem is given by (9.2.3). The proof is as follows.

Consider the system

$$\begin{aligned} \dot{x}(t) &= A(t)x(t) + B(t)u(t) \\ y(t) &= C(t)x(t) \end{aligned} \qquad 9.2.8$$

defined on the interval $[t_0 , T]$

The cost function (9.2.2) expressed in terms of the system states and the desired trajectory is

$$J = \int_{t0}^{T} \tilde{y}' Q\tilde{y} - x' C' Q \tilde{y} - \tilde{y}' Q Cx + \begin{bmatrix} x' & u' \end{bmatrix} \begin{bmatrix} C'QC & 0 \\ 0 & R \end{bmatrix} \begin{bmatrix} x \\ u \end{bmatrix} dt \qquad 9.2.9$$

From Section 9.1 we know that

$$-x'(t_0)\,P(t_0)\,x(t_0) = \int_{t_0}^{T} \begin{bmatrix} x' & u' \end{bmatrix} \begin{bmatrix} \dot{P} + PA + A'P & PB \\ B'P & 0 \end{bmatrix} \begin{bmatrix} x \\ u \end{bmatrix} dt \qquad 9.2.10$$

with the boundary condition $P(T) = 0$

Now equating (9.1.9) and (9.1.10) gives

$$J = x'(t_0)P(t_0)x(t_0) + \int_{t0}^{T} (\tilde{y}' Q\tilde{y} - x' C' Q \tilde{y} - \tilde{y}' Q Cx)dt + \Psi \qquad 9.2.11$$

where

$$\Psi = \int_{t0}^{T} \begin{bmatrix} x' & u' \end{bmatrix} \begin{bmatrix} \dot{P} + PA + A'P + C'QC & PB \\ B'P & R \end{bmatrix} \begin{bmatrix} x \\ u \end{bmatrix} dt \qquad 9.2.12$$

As in Section 9.1 it will be shown that the optimal control law is given by

$$u = -K x + v \qquad 9.2.13$$

where $v = R^{-1}B'g$

Substituting (9.2.13) into (9.2.12) gives

$$J = x'(t_0)P(t_0)x(t_0) + \int_{t0}^{T} (\tilde{y}' Q\tilde{y} - x' C' Q\,\tilde{y} - \tilde{y}' Q\,Cx)dt + \int_{t0}^{T} v' R\, v\, dt \qquad 9.2.14$$

Applying the control law (9.2.13) to (9.2.8) gives

$$\dot{x}' - v' B' = x' A_C' \qquad 9.2.15$$

where $A_C = A - BK$

From (9.2.5) it can be seen that

$$x' C' Q\ \tilde{y} = x'(\dot{g} + A_C' g) \qquad 9.2.16$$

where $A_C = A - BR^{-1} B' P = A - BK$ and $K = R^{-1} B' P$

Substituting (9.2.15) into (9.2.16) gives

$$x' C' Q\ \tilde{y} = x'(\dot{g} + A_C' g) = x'\dot{g} + (\dot{x}' - v' B')g = \frac{d}{dt}(x'g) - v' B' g \qquad 9.2.17$$

and the transpose of (9.2.17) gives

$$\tilde{y}' Q\, C\, x = \frac{d}{dt}(x'g) - g' B\, v \qquad 9.2.18$$

since Q is a symmetric matrix.

Now (9.2.17) and (9.2.18) can be substituted into (9.2.14) to give

$$J = x'(t_0)P(t_0)x(t_0) + 2\, x'g\,]_{t_0}^{T} + \int_{t0}^{T} (\tilde{y}' Q\tilde{y} + v' R\, v - v' B' g - g' B\, v)dt \qquad 9.2.19$$

$$= x'(t_0)P(t_0)x(t_0) - 2\, x'(t_0)g(t_0) + \int_{t0}^{T} (\tilde{y}' Q\tilde{y} - g' B\, R^{-1} B' g + \Omega)dt \qquad 9.2.20$$

where

$g(T) = 0$

$$\Omega = \int_{t0}^{T} (v - R^{-1}B'g)' R\, (v - R^{-1}B'g)\, dt \qquad 9.2.21$$

From (9.2.21) it is clearly seen that the minimum occurs when

$$v = R^{-1} B' g \qquad 9.2.22$$

since R is a positive definite symmetric matrix, and the quantity

$\int_{t0}^{T} (\tilde{y}' Q\tilde{y} - g' B R^{-1} B' g)dt$ does not depend on the control law.

The optimal control law is now found by substituting (9.2.22) into (9.2.13). This solution presents the problem of prior knowledge of all values of the desired output $\tilde{y}(t)$ .This problem is not necessarily easy to overcome.

9.2.2 ANDERSON AND MOORE'S APPROACH

Anderson and Moore [31] approach the model following problem in a slightly different manner to Athans [34]. Athans's [34] solution assumes that nothing is known about the model except that the model produces a desired output. Anderson and Moore [31] start with a special case of Athans's solution and derive a solution when the model's structure is known.

Anderson and Moore [34] tackle the problem by stating that if the states of the system follow some arbitrary states which are mapped to the desired output, then the output of the system must follow the desired output. The solution they present is not necessarily the optimal solution in all cases, since they only give the mapping between the desired output and the arbitrary states for a special class of system.

The optimal solution to the model following problem as presented by Anderson and Moore [34] is described in this section. The solution presented below is the optimal solution because the system output is required to directly track the desired output.

Suppose the system

$$\begin{aligned} \dot{x} &= Ax + Bu \\ y &= C\,x \end{aligned} \qquad 9.2.23$$

is required to track the output $\tilde{y}$ given by

$$\begin{aligned} \dot{z} &= Fz \\ \tilde{y} &= H\,z \end{aligned} \qquad 9.2.24$$

The error between the desired output $\tilde{y}(t)$ and the system's output y(t) is defined as

$$e(t) = \tilde{y}(t) - y(t) \qquad 9.2.25$$

and defining the error in terms of the model and system states gives

$$e = [\,-C \;\; H\,]\begin{bmatrix} x \\ z \end{bmatrix} \qquad 9.2.26$$

The cost function that is required to be minimised is

$$J = \int_{t0}^{T} [\,e'(t)\,Q(t)\,e(t) + u'(t)\,R(t)\,u(t)\,]\,dt \qquad 9.2.27$$

with the assumptions that Q(t) and R(t) are positive definite. In terms of the model states and the system states we have

$$J = \int_{t0}^{T} [\,\hat{x}'\,\hat{Q}\hat{x} + u'\;R\,u\,]\,dt \qquad 9.2.28$$

with the relationship $\dot{\hat{x}} = \hat{A}x + \hat{B}u$ where

$$\hat{x} = \begin{bmatrix} x \\ z \end{bmatrix} \quad \hat{A} = \begin{bmatrix} A & 0 \\ 0 & F \end{bmatrix} \quad \hat{B} = \begin{bmatrix} B \\ 0 \end{bmatrix} \quad \hat{Q} = \begin{bmatrix} C'\,Q\,C & -C'QH \\ -H'\,QC & H'QH \end{bmatrix} \qquad 9.2.29$$

The variables and matrices are now constructed as for the standard regulator:

$$u = -R^{-1}\,\hat{B}'\,\hat{P}\hat{x} \qquad 9.2.30$$

where $\hat{P}$ is the solution to the Riccati equation given by

$$-\dot{\hat{P}} = \hat{P}\hat{A} + \hat{A}'\,\hat{P} - \hat{P}\hat{B}R^{-1}\,\hat{B}'\,\hat{P} + \hat{Q}\,, \qquad \hat{P}(T) = 0 \qquad 9.2.31$$

and the minimum index is

$$J = \hat{x}'(t_0)\hat{P}(t_0)\hat{x}(t_0) \qquad 9.2.32$$

The result is expressed in terms of the original system variables and matrices using the definition given by (9.2.29). The $\hat{P}$ matrix is partitioned as

$$\hat{P} = \begin{bmatrix} P & P_{12} \\ P_{21} & P_{22} \end{bmatrix} \qquad 9.2.33$$

and so

$$-\dot{P} = PA + A'P - PBR^{-1}B'P + C'QC, \qquad P(T) = 0 \qquad 9.2.34$$

$$-\dot{P}_{12} = P_{12}F + A'P_{12} - PBR^{-1}B'P_{12} - C'QH, \qquad P_{12}(T) = 0 \qquad 9.2.35$$

$$-\dot{P}_{22} = P_{22}F + F'P_{22} - P_{12}'BR^{-1}B'P_{12} + H'QH, \qquad P_{22}(T) = 0 \qquad 9.2.36$$

The control law (9.2.30) is

$$u = K'x + K_1'z \qquad 9.2.37$$

where

$$K' = -R^{-1}B'P \qquad 9.2.38$$

$$K_1' = -R^{-1}B'P_{12} \qquad 9.2.39$$

It should be noted that P and P_{12} can be expressed in terms of the original system and model matrices, which will allow P and P_{12} to be solved. Thus the control law is a function of the system states and the model states. The minimum index is now given as

$$J = x'(t_0)P(t_0)x(t_0) + 2x'(t_0)P_{12}(t_0)z(t_0) + z'(t_0)P_{22}(t_0)z(t_0) \qquad 9.2.40$$

Anderson and Moore [31] show that the control law (9.2.37) is realisable without knowledge of z. Consider the control law

$$u = K'x - R^{-1}B'P_{12}z \qquad 9.2.41$$

If F and H are unknown, and z is unknown, then the products $g = -P_{12}z$ and $\Phi = z'P_{22}z$ can be determined for the model output $\tilde{y}(t)$ as follows.

Since

$$\frac{d}{dt}(g) = -\dot{P}_{12}z - P_{12}\dot{z} \qquad 9.2.42$$

substituting (9.2.35) and (9.2.24) into (9.2.42) gives

$$\dot{g} = -[A - BR^{-1} B' P]'g - C' Q \tilde{y} \qquad g(T)=0 \qquad 9.2.43$$

Similarly

$$\dot{\Phi} = \frac{d}{dt}(z' P_{22} z) = z' \dot{P}_{22} z + z' P_{22} \dot{z} + \dot{z}' P_{22} z \qquad 9.2.44$$

and substituting (9.2.36) and (9.2.24) into (9.2.44) gives

$$\dot{\Phi} = -(\tilde{y}' Q \tilde{y} - g' B R^{-1} B' g), \qquad \Phi(T) = 0 \qquad 9.2.45$$

Therefore the optimal cost is given as

$$J = x'(t_0)P(t_0)x(t_0) - 2\, x'(t_0)g(t_0) + \Phi(t_0) \qquad 9.2.46$$

and using the substitution $g = -P_{12}z$ into (9.2.41) gives the optimal control law as

$$u = K' x + R^{-1}B' g \qquad 9.2.47$$

This means that the optimal control developed by Anderson and Moore is identical to that described by Athans. The control law is now solved backwards in time, to determine g(t) which is used in the optimal control law.

9.3 NON-MINIMAL STATE SPACE REPRESENTATION

Hesketh [8] described a method known as non-minimal state space representation in which the system states are the derivatives of the inputs and outputs. Then, any linear design technique allows a controller to be constructed in proper transfer function form.

Non-minimal state space representation can also be applied to model following control. In fact this method lends itself well to this application and automatically addresses Young's limitation of perfect model matching and the need for the availability of all system states is not required.

Since non-minimal state space representation has the advantage that an output feedback controller is produced in proper transfer function form, then there is no need for an estimator or observer to be constructed. In using non-minimal state space representation the system matrices are higher order then the system itself. Thus, when any linear control techniques is used to design the controller, a higher number of poles are required to be placed than the order of the system would indicate. These extra poles can be considered as the poles for an observer, thus the observer construction is taken into account during the controller design phase and it does not have to be designed separately.

On the other hand the main limitations with using a non-minimal state space representation and output feedback controllers are:

1) Using the non-minimal state space representation may produce system matrices which are large and difficult to manipulate (this will be shown in subsequent sections).
2) Since non-minimal state space representation requires the system input to be a direct derivative of the actual system input, a sliding mode controller is difficult to implement.

A brief overview of designing a controller using non-minimal state space representation is given below. Consider a process described by

$$\frac{y(s)}{u(s)} = \frac{\sum_{k=0}^{nb} b_k s^k}{\sum_{k=0}^{na} a_k s^k} \qquad 9.3.1$$

A suitable non-minimal state space representation is:

$$\begin{aligned} \dot{x} &= Ax + Bs^{nb}u \\ y &= Cx \\ x &= [s^{na-1}\, y \ldots y\, s^{nb-1}\, u \ldots u]^T \end{aligned} \qquad 9.3.2$$

The procedure is illustrated by example. Let the system be

$$\frac{y}{u} = \frac{s+2}{s^2+s+1} \qquad 9.3.3$$

$$s^2y = 2u + su - y - sy \qquad 9.3.4$$

which when represented in non-minimal form is

$$\begin{bmatrix} su \\ s^2y \\ sy \end{bmatrix} = \begin{bmatrix} 0 & 0 & 0 \\ 2 & -1 & -1 \\ 0 & 1 & 0 \end{bmatrix} \begin{bmatrix} u \\ sy \\ y \end{bmatrix} + \begin{bmatrix} 1 \\ 1 \\ 0 \end{bmatrix} su$$

$$y = \begin{bmatrix} 0 & 0 & 1 \end{bmatrix} \begin{bmatrix} u \\ sy \\ y \end{bmatrix} \qquad 9.3.5$$

The controller design uses LQR with

$$J = \int_0^\infty (x^T Q x + su^T R su)$$

$$Q = \begin{bmatrix} 0 & 0 & 0 \\ 0 & 0 & 0 \\ 0 & 0 & 1 \end{bmatrix} \qquad 9.3.6$$

$$R = 1$$

Then the controller is

$$su = -Kx = -\begin{bmatrix} 0.9428 & 0.4714 & 0.5286 \end{bmatrix} x \qquad 9.3.7$$

Now the advantage of non-minimal state space representation becomes apparent when the controller is re-written as

$$u = \frac{-(0.4714\,s + 0.5286)y}{s + 0.9428} \qquad 9.3.8$$

Now if we look at the closed loop poles of the system given by (9.3.5) they are all stable and the poles are located at:

P1 = -1.0000, P2 = -0.7071 + 1.2247i, P3 = -0.7071 - 1.2247i

These poles are given for system (9.3.5) with a controller defined by (9.3.7). The question then is, are the same closed loop poles present for the system defined by (9.3.3) which is the original system and the actual controller that will be implemented given by (9.3.8)?

Using block diagram reduction, we obtain the transfer function for the system (9.3.3) and the controller (9.3.8).

$$\frac{y}{u} = \frac{s^2 + 2.9428s + 1.8856}{s^3 + 2.4142\,s^2 + 3.4142s + 2.0000} \qquad 9.3.9$$

Now, taking the roots of the dominator gives the closed loop poles of the system and the controller. Which are:

P_1 = -1.0000

P_2 = -0.7071 + 1.2247i

P_3 = -0.7071 - 1.2247I

These poles are the same as those for the closed loop system and controller defined (9.3.5) and (9.3.7). Thus, it is concluded that the use of non-minimal state space representation produces a stable controller for the original system and the controller produced has the same performance characteristics as that for a system which is placed in non-minimal format and a respective controller is designed for that system.

Thus it is shown that the use of non-minimal state space representation produces an output feedback controller that is stable and has a proper transfer function.

9.4 NON-MINIMAL STATE SPACE REPRESENTATION AND MODEL FOLLOWING

The use of non-minimal state space representation has been shown to be an effective means by which one can derive an output feedback controller that produces a proper transfer function. Clearly one of the initial limitations has been overcome. The next limitation to overcome is the problem of imperfect model matching. Using non-minimal state space representation allows one to represent the system under control and the model as a function of the error states and inputs. This will produce a controller that does not require the model to be the same order as the system and as shown previously a transfer function is given, this time in terms of the error state.

The use of non-minimal state space representation to derive a model following controller is again given by an example.

Consider a system defined by the transfer function

$$\frac{y}{u} = \frac{2}{s^2 + s + 1} \qquad 9.4.1$$

It is desired to track the model

$$\frac{y_m}{u_m} = \frac{1}{s + 1} \qquad 9.4.2$$

with the error state

$$e = y - y_m \qquad 9.4.3$$

The transfer function of the error system is

$$e = \frac{(s + 1)\, u - (s2 + s + 1) u_m}{s^3 + 2s^2 + 2s + 1} \qquad 9.4.4$$

A non-minimal form for the error system is

$$\begin{bmatrix} s^3u \\ s^2u \\ su \\ s^3u_m \\ s^2u_m \\ su_m \\ s^3e \\ s^2e \\ se \end{bmatrix} = \begin{bmatrix} 0&0&0&0&0&0&0&0&0 \\ 1&0&0&0&0&0&0&0&0 \\ 0&1&0&0&0&0&0&0&0 \\ 0&0&0&0&0&0&0&0&0 \\ 0&0&0&1&0&0&0&0&0 \\ 0&0&0&0&1&0&0&0&0 \\ 0&1&1&-1&-1&-1&-2&-2&-1 \\ 0&0&0&0&0&0&1&0&0 \\ 0&0&0&0&0&0&0&1&0 \end{bmatrix} \begin{bmatrix} s^2u \\ su \\ u \\ s^2u_m \\ su_m \\ u_m \\ s^2e \\ se \\ e \end{bmatrix} + \begin{bmatrix} 1 \\ 0 \\ 0 \\ 0 \\ 0 \\ 0 \\ 0 \\ 0 \\ 0 \end{bmatrix} s^3u + \begin{bmatrix} 0 \\ 0 \\ 0 \\ 1 \\ 0 \\ 0 \\ 0 \\ 0 \\ 0 \end{bmatrix} s^3u_m \qquad 9.4.5$$

In the design of the optimal controller, if the system is placed in the non-minimal state space format, then it can be seen that the new system matrix is uncontrollable. Thus the solution described in Section 9.2.2 can not directly be applied as Kalman's conditions for a complete solution to the Riccati equation require that the system matrices must be controllable.

To overcome the problem of uncontrollability, the system matrices can be transformed such that they are in the format described by (9.2.29). This will produce a component of the system matrices which consists of two components. They are

1) A component which is controllable and a controller must be designed for it.
2) An uncontrollable but marginally stable component for which a controller does not need to be designed.

In this format the solution to the model following problem described in Section 9.2.2 can now be applied.

Since the new system matrix is comprised of the system and the model, it is known that the uncontrollability is due to the fact that the input of the system cannot affect the output of the model. But since it is known that the model is marginally stable, controlling it is of no real relevance to the output of the system.

Thus an alternative method is not to transform the system matrices but merely treat the problem as a generalised eigenvalue problem. Thus only the components of the P matrix which affect the gain matrix K will determined. This means that the solution to the Riccati equation is optimal for only these components of the P matrix. We are not necessarily concerned with the determining the values of the other components of the P matrix since they do not affect the gain matrix. This method will be used to design an output feedback model following controller for the gantry crane system. A Matlab algorithm for this solution is given in appendix B.

As will be shown in the following section, the structure of the controller will consist of an output feedback controller and a feedforward controller. The feedforward component results because the model's input and its derivative are used as system states. This is an advantage because most feedback controllers rely on a change in the system's output before there is an error between the desired output and the system's output, and then the controller can attempt to compensate for the error. With feedforward control certain system states may react to an input change prior to the output being affected. Thus, feedforward control can minimise the transient error.

Non-minimal state space representation provides a valid means for representing a system in terms of its input and output. The one difficulty with this representation lies in the fact that the system matrices tend to be much larger then in a classical state space representation. Nevertheless with today's computing power large matrices are handled easily.

Also, the numerical problems using this state space representation tend to be ill-conditioned. This can be overcome by balancing prior to feedback / feedforward gain calculations.

9.5 CONTROLLER DESIGN

Sections 9.3 - 9.4 describes a method of placing a system into non-minimal state space representation such that an output feedback model following controller can be designed. Appendix B contains an algorithm for solving the LQR problem if the system is uncontrollable. Thus, an optimal output feedback model following controller can now be designed for the gantry crane system.

In this section a controller will be designed such that the cart's trajectory will follow a predefined model. Also since swing cancellation is a predominate feature of any crane controller, a controller for the swing angle will also be designed such that when the cart reaches its setpoint, the swing angle will be zero.

Unlike the previous sections that dealt with sliding mode control, in this section an integrator was not added to reduce the effects of steady state error. It is good practice to include an integrator in the controller design even when the system has an integrator. An integrator was not added into the controller design in order to determine how well the integrator in the system coupled with the controller (implemented as a transfer function) will compensate for the steady state error. Also the introduction of the integrator would increase the order of the system matrices significantly.

From Chapter 3 the model of the crane with a rope length equal to 1 m is:

$$\begin{bmatrix} \dot{x}_1 \\ \dot{x}_2 \\ \dot{x}_3 \\ \dot{x}_4 \end{bmatrix} = \begin{bmatrix} 0 & 1 & 0 & 0 \\ 0 & -5.73 & 1.014 & 0 \\ 0 & 0 & 0 & 1 \\ 0 & 5.73 & -10.81 & 0 \end{bmatrix} \begin{bmatrix} x_1 \\ x_2 \\ x_3 \\ x_4 \end{bmatrix} + \begin{bmatrix} 0 \\ 0.7376 \\ 0 \\ -0.7376 \end{bmatrix} u \qquad 9.5.1$$

where

x_1 = cart position = x x_2 = cart velocity = $\dot{x} = \dot{x}_1$

x_3 = swing angle = θ x_4 = swing velocity = $\dot{\theta} = \dot{x}_3$

u = the applied motor voltage

The transfer functions for the position of the cart and the swing angle are

$$\frac{y_c}{u} = \frac{0.7376s^2 + 7.2288}{s^4 + 5.7312s^3 + 10.8142s^2 + 56.1660s} \qquad 9.5.2$$

$$\frac{y_s}{u} = \frac{-0.7376s^2}{s^4 + 5.7312s^3 + 10.8142s^2 + 56.1660s} \qquad 9.5.3$$

where y_c and y_s are the outputs of the cart position and swing angle respectively and u is the input.

It is desired that the cart reaches setpoint at approximately 6 sec. and exhibits a first order response. Thus, there is no great instantaneous change and a large control voltage, unlike a step response where the sudden change in setpoint produces a large control voltage, and it is desired that the swing angle be zero when the cart reaches set point (i.e. steady state for the model).

Thus a suitable candidate for a model for which the cart to follow is

$$\frac{y_m}{u_m} = \frac{1}{s+1} \qquad 9.5.4$$

Since it is desired for the swing angle to have no oscillations then its model is

$$\frac{y_m}{u_m} = 0 \qquad 9.5.5$$

Now two error models will be constructed, one for the cart's trajectory and another for the swing angle. The error models are

$$e_1 = y_c - y_m \qquad 9.5.6$$

$$e_2 = y_s - 0 \qquad 9.5.7$$

From (9.5.2) - (9.5.7), we have

$$e_1 = \frac{(0.7376s^2 + 7.2288)u}{s^4 + 5.7312s^3 + 10.8142s^2 + 56.1660s} - \frac{1u_m}{s+1} \qquad 9.5.8$$

$$e_1 = \frac{TF_1u - TF_2u_m}{s^5 + 6.7312s^4 + 16.5454s^3 + 66.9802s^2 + 56.1660s} \qquad 9.5.9$$

where

$$TF_1 = 0.7376s^3 + 0.7376s^2 + 7.2288s + 7.2288$$

$$TF_2 = s^4 + 5.7312s^3 + 10.8142s^2 + 56.1660s$$

$$e_2 = \frac{-0.7376s^2 u}{s^4 + 5.7312s^3 + 10.8142s^2 + 56.1660s} \qquad 9.5.10$$

Now the full non-minimal state space model is

$$\begin{bmatrix} \dot{x}_1 \\ \dot{x}_2 \\ \dot{x}_3 \\ \dot{x}_4 \end{bmatrix} = \begin{bmatrix} A_{11} & 0 & 0 & 0 \\ 0 & A_{22} & 0 & 0 \\ A_{31} & A_{32} & A_{33} & 0 \\ A_{41} & 0 & 0 & A_{44} \end{bmatrix} \begin{bmatrix} x_1 \\ x_2 \\ x_3 \\ x_4 \end{bmatrix} + \begin{bmatrix} B_1 \\ 0 \\ 0 \\ 0 \end{bmatrix} s^5 u + \begin{bmatrix} 0 \\ B_2 \\ 0 \\ 0 \end{bmatrix} s^5 u_m \qquad 9.5.11$$

where

$$x_1 = \begin{bmatrix} s^4 u \\ s^3 u \\ s^2 u \\ su \\ u \end{bmatrix} \quad x_2 = \begin{bmatrix} s^4 u_m \\ s^3 u_m \\ s^2 u_m \\ su_m \\ u_m \end{bmatrix} \quad x_3 = \begin{bmatrix} s^4 e_1 \\ s^3 e_1 \\ s^2 e_1 \\ se_1 \\ e_1 \end{bmatrix} \quad x_4 = \begin{bmatrix} s^3 e_2 \\ s^2 e_2 \\ se_2 \\ e_2 \end{bmatrix}$$

$$\dot{x}_1 = \begin{bmatrix} s^5 u \\ s^4 u \\ s^3 u \\ s^2 u \\ su \end{bmatrix} \quad \dot{x}_2 = \begin{bmatrix} s^5 u_m \\ s^4 u_m \\ s^3 u_m \\ s^2 u_m \\ su_m \end{bmatrix} \quad \dot{x}_3 = \begin{bmatrix} s^5 e_1 \\ s^4 e_1 \\ s^3 e_1 \\ s^2 e_1 \\ se_1 \end{bmatrix} \quad \dot{x}_4 = \begin{bmatrix} s^4 e_2 \\ s^3 e_2 \\ s^2 e_2 \\ se_2 \end{bmatrix}$$

$$A_{11} = A_{22} = \begin{bmatrix} 0 & 0 & 0 & 0 & 0 \\ 1 & 0 & 0 & 0 & 0 \\ 0 & 1 & 0 & 0 & 0 \\ 0 & 0 & 1 & 0 & 0 \\ 0 & 0 & 0 & 1 & 0 \end{bmatrix} \qquad A_{31} = \begin{bmatrix} 0 & 0.74 & 0.74 & 7.23 & 7.23 \\ 0 & 0 & 0 & 0 & 0 \\ 0 & 0 & 0 & 0 & 0 \\ 0 & 0 & 0 & 0 & 0 \\ 0 & 0 & 0 & 0 & 0 \end{bmatrix}$$

$$A_{32} = \begin{bmatrix} -1 & -5.73 & -10.81 & -56.17 & 0 \\ 0 & 0 & 0 & 0 & 0 \\ 0 & 0 & 0 & 0 & 0 \\ 0 & 0 & 0 & 0 & 0 \\ 0 & 0 & 0 & 0 & 0 \end{bmatrix} \quad A_{33} = \begin{bmatrix} -6.73 & -16.54 & -66.98 & -56.17 & 0 \\ 1 & 0 & 0 & 0 & 0 \\ 0 & 1 & 0 & 0 & 0 \\ 0 & 0 & 1 & 0 & 0 \\ 0 & 0 & 0 & 1 & 0 \end{bmatrix}$$

$$A_{41} = \begin{bmatrix} 0 & 0 & -0.74 & 0 & 0 \\ 0 & 0 & 0 & 0 & 0 \\ 0 & 0 & 0 & 0 & 0 \\ 0 & 0 & 0 & 0 & 0 \\ 0 & 0 & 0 & 0 & 0 \end{bmatrix} \quad A_{44} = \begin{bmatrix} -5.73 & -10.81 & -56.17 & 0 \\ 1 & 0 & 0 & 0 \\ 0 & 1 & 0 & 0 \\ 0 & 0 & 1 & 0 \end{bmatrix}$$

$$B_1 = B_2 = \begin{bmatrix} 1 \\ 0 \\ 0 \\ 0 \\ 0 \end{bmatrix}$$

In the design of the controller using the LQR technique, it is noted that only the states relating to the respective error signals need to be compensated for by weights in the Q matrix, and since the input signal is the fifth derivative of the actual control signal this does not require a heavy weighting.

Thus, using the technique described in the previous section and after many simulations using different weightings for the Q and the R matrices a satisfactory controller can be designed with the following Q and R matrices.

```
Q = zeros(19,19);
Q(11,11)=0;
Q(12,12)=0;
Q(13,13)=1; this weights the second derivative of the e1 state slightly
Q(14,14)=10; this weights the first derivative of the e1 state heavily
Q(15,15)=100; this weights the e1 state the most
Q(18,18)=10; this weights the first derivative of the e1 state heavily
Q(19,19)=100; this weights the e2 state the most
Q=Q*100;
```

The weighting of the fifth derivative of the control input is minimal to provide for a faster settling time. Therefore the R matrix was chosen to be R=0.0001

The feedback gains that are produced by using the above Q and R matrices are:

$$K = [\ K_1 \quad 0\ 0\ 0\ 0\ 0\ K_2 \quad K_3\ ] \qquad 9.5.12$$

where

$$K_1 = [14.6 \quad 106.3 \quad 376.9 \quad 1104.7 \quad 813.4]$$
$$K_2 = [141.9 \quad 1003 \quad 2601.4 \quad 9771.9 \quad 10000]$$
$$K_3 = [-17.5 \quad -1269.1 \quad -185.8 \quad -450.4]$$

Since the control input is s^5u then the feedback controller is as follows

$$s^5u = -Kx \qquad 9.5.13$$

Thus, the controller as a transfer function is

$$u = \frac{-TF_3\, e_1 - TF_4\, e_2}{s^5 + 14.6s^4 + 106.3s^3 + 376.9s^2 + 1104.7s + 813.4} \qquad 9.5.14$$

where

$$TF_3 = (141.9s^4 + 1003s^3 + 2601.4s^2 + 9771.9s + 10{,}000)$$

$$TF_4 = (-170.5s^3 - 1269.1s^2 - 185.8s + 450.4)$$

The next point to consider is the location of the closed loop poles. All the closed loop poles should be stable except for those relating to model. These poles lie at (0,0i) because they cannot be directly controlled from the input into the system.

Thus, the closed loop poles of the system are:

P_1 = -0.8286 + 3.8671i	P_2 = -0.8286 - 3.8671I	P_3 = -1.0818 + 2.5331I
P_4 = -1.0818 - 2.5331I	P_5 = -2.3316 + 2.1567i	P_6 = -2.3316 - 2.1567i
P_7 = -3.1029 + 1.0528i	P_8 = -3.1029 - 1.0528I	P_9 = -5.6246
P_{10} = -5.5931	P_{11} = -0.069035 + 3.1682i	P_{12} = -0.0690 - 3.1682i
$P_{13} = -4.2124*10^{-16}$	P_{14} = -1.0000	P_{15} = 0
P_{16} = 0	P_{17} = 0	P_{18} = 0
P_{19} = 0		

As can be seen P_1 - P_{13} are all stable and relate to the error states of the system. Pole P_{14} is the pole of the model itself, and poles P_{15} - P_{19} are the five states that relate to the model input and cannot be controlled from this input.

The key aspect to note about (9.5.14) is that there is no feedforward term, that is a term which is related to the model input. This is brought about because of the integrator in the transfer function(9.5.2) and (9.5.3).

The only way in which the error can be zero if there is an integrator in the forward path is if the input into the integrator is zero. Thus the error signal must be zero. For this reason the controller does not have any terms associated with the model input.

Consider the following simple example. Let the plant be defined as an integrator

$$\frac{y}{u} = \frac{1}{s} \qquad 9.5.15$$

Now let the model that the plant is desired to follow be

$$y_m = u_m \qquad 9.5.16$$

Thus the non-minimal state space representation in terms of the error ($y - y_m$) is

$$\begin{bmatrix} \dot{u} \\ \dot{u}_m \\ \dot{e} \end{bmatrix} = \begin{bmatrix} 0 & 0 & 0 \\ 0 & 0 & 0 \\ 1 & 0 & 0 \end{bmatrix} \begin{bmatrix} u \\ u_m \\ e \end{bmatrix} + \begin{bmatrix} 1 \\ 0 \\ 0 \end{bmatrix} \dot{u} + \begin{bmatrix} 0 \\ 1 \\ 0 \end{bmatrix} \dot{u}_m \qquad 9.5.17$$

Substituting $A = \begin{bmatrix} 0 & 0 & 0 \\ 0 & 0 & 0 \\ 1 & 0 & 0 \end{bmatrix}$ $B = \begin{bmatrix} 1 \\ 0 \\ 0 \end{bmatrix}$ $Q = \begin{bmatrix} 0 & 0 & 0 \\ 0 & 0 & 0 \\ 0 & 0 & 1 \end{bmatrix}$ $R = 1$ into the Riccati equation defined by (9.4.37) gives

$$\begin{bmatrix} (P_{31} + P_{13} - P_{11}^{\,2}) & (P_{32} - P_{11}P_{12}) & (P_{33} - P_{11}P_{13}) \\ (P_{23} - P_{21}P_{11}) & (-P_{21}P_{12}) & (-P_{21}P_{13}) \\ (P_{33} - P_{31}P_{11}) & (-P_{31}P_{12}) & (-P_{31}P_{13} + 1) \end{bmatrix} = 0 \qquad 9.5.18$$

To determine the values of the P matrix start by considering the equation

$$-P_{31}P_{13}+1=0 \qquad 9.5.19$$

This implies that neither P_{31} nor P_{13} can be zero. This is because they are inversely proportional to one another. Thus, if either P_{31} or P_{13} is zero then the other is infinite.

Now consider the following equations

$$-P_{21}P_{13} = 0 \quad -P_{31}P_{12} = 0 \quad -P_{31}P_{12} = 0 \qquad 9.5.20$$

From the fact that neither P_{31} nor P_{13} can be zero it follows that P_{12} and P_{21} are zero.

Now consider the following equations

$$P_{31} + P_{13} - P^2_{11} = 0 \qquad 9.5.21$$

$$P_{33} - P_{31}P_{11} = 0 \qquad 9.5.22$$

$$P_{33} - P_{13}P_{11} = 0 \qquad 9.5.23$$

substituting (9.5.22) into (9.5.23) gives

$$P_{31}P_{11} - P_{13}P_{11} = 0 \qquad 9.5.24$$

$$P_{11}(P_{31} - P_{13}) = 0 \qquad 9.5.25$$

Equation (9.5.25) implies that either P_{11} or $(P_{31} - P_{13})$ must equal zero. From (9.5.21) it can be seen that P_{11} cannot be zero. Because if P_{11} was zero then (9.5.21) would imply that $P_{31} = -P_{13}$ and from (9.5.19) it can be seen that this is not true. Thus, P_{11} cannot equal zero. So for (9.5.25) to be true then

$$(P_{31} - P_{13}) = 0 \qquad 9.5.26$$

This then implies that for (9.5.19) and (9.5.26) to hold, then $P_{31} = 1$ and $P_{13} = 1$. Thus substituting $P_{31} = 1$ and $P_{13} = 1$ into (9.5.21) gives $P_{11} = \pm\sqrt{2}$. Since P is positive definite then $P_{11} = \sqrt{2}$. Substituting the values of P_{11} and P_{13} into (9.4.23) give $P_{33} = \sqrt{2}$.

Now all the coefficients in the P matrix have been found except for P_{22} and P_{32}. Thus the P matrix is as follows.

$$P = \begin{bmatrix} \sqrt{2} & 0 & 1 \\ 0 & x & 0 \\ 1 & x & \sqrt{2} \end{bmatrix} \qquad 9.5.27$$

The question is, 'do the values of P_{22} and P_{32} play any significant role in the determination of the feedback gain matrix K?'

It was stated previously that $K = R^{-1}B'P$. Observing this equation with the respective values of R, B and P gives

$$K = 1\begin{bmatrix} 1 & 0 & 0 \end{bmatrix}\begin{bmatrix} \sqrt{2} & 0 & 1 \\ 0 & x & 0 \\ 1 & x & \sqrt{2} \end{bmatrix} \qquad 9.5.28$$

Observing (9.5.28) reveals that the values of P_{22} and P_{32} are meaningless in the determination of the K matrix, since they will be multiplied by zero. Thus the final solution for the feedback gain matrix K is

$$K = [\sqrt{2} \;\; 0 \;\; 1] \qquad 9.5.29$$

From this simple example it is concluded that when an integrator exists in the plant, the feedback gains which are associated with the model input and thus the feedforward path are zero. This means that there is no feedforward term in the overall controller structure for a plant which has an integrator in its forward path.

Note that in the above example the method for determining the coefficients of the P matrix requires observation of the set of equations that are produced from the Riccati equation. In Appendix B, the Matlab routine for the determination of the P an K matrix is given. The routine yields the same P and K matrix as given by (9.5.28) and (9.5.29).

CHAPTER 10 SIMULATION AND IMPLEMENTATION OF THE MODEL FOLLOWING CONTROLLER

This chapter contains a discussion of the simulation and the implementation of the controller designed in Chapter 9, a comparison between the sliding mode controller implemented in Chapter 6 and the implementation of the output feedback model following controller designed in Chapter 9, and a description of how the output feedback controller can be implemented as a sliding mode controller.

The output feedback controller designed in Chapter 9 deals solely with cart positioning and swing cancellation. In order to incorporate a gain scheduling of the rope length, one needs to solve the Riccati equation described in Chapter 9 in terms of rope length variable ℓ. This would become quite mathematically complex and thus was not attempted.

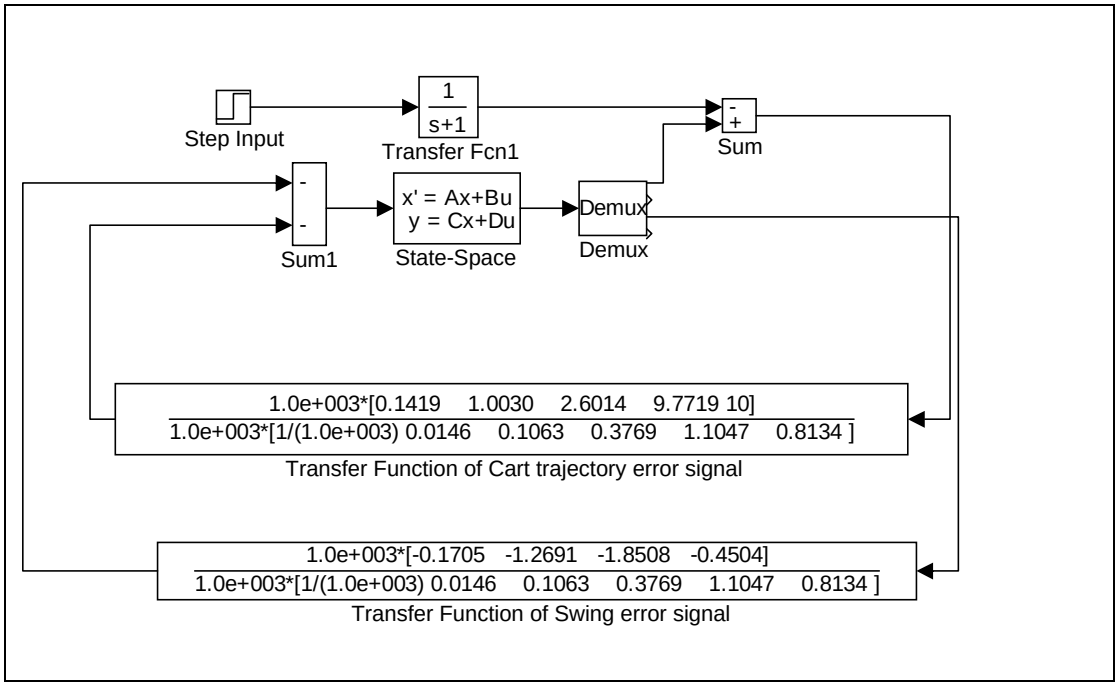

Figure 10.1 Block diagram of output feedback controller

10.1 SIMULATION OF THE MODEL FOLLOWING CONTROLLER

10.1.1 CART RESPONSE

The positioning of the cart in the control of a crane system is of utmost importance, as it is desired that the cart be moved to a known setpoint at which the goods are to be raised or lowered. With the sliding mode implementation, the cart's position is determined by a step function setpoint change. This produces a sharp instantaneous control signal and in an industrial application this is clearly not practical because

1) The cart cannot react to the sharp and sudden changes that are requested by the control signal.
2) Even if the cart can react to sharp and sudden changes that are requested by the control signal, this may cause the goods to swing very vigorously which could be dangerous.

Thus, the cart should follow a gradually changing setpoint such as a first order step response. This then produces a control signal that requests the cart to move smoothly and gradually as the setpoint changes, eliminating any sudden changes in the control signal.

The cart’s response should have little (as in Chapter 6) or no overshoot. Basically a critically damped response is required.

Simulating different Q and the R weighting matrices, (using the non-minimal state space representation and using the method described in Chapter 9 to develop a linear quadratic regulator) a critically damped response could not be achieved, thus requiring a compromise between the level of overshoot and the required settling time. This determined the Q and R weighting matrices given in Section 9.5.

Figure 10.1.1 illustrates the cart’s position as it follows the model. Notice that the level of overshoot from the steady state value of the model (i.e. cart’s final setpoint) is minimal, and the settling time is just under 6 sec.

In comparison with the sliding mode approach where the cart settles in approximately 5 sec., the trade off with the output feedback controller of a slightly longer settling time and virtually no overshoot becomes apparent. Even in the design of the sliding mode controller in Chapter 6 faster settling time was traded off against overshoot. Though the level of overshoot was quite small, it produced a slightly shorter settling time.

Overall the cart's response is quite adequate for a real-time implementation of the controller and the settling time is not vastly different from that of the sliding mode controller.

10.1.2 SWING ANGLE

One of the main advantages of using output feedback control is that a separate observer design is not needed. This advantageous feature also produces a disadvantage that is highlighted by Figure 10.1.2. The swing angle has a longer settling time and is not as smooth as Figure 6.1.2.

From Figure 10.1.2 it can be seen that the settling time of the swing angle is approximately 10 sec. But within the period from 6 to 10 sec. the swing angle is very small and in a real-time implementation these small angles are effectively zero. The lengthy delay in the complete cancellation of the swing angle is caused because overshoot was traded off against settling time.

10.1.3 CONTROL EFFORT

The most important aspect of the output feedback model following controller becomes apparent when one looks at the control effort or the control signal. Since the model's output is gradually changing with respect to time, the controller does not produce a sharp change in the control signal. Unlike the sliding mode controller where the setpoint was designated by a step change which produced sharp changes in the control signal.

Because the cart's position is required to follow a first order response, the control signal is gradually changing as the error between the model's and the system's output becomes apparent to the controller. Since the controller is a transfer function it also acts as a filter for the control signal which in turn will provide for a nice smooth control signal.

Thus, for practical applications where sharp changes to the control input are not desired, this method of designing a controller clearly has a distinct advantage.

Note that in Figure 6.1.3 there was an instantaneous voltage of 4.5 V applied to the motor, which in practice corresponds to approximately 8 V to compensate for the dead band region. These quick changes would also cause a change in the swing angle that could be viewed as noise in practice. This will be discussed latter in the real-time implementation.

A key point to note is that beyond the 0.5 second mark (i.e. time = 0.5 sec.), the waveform of this control signal is virtually identical to that of the sliding mode controller Figure 6.1.3. Thus, once the system is in motion and the system states are moving towards their respective setpoint, the control action is the same for both the output feedback controller and the sliding mode controller.

Cart and model step response

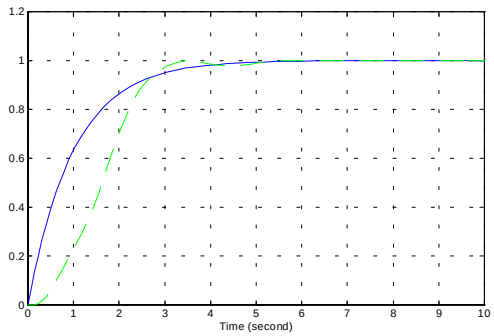

Figure 10.1.1

Swing angle step response

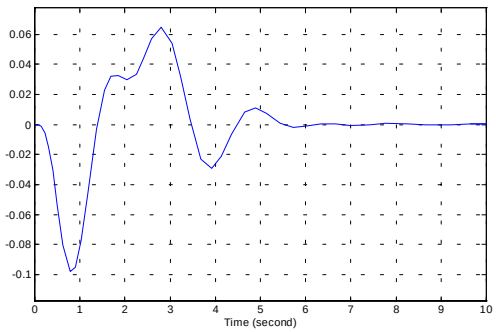

Figure 10.1.2

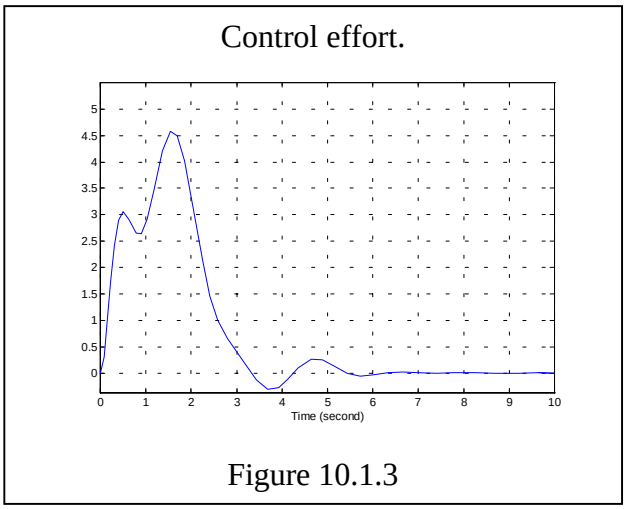

Figure 10.1.3

10.2 REAL-TIME IMPLEMENTATION

A comparison between the sliding mode controller implemented in Chapters 6 and 8, and the output feedback model following controller is given in this section.

Unlike the sliding mode controllers implemented in Chapters 6 and 8 which required an alpha-beta filter to estimate the cart and swing velocities, the output feedback controller does not require the design of a separate state observer or estimator for the unavailable states. Thus, it should be easier to implement in real-time.

It is noted that the system has an integrator in the forward path. Even though it is good practice to include some form of integral control to eliminate steady state error and not to rely on integrators which may be present in the system's structure, additional integral control was not added into the output feedback controller's structure, unlike the design of the sliding mode controller. This was done to determine if the integrator in the plant coupled with using a dynamic controller would alleviate any steady state error.

For completeness, the hunting and dead band compensation used in this section are the same as Section 6.4.

10.2.1 CART RESPONSE

Figure 10.2.1 illustrates the reasonably accurate tracking of the desired first order response despite the fact that a dynamic linear controller is being used to control the non-linear crane system and a fourth order system is asked to follow a first order response. As with most linear controllers they require an accurate model of the real-time system in order for the real-time system to reflect the simulated system.

Comparing the simulated step response of the cart Figure 10.1.1, it can be seen that the real-time system has a slightly higher overshoot then the simulated system. This is because errors which arise from the non-linearities in the real-time system take time to be compensated for by the controller, since robustness in the presence of non-linearities was not built into the controller design. This leads to higher overshoot as can be seen in Figure 10.2.1.
Since the system is fourth order, the level of overshoot could be minimised if a fourth order model was the required model for the system to follow. Nevertheless, the purpose of this experiment was to prove that there is no need for the perfect model matched conditions as described by Young [16].

It has also been shown that the real-time system does exhibit very similar characteristics to the simulated system, which means that the model of the real-time system is quite accurate.

10.2.2 SWING ANGLE

One of the key features of using the output feedback controller implemented as a transfer function is that it produces a smoother control signal. This is because the transfer function can be seen as a filter for the control signal. Figure 10.2.2 illustrates the swing angle. It is clear from this figure that the swing angle appears to exhibit a much more sinusoidal motion than that of the sliding mode controller in Chapter 6 and 8. This is because even though there is still noise on the swing angle signal the control signal is smoother and does not fully attempt to compensate for the noise, unlike the sliding mode controller.

Since the sliding mode controller in Chapter 6 and 8 is a more robust controller it attempts to compensate for any disturbances, even noise. This produces a noisier control signal which induces a quick change in the direction of the swing angle which in turn can be viewed as noise.

The simulated response of the swing angle Figure 10.1.2 and the real-time response of the swing angle are virtually identical. Note that they both have approximately the same settling time. The real-time response of the swing angle has a constant value between 2 and 2.4 sec. and then increases again to a value of 0.1 rad. This is also seen by the simulated system where the swing angle's value is constant between 1.5 to 2 sec. and then increase to a value of 0.06 rad. The real-time system displays slightly higher values, because of the linearisation that was performed in developing the model.

In Figure 10.2.1 it was noted that the overshoot was also slightly higher than for the simulated system. Note that the time from which the overshoot occurs is also the time frame in which the swing angle is slightly higher then that for the simulated system. Thus the increase in swing angle may be attributed to the cart's overshoot because the controller is not adjusting rapidly enough to the cart's motion.

Between 7 - 7.2 sec. the swing value moves outside the band that was specified to compensate for hunting. This produces a control acting to compensate for the swing angle and as can be seen from Figure 10.1.1 the cart moves slightly in order to cancel the swing angle. This characteristic is also observed between 9.6 and 10 sec.
Note that the initial value of the swing angle is not exactly zero. This is because the cart has slightly moved and thrown the initial condition slightly out before the controller could be started.

Even though Figure 10.2.2 displays a noisy signal, the overall performance of the controller does not seem to be greatly affected, and the real-time response tends to match the simulated response quite adequately.

10.2.3 CONTROL EFFORT

As was stated previously, one of the key features of using a transfer function as a controller is that it provides filtering of the control signal. Figure 10.2.3 illustrates the real-time control signal. Note that this signal is significantly smoother than that of the sliding mode controller in Chapter 6 and 8. This smoother signal may be seen as advantageous, because it produces smoother motion of the cart and the swing angle.

In the sliding mode approach, the control signal is noisier because of the robustness of the controller as it is attempting to compensate for any disturbances and because it uses all the states of the system in calculating the control signal. Because the velocities have only been very basically estimated they are noisy and this also contributes to the noisy control signal.

The most important aspect of model following can be observed by Figure 10.2.3 and that is a slowing increasing control signal. Unlike the sliding mode controller where the step change caused an instantaneous and large initial voltage of approximately 5 V, the output feedback model following produces a signal which gradually increases to 5 V.

This is because as the error between the model and the system is slowly increasing it produces a slowly increasing control signal.

Note once again that between 7 - 7.2 sec. there is a slight kick given by the controller, because the swing angle has gone outside the bounds defined for the hunting compensation. Note also that the negative voltages are much larger then those simulated, because a voltage of -4.5 V was added to compensate for any dead band which is quite large in this direction.

As the initial error values are quite small the control signal is small and because of the dead band region it takes some time before the cart actually moves. Even though the cart’s position and swing angle is not completely zero at the start, there is still a slight time delay before an ample voltage can be reached in order to move the cart. Nevertheless, Figure 10.2.3 has a very similar waveform to that of the simulated system in Figure 10.1.3.

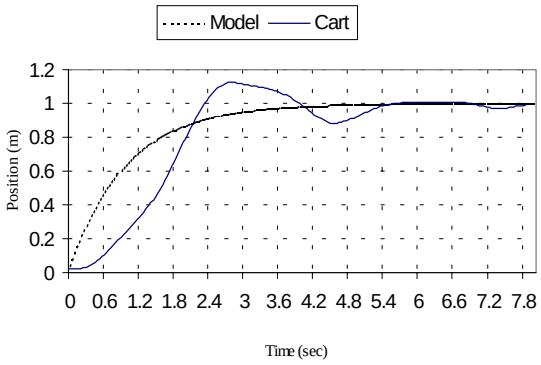

Figure 10.2.1

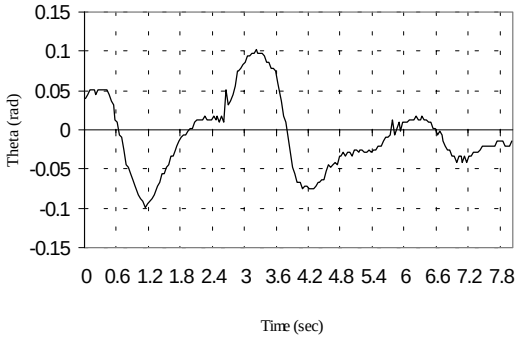

Figure 10.2.2

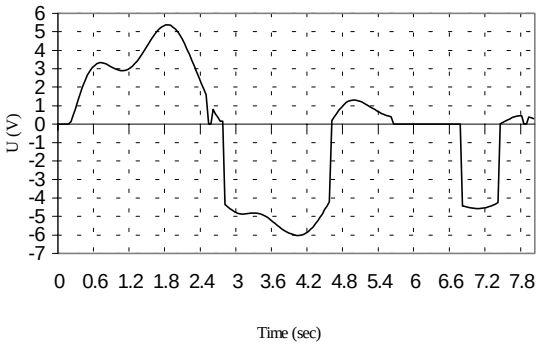

Figure 10.2.3

10.3 OUTPUT FEEDBACK SLIDING MODE CONTROL

Throughout this thesis, state feedback sliding mode control has been observed to be robust in the presence of bounded uncertainties and matched disturbances. To achieve some level of robustness in the output feedback model following controller it would be desirable to incorporate sliding mode action. Jiang, Hesketh and Clements [9] proposed output feedback model following sliding mode control based on a non-minimal state space model and using H_∞ design techniques. This controller has elements of a PI structure.

Since the aim of this thesis is to design and implement a robust non-linear controller for the gantry crane system, it is proposed that the method described by Jiang, Hesketh and Clements [9] be used to design a controller for the real-time crane system. However, the method in [9] only deals with a SISO system and since the crane is a MIMO system, this method needs to be modified to cater for the MIMO system. In this section the modifications needed are described.

The method described in this section produces a controller that is non-linear and robust in the presence of a wide variety of uncertainties and disturbances because it is designed by a combination of H_∞ and sliding mode control techniques. Since the controller produced will be in output feedback format (i.e. dynamic controller), it will retain the properties of the output feedback model following controller described in Chapter 9. These mainly are, the lack of need to have all states available and filtering of the control signal.

If a change in rope length is viewed as an external disturbance on the cart and swing dynamics, then a controller for cart setpoint control and swing cancellation which is robust with a varying rope length can be achieved via the method described in [9] with the appropriate modification. In this section rope length control is achieved using the controller described in Chapter 7. Thus, all three dynamics are controlled.

10.3.1 CONTROLLER DESIGN

The controller design described here is based on [9]. Consider the system

$$[D(s) + \Delta D(s)]y(t) = [N(s) + \Delta N(s)]u(t) + d(t) \qquad 10.3.1$$

and the error signal

$$e(t) = y(t) - y_r(t) \qquad 10.3.2$$

where

$y_r(t)$ is a given reference signal that the system is desired to track.

The system 10.3.1 can be represented in non-minimal format as

$$\dot{x} = (A + \Delta A(t))x(t) + B_1 u(t) + B_2[\,\hat{d}(t) - \hat{y}_r(t)\,] \qquad 10.3.3$$
$$y(t) = Cx(t)$$

where

$$x(t) = \left[e(t)\ \ \dot{e}(t) \ldots e^{(n-1)}(t)\,,\, u(t)\ \ \dot{u}(t) \ldots u^{(n-1)}(t) \right]^T$$

$$\hat{d}(t) = d(t) - \Delta D(s) y_r(t)$$
$$\hat{y}_r(t) = D(s) y_r(t)$$
$$\Delta A(t) = B_2 F_1 \Delta(t) H_2$$

To develop a robust controller it is desired that H_∞ control techniques be used. Thus, by adding a measurement signal z(t) and introducing F_2, H_1 and E for performance specification and input disturbance rejection, the system given in (10.3.3) can be written as

$$\dot{x} = Ax(t) + F\begin{bmatrix} w_1(t) \\ w_2(t) \end{bmatrix} + B_1 u(t)$$

$$\begin{bmatrix} z_1(t) \\ z_2(t) \end{bmatrix} = Hx(t) + Eu(t) \qquad 10.3.4$$

$$w_2(t) = \Delta(s)\, z_2(t)$$

where w_1 is an external signal including the disturbance and

$$F = [F_2 \ \ F_1], \qquad H = \begin{bmatrix} H_1 \\ H_2 \end{bmatrix}, \qquad E = \begin{bmatrix} \alpha \\ 0 \\ : \\ : \\ 0 \end{bmatrix}, \quad H^T E = 0$$

Now, if there exists a P > 0 satisfying the Riccati equation

$$0 = PA + A^{T}P + P\left(\frac{1}{\gamma^{2}} F D^{-1} F^{T} - \frac{1}{\alpha^{2}} B_1 B_1^{T}\right)P + H^{T} D H \qquad 10.3.5$$

where D is a scaling matrix, let the control law is given as

$$u^{(n)}(t) = -Kx(t) = -L(s)e(t) - P(s)u(t) \qquad 10.3.6$$

where

$$K = \frac{1}{\alpha^{2}} B_1^{T} P \qquad 10.3.7$$

and P is the solution to (10.3.5)

By rearranging (10.3.6), an output feedback control is given as

$$u(t) = \frac{L(s)}{s^{n} + P(s)} e(t) + \hat{y}_r(t) \qquad 10.3.8$$

Thus, a suitable output feedback sliding mode controller is a given as

$$u(t) = \left(f_1(t) + \frac{f_2(t)}{s}\right) f_3(t) + \hat{y}_r(t) \qquad 10.3.9$$

where $f_1(t)$ and $f_2(t)$ are bounded positive non-linear functions,

$$f_3(t) = \frac{\beta L(s)}{s^{n} + \beta P(s)} e(t) \qquad 10.3.10$$

and $\beta>1$ is a high gain function which forces the states of the closed loop system on to the sliding surface.

Since it is desired to control all three dynamics of the gantry crane system, a non-minimal state space representation of the cart position and swing angle which includes external disturbances will be developed. The disturbances on the system dynamics are caused by a change in the rope length.

It is important in using this approach that the plant be controllable and observable under all admissible modelling uncertainties. It is known that the non-minimal model developed in Chapter 9 is uncontrollable because the input signal of the reference model and it's derivatives are used as system states when the non-minimal state space model was developed. Thus, a new non-minimal state space model needs to be constructed without using the input signal of the reference model and its derivatives as states.

From Chapter 9 the transfer functions for the position of the cart and the swing angle are

$$\frac{y_c}{u} = \frac{0.7376s^2 + (7.2288 + \partial_1)}{s^4 + 5.7312s^3 + (10.8142 + \partial_2)s^2 + (56.1660 + \partial_3)s} \qquad 10.3.11$$

$$\frac{y_s}{u} = \frac{(-0.7376 + \partial_4)s^2}{s^4 + 5.7312s^3 + (10.8142 + \partial_2)s^2 + (56.1660 + \partial_3)s} \qquad 10.3.12$$

where $\partial_1 ... \partial_4$ are the disturbances caused by a change in the rope length and u, y_c and y_s are the inputs and outputs of the cart position and swing angle respectively.

Thus the error model for the cart and swing are

$$e_1 = y_c - y_{r1} = \frac{0.7376s^2 + (7.2288 + \partial_1)}{s^4 + 5.7312s^3 + (10.8142 + \partial_2)s^2 + (56.1660 + \partial_3)s} u - y_r \qquad 10.3.13$$

$$e_2 = y_s - y_{r2} = \frac{(-0.7376 + \partial_4)s^2}{s^4 + 5.7312s^3 + (10.8142 + \partial_2)s^2 + (56.1660 + \partial_3)s} u \qquad 10.3.14$$

where

$y_{r1} = \frac{1}{s+1} u_m =$ the output reference signal that the cart is desired to follow

$y_{r2} = 0 =$ the output reference signal that the swing angle is desired to follow

From (10.3.13) and (10.3.14) a non-minimal state space representation of the system is

$$\begin{bmatrix} us^4 \\ us^3 \\ us^2 \\ us \\ e_1s^4 \\ e_1s^3 \\ e_1s^2 \\ e_1s \\ e_2s^4 \\ e_2s^3 \\ e_2s^2 \\ e_2s \end{bmatrix} = \begin{bmatrix} 0 & 0 & 0 & 0 & 0 & 0 & 0 & 0 & 0 & 0 & 0 & 0 \\ 1 & 0 & 0 & 0 & 0 & 0 & 0 & 0 & 0 & 0 & 0 & 0 \\ 0 & 1 & 0 & 0 & 0 & 0 & 0 & 0 & 0 & 0 & 0 & 0 \\ 0 & 0 & 1 & 0 & 0 & 0 & 0 & 0 & 0 & 0 & 0 & 0 \\ 0 & A_{52} & 0 & A_{54} & A_{55} & A_{56} & A_{57} & 0 & 0 & 0 & 0 & 0 \\ 0 & 0 & 0 & 0 & 1 & 0 & 0 & 0 & 0 & 0 & 0 & 0 \\ 0 & 0 & 0 & 0 & 0 & 1 & 0 & 0 & 0 & 0 & 0 & 0 \\ 0 & 0 & 0 & 0 & 0 & 0 & 1 & 0 & 0 & 0 & 0 & 0 \\ 0 & 0 & A_{93} & 0 & 0 & 0 & 0 & 0 & A_{99} & A_{910} & A_{911} & 0 \\ 0 & 0 & 0 & 0 & 0 & 0 & 0 & 0 & 1 & 0 & 0 & 0 \\ 0 & 0 & 0 & 0 & 0 & 0 & 0 & 0 & 0 & 1 & 0 & 0 \\ 0 & 0 & 0 & 0 & 0 & 0 & 0 & 0 & 0 & 0 & 1 & 0 \end{bmatrix} \begin{bmatrix} us^3 \\ us^2 \\ us \\ u \\ e_1s^3 \\ e_1s^2 \\ e_1s \\ e_1 \\ e_2s^3 \\ e_2s^2 \\ e_2s \\ e_2 \end{bmatrix} + \begin{bmatrix} 1 \\ 0 \\ 0 \\ 0 \\ 0 \\ 0 \\ 0 \\ 0 \\ 0 \\ 0 \\ 0 \\ 0 \end{bmatrix} - \begin{bmatrix} 0 \\ 0 \\ 0 \\ 0 \\ 1 \\ 0 \\ 0 \\ 0 \\ 0 \\ 0 \\ 0 \\ 0 \end{bmatrix} y_{r1} * D(s) \qquad 10.3.15$$

$$y = \begin{bmatrix} 0 & 0 & 0 & 0 & 0 & 1 & 0 & 0 & 0 & 0 \\ 0 & 0 & 0 & 0 & 0 & 0 & 0 & 0 & 0 & 1 \end{bmatrix} \begin{bmatrix} us^3 \\ us^2 \\ us \\ u \\ e_1s^3 \\ e_1s^2 \\ e_1s \\ e_1 \\ e_2s^3 \\ e_2s^2 \\ e_2s \\ e_2 \end{bmatrix}$$

where

$A_{52} = 0.7376$ $A_{54} = 0.7376 + \partial_1$ $A_{55} = -5.7312$ $A_{56} = -10.8142 + \partial_2$

$A_{57} = -56.166 + \partial_3$ $A_{93} = -0.7376 + \partial_4$ $A_{99} = -5.312$ $A_{910} = -10.8142 + \partial_2$

$A_{911} = -56.166 + \partial_3$ $D(s) = s^4 + 5.7312s^3 + (10.8142 + \partial_2)s^2 + (56.1660 + \partial_3)s$

To use the H_∞ technique it is required to represent the system (10.3.15) as the generalised system (10.3.4). Thus, it can be seen from (10.3.15) that

$$A = A + \Delta A,\ B_1 = B,\ F = [0\ F_1],\ H = \begin{bmatrix} 0 \\ H_2 \end{bmatrix},\ E = \begin{bmatrix} \alpha \\ 0 \end{bmatrix} \qquad 10.3.16$$

where

$$\Delta A = F_1 \Delta H_2$$

$$F_1 = \begin{bmatrix} 0&0&0&0&0&0 \\ 0&0&0&0&0&0 \\ 0&0&0&0&0&0 \\ 0&0&0&0&0&0 \\ 1&1&1&0&0&0 \\ 0&0&0&0&0&0 \\ 0&0&0&0&0&0 \\ 0&0&0&0&0&0 \\ 0&0&0&1&1&1 \\ 0&0&0&0&0&0 \\ 0&0&0&0&0&0 \\ 0&0&0&0&0&0 \end{bmatrix} \quad \Delta = \begin{bmatrix} \partial_1&0&0&0&0&0 \\ 0&\partial_2&0&0&0&0 \\ 0&0&\partial_3&0&0&0 \\ 0&0&0&\partial_4&0&0 \\ 0&0&0&0&\partial_2&0 \\ 0&0&0&0&0&\partial_3 \end{bmatrix} \quad H_2 = \begin{bmatrix} 0&0&0&1&0&0&0&0&0&0&0&0 \\ 0&0&1&0&0&1&0&0&0&1&0&0 \\ 0&0&0&0&0&0&1&0&0&0&0&0 \\ 0&0&0&0&0&0&0&0&0&0&1&0 \\ 0&0&1&0&0&0&0&0&0&0&0&0 \\ 0&0&0&0&0&0&0&0&0&1&0&0 \end{bmatrix}$$

Having determined all the system, disturbance and performance specification matrices, the Riccati equation given by (10.3.5) can now be solved in principle using the algorithm given in Appendix C.

However, when this algorithm in Appendix C was used, a set of feedback gains which stabilises the system could not be determined because a $P > 0$ could not found. This results from the uncontrollable states which are introduced in transforming a multivariable system in to non-minimal format. This problem does not appear in the SISO case (see [9]).

The system given by (10.3.15) is a 12^{th} order system and if state variable feedback control is used in closed loop the system is still 12^{th} order. From Chapter 5 and 9 we know the system is 4^{th} order and the output feedback controller will be 4^{th} order. Therefore, in closed loop the system will be 8^{th} order, as some uncontrollable modes have been cancelled.

Consider the closed loop system

$$\begin{aligned} \dot{x} &= Ax + Bu \\ y &= Cx \\ u &= \frac{L(s)}{s^n + P(s)} x \end{aligned} \qquad 10.3.17$$

and the non-minimal state space representation of (10.3.17) given as

$$\begin{aligned} \dot{\hat{x}} &= \hat{A}\hat{x} + \hat{B}\hat{u}s^n \\ \hat{y} &= \hat{C}\hat{x} \\ \hat{u}s^n &= K\hat{x} = \begin{bmatrix} L(s) & P(s) \end{bmatrix} \begin{bmatrix} x & u \end{bmatrix} \end{aligned} \qquad 10.3.18$$

Now if (10.3.18) is transformed into controllable form

$$\overline{A} = T * \hat{A} * T^{-1} = \begin{bmatrix} A_{nc} & 0 \\ A_{21} & A_c \end{bmatrix} \quad \overline{B} = T * \hat{B} = \begin{bmatrix} 0 \\ B_c \end{bmatrix} \quad \overline{C} = \hat{C} * T^{-1} = \begin{bmatrix} C_{nc} & C_c \end{bmatrix} \qquad 10.3.19$$

where A_c and B_c are controllable, the state variable feedback controller can be designed on the controllable subsystem.

Observing the closed loop system

$$\begin{aligned} \dot{x}_c &= A_C x_C + B_C u \\ y_C &= C_C x_C \\ u &= K_C x_C \end{aligned} \qquad 10.3.20$$

It was found that closed loop system (10.3.20) will be of the same order as the original closed loop system given by (10.3.17) and the closed loop poles of these two systems are the same.

Thus, an output feedback controller can be designed for the system (10.3.15) if it is transformed into controllable form. However, it should be noted that the controller for the system (10.3.18) will then be given as $\hat{u}\, s^n = \begin{bmatrix} 0 & K_c \end{bmatrix} \hat{x}$ and must be transformed into an output feedback controller for the original system. This new controller stabilises the original system (10.3.17). The problem with this method is that the disturbances are also transformed.

To transform the system (10.3.15) into its controllable / uncontrollable subspaces, the Matlab function CTRBF is used. This gives

$$A_{nc} = \begin{bmatrix} 0.0001 & 0.0089 & 0.0000 & 0.0000 \\ -0.0174 & 0.7918 & 1.0616 & 0.0000 \\ -0.0916 & -10.3441 & -0.8932 & 0.2330 \\ 1.1124 & 6.8866 & 0.1313 & -5.6299 \end{bmatrix}$$

$$A_c = \begin{bmatrix} 0.0007 & 0.1747 & 0.0000 & 0.0000 & 0.0000 & 0.0000 & 0.0000 & 0 \\ -0.6003 & -0.2371 & 5.7676 & 0.0000 & 0.0000 & 0.0000 & 0.0000 & 0 \\ -0.0052 & -0.8836 & 0.0140 & 1.0115 & 0.0000 & 0.0000 & 0.0000 & 0 \\ 0.4293 & 0.5543 & -4.1088 & -0.9958 & 1.6102 & 0.0000 & 0.0000 & 0 \\ 0.6439 & -1.3174 & -6.2507 & 2.2994 & -1.5264 & 3.0327 & 0.0000 & 0 \\ -0.7115 & 1.4557 & 6.9068 & -2.5407 & 1.6867 & -2.9866 & 1.4451 & 0 \\ 0.0000 & 0.0000 & 0.0000 & 0.0000 & 0.0000 & 0.0000 & 0.0000 & 1 \\ 0 & 0 & 0 & 0 & 0 & 0 & 0 & 0 \end{bmatrix} \quad 10.3.21$$

$$B_C = \begin{bmatrix} 0 & 0 & 0 & 0 & 0 & 0 & 0 & 1 \end{bmatrix}^T$$

From (10.3.21) it can be seen that the uncontrollable subsystem is 4^{th} order. This is exactly the number of extra states in the closed loop non-minimal system when compared to the closed loop system of the original system and the output feedback controller.

The poles of the 4^{th} order subsystem A_{nc} in (10.3.21) are

$$P_1 = -5.5931 \qquad P_2 = 0.0000$$
$$P_3 = -0.0690 + 3.1681i \qquad P_4 = -0.0690 - 3.1681i \qquad 10.3.22$$

Three poles are stable but the pole at 0 causes instability. The unstable pole occurs because of the pole zero cancellation in (10.3.14).

In order to use H_∞ control techniques it is required to formulate the F, H and E matrices as described in (10.3.4). These matrices for the non-minimal system are given in (10.3.16), but these need to be transformed such that a new F, H and E matrices are given for the controllable subsystem. This is not easily done by simple transformation, and in general this needs further investigation which is beyond the scope of this thesis.

To achieve a controller using H_∞ control techniques, arbitrary F, H and E matrices will be chosen such that the controllable system subsystem will be of the form described by (10.3.16). Thus

$$F = \begin{bmatrix} 1 & 0 & 0 & 0 & 0 & 0 & 0 & 0 \\ 0 & 1 & 0 & 0 & 0 & 0 & 0 & 0 \\ 0 & 0 & 1 & 0 & 0 & 0 & 0 & 0 \\ 0 & 0 & 0 & 1 & 0 & 0 & 0 & 0 \\ 0 & 0 & 0 & 0 & 1 & 0 & 0 & 0 \\ 0 & 0 & 0 & 0 & 0 & 1 & 0 & 0 \\ 0 & 0 & 0 & 0 & 0 & 0 & 1 & 0 \\ 0 & 0 & 0 & 0 & 0 & 0 & 0 & 1 \end{bmatrix} \quad H = \begin{bmatrix} 25 & 2 & 15 & 0 & 0 & 0 & 0 & 0 \\ 0 & 1 & 0 & 0 & 0 & 0 & 0 & 0 \\ 0 & 0 & 0 & 0 & 0 & 0 & 0 & 0 \\ 0 & 0 & 0 & 1 & 0 & 0 & 0 & 0 \\ 0 & 0 & 0 & 0 & 1 & 0 & 0 & 0 \\ 0 & 0 & 0 & 0 & 0 & 1 & 0 & 0 \\ 0 & 0 & 0 & 0 & 0 & 0 & 1 & 0 \\ 0 & 0 & 0 & 0 & 0 & 0 & 0 & 1 \end{bmatrix} \quad E = \begin{bmatrix} 0 \\ 0 \\ 0.1 \\ 0 \\ 0 \\ 0 \\ 0 \\ 0 \end{bmatrix} \qquad 10.3.23$$

Using the algorithm in Appendix C gives the feedback gains

$$K_c = [989.76 \;\; 136.50 \;\; -63.18 \;\; 107.71 \;\; 174.09 \;\; 127.92 \;\; 71.73 \;\; 13.85] \qquad 10.3.24$$

which stabilises the controllable subsystem (10.3.21) with the H_∞ norm $\gamma = 30.4123$.

The closed loop poles of the system (10.3.21) with the controller (10.3.24) are

$$\begin{aligned} &P_1 = -5.9806 + 0.3256i \;\; P_2 = -5.9806 - 0.3256i \;\; P_3 = -0.3499 + 3.2713i \\ &P_4 = -0.3499 - 3.2713i \;\; P_5 = -0.6220 + 1.1682i \;\; P_6 = -0.6220 - 1.1682i \\ &P_7 = -2.8404 + 1.5228i \;\; P_8 = -2.8404 - 1.5228i \end{aligned} \qquad 10.3.25$$

which are all stable.

Now, by performing a reverse transformation on (10.3.24) a state variable feedback controller is given for the non-minimal model (10.3.15). The feedback gains for the non-minimal system (10.3.15) are

$$\begin{aligned} \hat{K} &= [0 \;\; K_c] * T^{-1} \\ &= [13.85 \;\; 71.73 \;\; 159.56 \;\; 204.75 \;\; 27.44 \;\; 15.37 \;\; 26.81 \;\; 977.34 \;\; -6.85 \\ &\quad -189.37 \;\; -2.10 \;\; 17.7545] \end{aligned} \qquad 10.3.26$$

If we observe the closed loop system of the non-minimal model (10.3.15) and the controller (10.3.26) it can be seen that this system's poles are (10.3.25) which are the poles of the controllable and (10.3.22) which are the poles of the uncontrollable system.

As was stated previously, even though the non-minimal model has an unstable pole, this will disappear in the transformation of the output feedback controller.

Thus, the output feedback controller for the system in Chapter 5 is

$$u = -(f_{e1} + f_{e2}) \qquad 10.3.27$$

where

$$f_{e1} = \frac{27.4402s^3 + 15.3768s^2 + 26.8117s + 977.3428}{s^4 + 13.8549s^3 + 71.7338s^2 + 159.5639s + 204.7549} e_1$$

$$f_{e2} = \frac{-6.8479s^3 - 189.3709s^2 - 2.1013s + 17.7545}{s^4 + 13.8549s^3 + 71.7338s^2 + 159.5639s + 204.7549} e_2$$

with the closed loop poles for the system given in Chapter 5 and the controller (10.3.27) at

$$\begin{aligned} &P_1 = -5.9806 + 0.3256i \quad P_2 = -5.9806 - 0.3256i \quad P_3 = -0.3499 + 3.2713i \\ &P_4 = -0.3499 - 3.2713i \quad P_5 = -0.6220 + 1.1682i \quad P_6 = -0.6220 - 1.1682i \\ &P_7 = -2.8404 + 1.5228i \quad P_8 = -2.8404 - 1.5228i \end{aligned} \qquad 10.3.28$$

It has been described above that output feedback sliding mode controller can be achieved if H_∞ control techniques are initially used to design the state variable feedback controller which is then transformed into an output feedback controller.

Thus, from (10.3.9) an output feedback sliding mode controller is given as

$$u = -1*(1 - \frac{0.2sat(0.5)}{s})*(F_{e3} + F_{e4}) \qquad 10.3.29$$

where

$$f_{e3} = \frac{2*(7.4402s^3 + 15.3768s^2 + 26.8117s + 977.3428)}{s^4 + 2*(13.8549s^3 + 71.7338s^2 + 159.5639s + 204.7549)} e_1 \qquad 10.3.30$$

$$f_{e4} = \frac{2*(-6.8479s^3 - 189.3709s^2 - 2.1013s + 17.7545)}{s^4 + 2*(13.8549s^3 + 71.7338s^2 + 159.5639s + 204.7549)} e_2 \qquad 10.3.31$$

10.3.2 SIMULATION

Since the output feedback sliding mode controller has been designed using a combination of H_∞ control techniques and sliding mode techniques, we expect the controller to be robust in the presence of a wide range of uncertainties and disturbances. The output feedback sliding mode controller has been designed for cart set point control and swing cancellation where a change in the rope length can be viewed as an external disturbance on the cart and swing dynamics. Thus, the controller should have the same performance if the rope length is fixed or if the rope length is varied. Using this approach means that all three dynamics (cart position, swing angle and rope length) are controlled. The output feedback sliding mode controller is used for the cart and swing control and the state variable feedback controller described in Chapter 7 is used for the rope length control.

As described in the previous section, model following control can easily be incorporated. Thus a suitable reference model (as in Chapter 9) for the cart position is

$$y_r = \frac{1}{s+1} u_m \qquad 10.3.32$$

where u_m is the input to the cart reference model and since the swing angle oscillations are desired to be 0, then the model for the swing angle is $y_r = 0$.

The Figure 10.3.1 illustrates the block diagram of the output feedback sliding mode controller and the rope length controller.

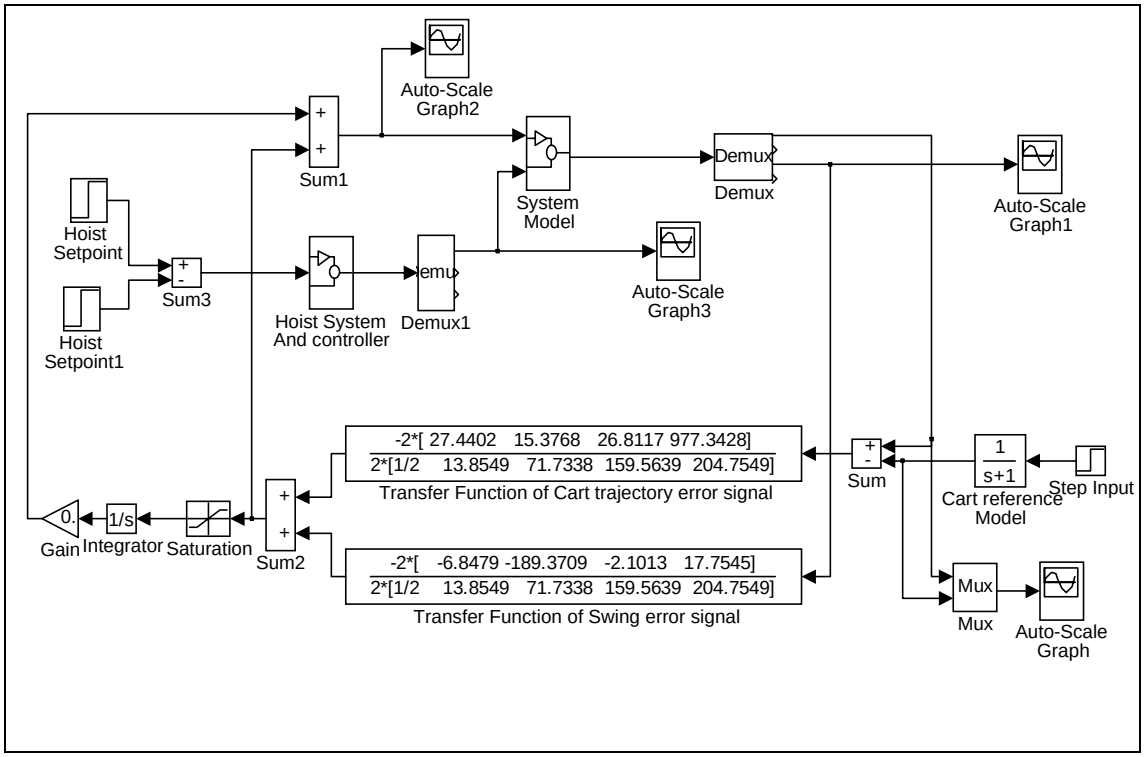

Figure 10.3.1

To determine the robustness of the output feedback sliding mode controller, a comparison will be made between the output feedback controller while the rope length is being varied (Figures 10.3.2 - 10.3.5), and when the rope length is fixed (Figures 10.3.6 - 10.3.8). A comparison will also be made between this controller and the controllers designed in the previous chapters.

As can be seen from Figures 10.3.2 - 10.3.8 whether the rope length is varied or fixed it does not affect the controller's performance. In both simulations (i.e. rope length varying and rope length fixed) the settling time for the cart position and swing angle is the same. Also in both simulations the cart follows the reference model quite accurately and the swing is cancelled. Thus, the controller is robust in the presence of uncertainties and disturbances.

The most noticeable difference between the two simulations is the slight change in direction in the swing angle in Figure 10.3.3 which is not present in Figure 10.3.7. This change in direction is caused by the rope length being very short, since the frequency of oscillations of the goods is greater for a short rope length than for a large rope length. This in turn produces a change in direction of the swing angle over a shorter time period. Once the rope length has increased, the responses of the swing angle in both simulations (i.e. Figures 10.3.3 and 10.3.7) are virtually identical.

Comparing the output feedback sliding mode controller with the gain scheduled sliding mode controller it can be seen that the output feedback sliding mode controller has a longer settling time. This is because the output feedback sliding mode controller was designed using H_∞ control technique which is a conservative technique to cater for disturbances. The conservative nature of the control technique can be seen not only by the reduction in the magnitude of the swing angle when compared to the magnitude of the swing angle in the gain scheduled sliding mode controller, but also by an increase in the system's settling time, especially the swing angle. Nevertheless with a better choice of the F, H and E matrices a settling time which is close to the gain scheduled sliding mode control could be achievable, but this would be traded off against and increase in the magnitude of the swing angle.

The choice of the F, H and E matrices was determined from a practical point of view where it is desired that the cart and swing angle settle as fast as possible. From Figure 10.3.3 it can be seen that after 8 sec. the swing angle is very small and practically speaking, these values in the swing angle would be seen as 0 rad. If the limits for hunting compensation (as described in Chapter 6) were imposed on the output feedback sliding mode controller, then from simulation it is determined that if the controller was implemented in real-time, then the cart and swing angle would have a settling time of 8 sec. Thus from a practical point of view the choice of the F, H and E matrices given in (10.3.23) is justified because a real-time implementation of the controller would produce a settling time that is close to the gain scheduled sliding modes controller's settling time.

If it is desired to totally cancel the swing in the shortest time possible, then other F, H and E matrices would be needed. But it must be remembered that this will cause an increase in the cart's settling time.

Unfortunately, at the time when the output feedback controller was designed, the real-time crane system was inoperable. Thus, a real-time implementation of this controller was not achieved. Based on the fact that all the previous controllers did not require any on-line tuning and exhibited the same performance characteristics as in simulation, there is good reason to believe that the real-time implementation of output feedback sliding mode controller would have the same performance characteristics as the simulation.

Overall, it has been shown that a robust model following output feedback controller can be achieved when a combination of H_∞ and sliding mode control techniques are used.

Cart and Model step response

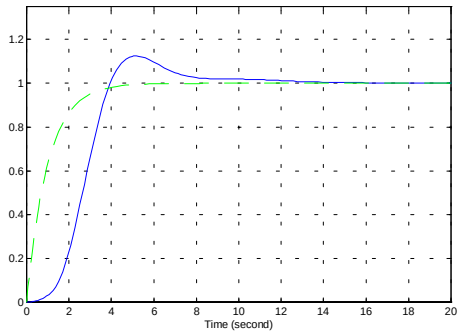

Figure 10.3.2

Swing angle step response

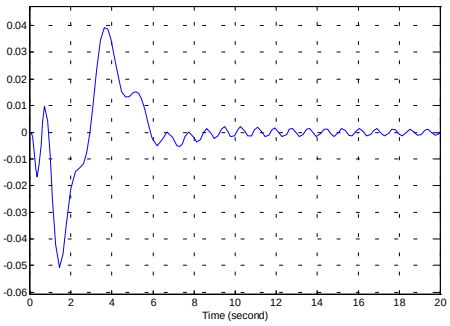

Figure 10.3.3

Control effort

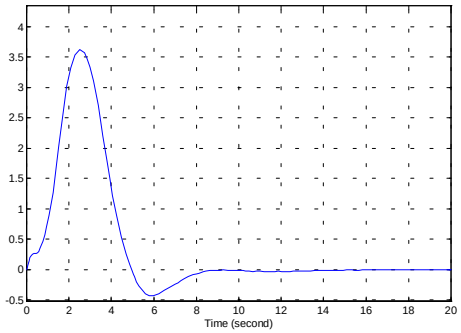

Figure 10.3.4

Rope length response

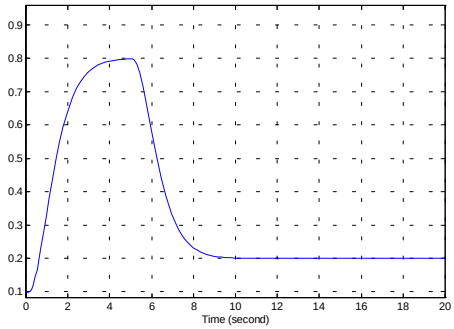

Figure 10.3.5

Cart and Model response

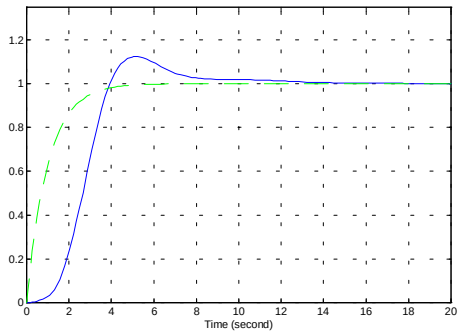

Figure 10.3.6

Swing angle step response

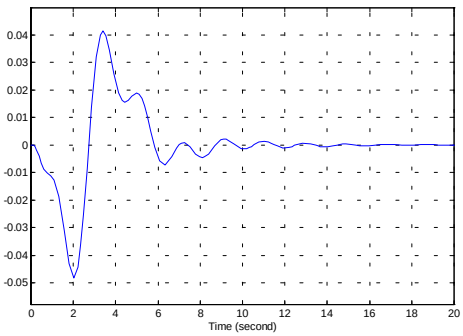

Figure 10.3.7

Control effort

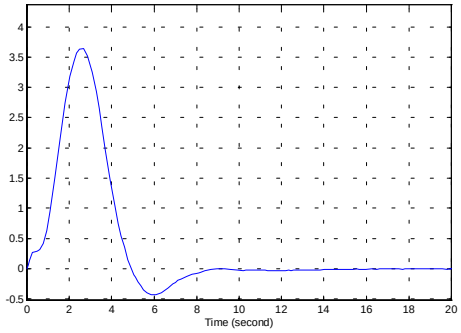

Figure 10.3.8

10.4 SUPERVISORY CONTROL

An experienced crane operator can adequately drive the crane to a desired setpoint without the load swinging (i.e. oscillating). Using this information it is possible to derive an open loop controller based on the operator's action. The problem with using this method is that the operator is mentally continually changing the driving strategy based on the new surrounding condition, i.e. wind changes, load changes, new cart set point etc. Thus, the information gained must be constantly updated.

A discussion on how a combination of feedforward and feedback control can be used to form a supervisory controller is given in this section. The operator drives the crane (this is the feedforward component) and the sliding mode controller (which is the feedback component) compensates as the system's output strays from the desired trajectory. The system's output may stray from the desired trajectory because of the operator's inappropriate action or because of any uncertainties which lie in the system or by external disturbances.

This approach means that an operator directly influences the system's performance, where as in using feedback or model following control, the operator only provides the desired setpoint or trajectory and thus, the operator does not directly influence the system's performance.

The open loop responses of system's outputs are observed as the operator drives the crane. A mathematical model which resembles the open loop responses of the outputs is then generated. This model is used as the desired trajectory (response) that the system's outputs are required to follow when the feedback controller (supervisory controller) is activated.

As the operator drives the crane the response of the system's outputs should closely resemble the desired response, thus errors between these two response should be small. The advantage of using the operator's action as the feedforward signal when the supervisory controller is activated is that the feedback controller does not have to work as hard because errors between the desired response and the actual response are small.

Thus, the control action does not necessarily have to be large to produce the desired response, since the feedforward action already produces an approximate desired response.

A practical disadvantage with using a supervisory controller is that the operators must be retrained so that they do not attempt correct for any deviations in the system's performance from the desired trajectory. The operators must be trained just to drive the crane and allow the supervisory controller to compensate for any errors between the system's outputs and the desired trajectory.

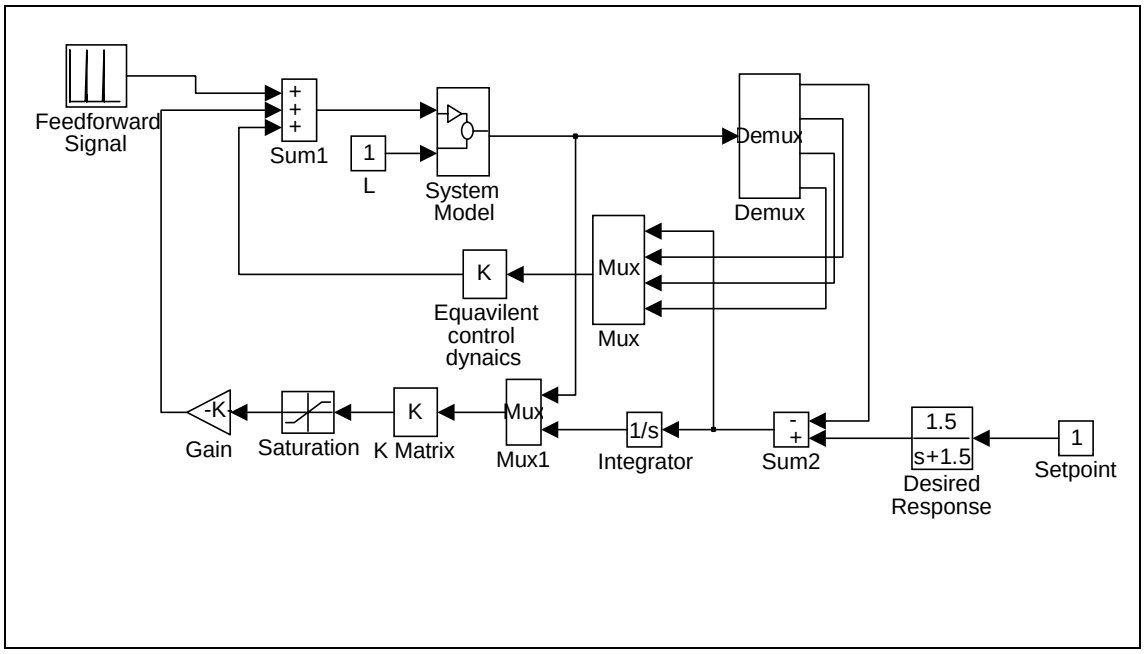

Figure 10.4.1 Block diagram of supervisory controller

The feedforward signal, as an operator might drive the system, was generated by a series of ramp functions. A bang-bang control signal could be used, but realistically an operator would not drive a crane like this. They are more likely to gradually increase the control signal. Thus, a series of ramp functions was used. Figure 10.4.2 illustrates the feedforward signal used.

The feedforward signal used is not as smooth as the other control signals calculated earlier. This is because all the previous control signals were calculated via the controller and thus produce very smooth signals. Figure 10.4.2 is a feedforward signal that was developed by experimentation. The conditions were that the cart had to settle in approximately 4 sec. to a value of 1 m and exhibit a first order step response. Also the swing angle had to be brought to rest at 0 rad. Thus, the feedforward signal was generated such that the system would exhibit the above conditions, which are conditions that a real life crane operator may have to meet.

Figures 10.4.3 and 10.4.4 illustrate the open loop step response when the feedforward signal illustrated by Figure 10.4.2 is applied to the model of the crane. Notice that the cart settles in approximately 5 sec. and has an envelope shape of a first order system. The swing angle has been bought under control in 5 sec. Since these figures were generated from simulation the swing angle is not zero because a frictionless model was assumed. But after 5 sec. the swing angle is so small that it is negligible and thus, can be said to be zero.

Since the desired response of the cart (Figure 10.4.2) is similar to a first order response, with the constraints that there should be no overshoot and the cart should reach it's setpoint in approximately 5 sec., then the response that the cart should follow is given by the transfer function $\frac{1.5}{s+1.5}$. Figure 10.4.5 illustrates this response.

The feedback controller that will be used is the sliding mode controller described in Chapter 5. This controller was chosen because the structure already incorporates a setpoint controller. In Chapter 5 the setpoint was designated by a step function. This is not ideal as a step change in the setpoint means that the controller produces a large input signal to compensate for the sudden setpoint change. However in this instance the setpoint will be described by a transfer function and thus, there are only small changes in the setpoint until the final value is reached. This fact, coupled with the fact that the feedforward signal already produces an approximate desired response, means that the controller should not produce large input signals.

Another reason for using the sliding mode controller developed in Chapter 5 is that the desired response that one would like the cart to follow can be easily changed without changing the controller structure. If one was to use the model following controller developed in Chapter 9, then if the desired model was to be changed the controller would also need to be changed. Thus, the sliding mode controller developed in Chapter 5 seems to be a more practical controller, because the sliding mode controller can be initially developed, then all that changes is the desired response that we want the cart to follow.

10.4.1 CART RESPONSE

The primary control of the cart is the open loop feedforward signal described by Figure 10.4 .2. With the introduction of the feedback controller the cart step response (Figure 10.4.6) closely resembles Figure 10.4.3, but exhibits a much smoother response as setpoint is reached. Thus, the feedback controller has ironed out all the jagged features of Figure 10.4.3 giving a smother response. The whole point of implementing the feedback controller is to keep the system on the desired trajectory.

Notice in Figure 10.4. 6 that the settling time is slightly longer. This is because the feedback controller will attempt to bring all the system states under control at the same time. Since the swing angle in Figure 10.4.7 is not brought completely under control (i.e. swing angle = 0) until 6.5 sec. the feedback controller brings the cart to setpoint at the same time. But if we consider the system at the 5 second mark (i.e. time = 5 sec.), it can be seen that the cart is very close to the final setpoint value and the swing angle is so small that it can be taken as zero. Thus, the system could be said to settle in 5 sec.

As the controller is only accounting for the small errors in the system's response compared to the desired trajectory, the gain in front of the saturation function had to increased to a value of 20 so that the system would be pushed more rapidly on to the sliding surface. If the same value for α was used as in Chapter 5, the system would take longer to settle. This is because the errors are small which produce a small control action and thus only move the system towards the sliding surface at a slow rate.

10.4.2 SWING ANGLE

It can be seen from Figure 10.4.7 that the introduction of the feedback controller has cancelled the oscillation of the swing angle after the 5 second mark (i.e. time = 5 sec.). The feedforward signal produces an approximate response and thus some oscillations of the swing angle are not completely cancelled. This was done to show how the feedback controller takes care of the small error that maybe incurred as the operator drives the crane to the desired response.

Notice that in Figure 10.4.7 the swing has been cancelled. This is primarily due to the feedback controller, as the feedforward controller does not entirely cancel the swing (Figure 10.4.4). The feedforward controller drives the system as close as possible to the desired response, thus only minimising the swing, and then the feedback controller takes care of the rest.

From Figure 10.4.7 it can be seen that the feedback controller helps to produce a smoother response of the swing angle. The swing angle oscillation between 4 and 5 sec. in Figure 10.4.4 has been eliminated by the feedback controller (which means that the operator may have performed an inappropriate control action) and the swing angle has been virtually bought under control within 5 sec.

10.4.3 CONTROL EFFORT

Figure 10.4.8 illustrates the control effort of combined feedforward signal and the feedback control signal. With the introduction of the feedback controller, the control signal illustrated by Figure 10.4.8 is a much smoother than that of the feedforward signal Figure 10.4.2. It can be seen that the feedback controller has taken out any unnecessary or incorrect control actions that the operator may perform.

The key point to note is that since the feedforward signal is the operator driving the crane, then large step changes in the control signal do not occur. This is because the operator would probably gradually increase or decrease the voltage that is applied to the motor in order to place the cart at the desired setpoint and cancel the swing. Generally, operators do not use large step changes in the voltage that is applied to the motor to

place the cart to the desired setpoint and cancel the swing. Thus, unlike Chapter 6 where a step change was used which produced a sudden and large change in the control signal, the control signal that is produced using a combination of feedforward and feedback control means the control signals can be kept to a minimum value to achieve the desired response.

Feedforward control signal

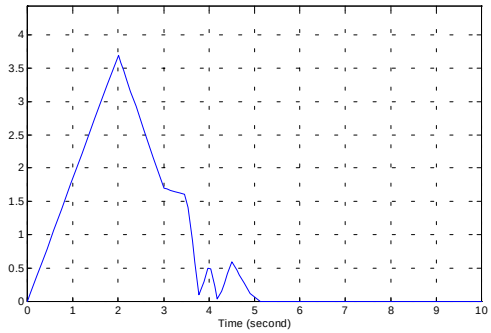

Figure 10.4.2

Cart open loop response

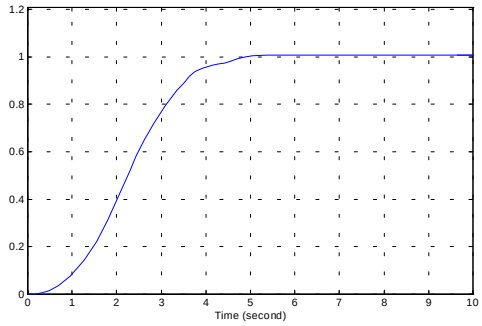

Figure 10.4.3

Swing angle open loop response

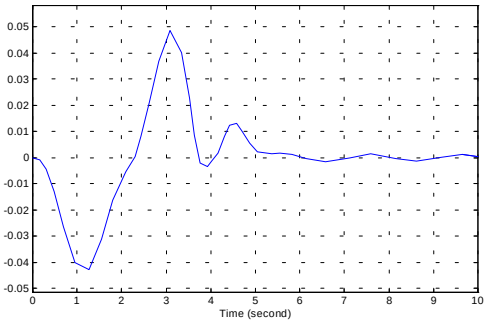

Figure 10.4.4

Desired response

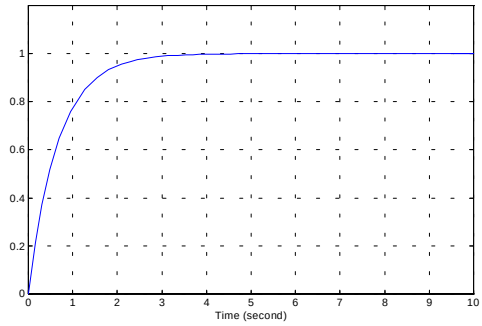

Figure 10.4.5

Cart position closed loop response

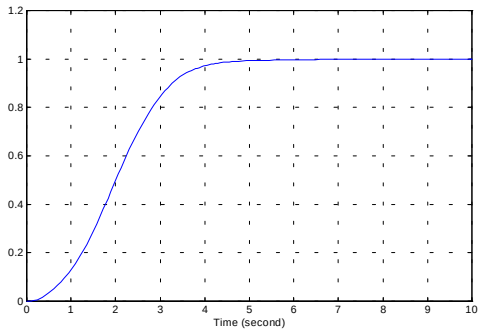

Figure 10.4.6

Swing angle closed loop response

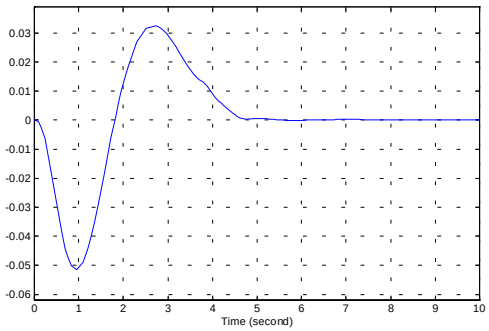

Figure 10.4.7

Control effort

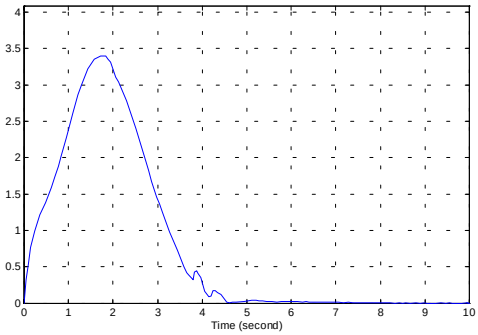

Figure 10.4.8

10.5 CONCLUSION

A discussion of the design and implementation of an output feedback model following is given in Chapters 9 and 10, from which it is concluded that the initial assumption by Young [16] to perfect model matching is not needed. In particular, in Chapter 9 it is shown that if the system is placed in a non-minimal state space format, then by manipulation of the LQR an output feedback model following controller can be designed and Young's assumptions are not needed. A generalised eigenvalue method was used to solve the LQR in Chapter 9. This approach means that Kalman's conditions do not necessarily need to hold to solve the LQR problem. Using the alternative method the output feedback model following controller was designed and implemented.

It was shown that real-time results matched the simulated results. Thus, it is concluded that the model of the gantry crane system is precise and no online tuning is required in the controller implementation.

It is also shown that the output feedback model following controller produces a much smoother control signal (both in simulation and in the real-time implementation) than the sliding mode controller, because it was implemented as a transfer function and thus any noise was filtered out. Thus, it is concluded that if it is desired to have a smooth control signal to reduce mechanical stress on the system, then the output feedback model following controller is an appropriate solution.

It is shown that output feedback model following control could be extended to incorporate sliding mode control if the H_∞ Riccati equation was used instead of the LQR Riccati equation. Using this approach it was shown that two independent controllers could be designed quite successfully, controlling all three dynamics (i.e. cart position swing angle and rope length).

The output feedback model following sliding mode controller was used for cart setpoint and swing control and a simple state variable feedback controller was used for rope length control. This output feedback sliding mode controller was found to have virtually no degradation in performance as the rope length was varied, compared to using a fixed rope length. Thus confirming the controller's robustness in the presence of uncertainties and disturbances.

In Chapter 10 a combination of both feedforward and feedback control is used to design a controller that would make the system follow a desired trajectory. The advantage of having both control actions means that the control does not have to work as hard as most of the control can achieved by the feedforward signal. It is concluded that in practice an operator can be used as the feedforward signal and then the feedback controller can be used to correct the trajectory of the system's outputs as they stray from the desired trajectory.

CHAPTER 11 CONCLUSIONS AND RECOMMENDATIONS

11.1 CONCLUSIONS

The work presented in this thesis describes the development of a class of robust non-linear controllers that can be implemented in real-time to control the gantry crane system. This thesis also gives a detailed discussion of the advantages and disadvantages of the different controllers. The choice of controller that is implemented is left up to the engineer once the performance criteria are chosen.

As part of good engineering practice, it is required to simulate the controller's performance before implementing the controller. For this, a mathematical model that realistically describes the behaviour of the gantry crane system is needed. In order to determine a realistic mathematical model of the gantry crane system, a comparison between two different models were developed and investigated. One model consists of a complete mathematical model of the gantry crane system which tightly couples the cart, swing and hoist dynamics and the other model is a loosely coupled model. The loosely coupled model is comprised of one model for the hoist dynamics and another model for the cart and swing dynamics. These two models are coupled by a term which include the rope length as a parameter.

From the work presented in this thesis, it is concluded that the loosely coupled model gives a more accurate representation of the gantry crane system than the complete mathematical model. The loosely coupled model is used to simulate all the controllers developed in this thesis.

This conclusion is based on the fact that as the goods swing in the real-time system, the cart moves as well, but the rope length is constant. This occurs because of friction between the rope and the drum. This property is only seen in simulation when friction is neglected by using the loosely coupled model. To observe this property in simulation using the complete mathematical model friction must not be neglected.

Throughout the thesis all controller design and simulation is performed on the loosely coupled model. When the controllers were implemented they produced the same performance as in simulation without the need for additional on-line tuning. This result is further justification for the use of the loosely coupled model.

Since a completely accurate mathematical model of the gantry crane system is difficult to develop, it follows that a robust controller is required which caters for a wide variety of modelling uncertainties. Sliding mode control is used throughout this thesis because it is a simple, yet robust non-linear controller design technique that caters for bounded uncertainties and matched disturbances. Therefore, it is concluded that a controller designed using this technique should be robust in the presence of modelling uncertainties when implemented on the gantry crane system.

An objective of this thesis is to determine just how robust sliding mode control is with respect to modelling uncertainties. This objective is achieved by comparing the simulated and real-time performance of two controllers. These controllers were a non gain scheduled sliding mode controller and a gain scheduled sliding mode controller where the gain scheduling parameter is the rope length. It is found that the gain scheduled sliding mode controller does not vastly improve the controller's performance when compared to the non gain scheduled sliding mode controller. Thus, one major conclusion is that a sliding mode controller can be designed for a simplified mathematical model of the gantry crane system, and when this controller is implemented, it behaves similarly to the simulated system which consists of the simplified model and controller.

Another objective of this thesis is to achieve setpoint control for the cart position and rope length at the same time. This is accomplished by introducing a new state which is the integral error of the cart position and the desired setpoint and similarly for the rope length. A change in the desired position (i.e. setpoint) is driven by a step change. It is observed that a large setpoint change would initially produce very large control signals as the setpoint changed from one value to another.

The implementation of the sliding mode controller required that all the system states be available. On the real-time system the only directly available states are the cart position, swing angle and rope length and thus all the respective velocities need to be estimated. Sufficiently good state estimation is achieved using a simple alpha-beta state estimator.

It is observed that the implementation of the sliding mode controller produces a noisy control signal. This occurs because all the directly available states are influenced by noise. Having a noisy control signal causes the cart to jitter and it is difficult to achieve complete setpoint control. A cleaner control signal can be achieved by implementing a Kalman filter on either the states which are influenced by noise or on the control signal itself. But doing this would add another dimension of complexity to the final control solution.

Since the implementation of the sliding mode controller requires the implementation of an estimator for the unavailable states, produces a noisy control signal, and produces a large control signal for a large setpoint change, it follows that a controller which caters for all these factors is needed. Therefore, the work in this thesis leads to the investigation of dynamic output feedback model following controllers (DOFMFC). From the literature review it is concluded that DOFMFC would cater for all of these problems.

The limitation with most of the existing literature when model following control is discussed, is the requirement of perfect model matching to occur. The design of a dynamic output feedback model following controller, that does not require perfect model matching to occur is developed in this thesis. This is achieved by representing both the system model and a model that the system is required to track in non-minimal state space format. Then LQR techniques are used to produce the controller. The non-minimal state space model is uncontrollable, and standard techniques to solve the Riccati equation for the LQR can not be applied. This thesis shows that the LQR Riccati equation can be solved by using a generalised eigenvalue solution.

Representing the system in non-minimal state space format gives a dynamic output feedback controller that has a proper transfer function and produces both feedforward and feedback components in the final controller structure. It is shown that the feedforward component is only produced if the plant does not have an integrator in the forward path.

Comparing the implementation of the DOFMFC with the sliding mode controller reveals that the DOFMFC has a slightly longer settling time, produces a less noisy control signal, and negates the need to have all the states available. The major limitation with the DOFMFC is that its performance is not guaranteed as the rope length is varying.

This thesis shows that a DOFMFC which overcomes this limitation can be achieved by using a combination of H_∞ and sliding mode control techniques. It is found that uncontrollable modes are produced when MIMO systems are placed in non-minimal state space representation. Because of the uncontrollable modes, a positive P for the Riccati equation which pertains to H_∞ control cannot be found. It is shown that in order to achieve a positive P, then the non-minimal model for the MIMO system must be transformed into controllable / uncontrollable portions.

This thesis shows that if a controller is designed solely for the controllable portion, then the closed loop poles of the controllable portion and the controller would be the same as the closed loop poles of the original model and the output feedback controller.

A comparison of this controller is given with a fixed rope length and a varying rope length, and it is concluded that this controller's performance is not affected by a varying rope length. Unfortunately an implementation of this controller was not possible because the crane was inoperable at this point. Since all the controllers implemented in this thesis performed similarly to the simulation without the need for additional on-line tuning, then there is good reason to conclude that an implementation of this controller would have similar performance characteristics as the simulation.

This thesis also describes an alternative method to develop a supervisory controller which is a combination of a feedforward component and a feedback component. The feedforward component is generated by the crane's operator, and the feedback component is the sliding mode controller. A model of the desired output is previously generated from observation of the operator's actions. This is then used as the reference model that the system is required to track. The operator then drives the crane. This is used as the feedforward signal. As the system's output strays from the desired trajectory either because of the operator's inappropriate action or external disturbances influencing the system's performance, the feedback sliding mode controller compensates and keeps the system's output tracking the desired trajectory.

It is therefore concluded that a controller which is comprised of both a feedforward and feedback component does not have to be developed by using model following techniques.

In conclusion, this thesis shows that dependent upon the performance criteria that the controller is required to meet, there exist a number of different control techniques based on sliding mode control and its variations that can be used to develop a controller for the gantry crane system.

11.2 RECOMMENDATIONS

Throughout this thesis a number of different controllers have been developed to control the gantry crane system. Most have been simulated and implemented in real-time on a scale model of the gantry crane system. This thesis has addressed some of the issues which arise when a practical implementation of controllers is attempted. However, there do exist areas where work can be conducted to improve the real-time performance of the controllers. These areas are the mechanical model of the crane system, and the controller design.

It has been noted throughout this thesis that the real-time crane system has many non-linearities in the mechanical structure of the gantry crane system. These non-linearities can be attributed to friction, noise and the fact the frame on which the cart travels is not level and shakes when the cart moves since it is made out of timber.

The non-linearities in the system caused a dead-band region in the motor which had to be compensated for. They also caused parameter fluctuations in the measurement of the cart position, rope length and the swing angle. This meant that the controller had to work harder in order to compensate for the parameter fluctuations while attempting to cancel the swing and position the cart and the rope length to the desired setpoint.

To eliminate the parameter fluctuations in the cart position signal and the swing angle signal which are caused by a non level track and the shaking of the frame as the cart moves, it is recommended that the system be rebuilt out of steel or aluminium to improve rigidity of the system.

The cart currently runs along a set of wooden tracks which are lined with rubber. The rubber in conjunction with the knurling of the steel wheels of the cart and the mass of the cart provides traction for the cart. Traction is actually the frictional component between the cart’s wheels and the track. This frictional component produces a large dead band region which must be overcome by the cart’s motor in order to move the cart.

Since the cart's motor is small, it cannot produce the required level of torque to overcome the friction when a small current is applied to the cart's motor. Thus, it is recommended that the cart's motor be replaced with a more powerful motor that produces the torque required when a small current is applied to the motor. This would then minimise the dead band region.

It is very difficult to totally eliminate friction from a system, but the magnitude of the frictional component can be reduced easily. In order to minimise the magnitude of the frictional component it is recommended that a cog and chain system be developed to move the cart along the track. This eliminates the need to have the wheels knurled or to line the track with rubber to provide traction. Implementing a cog and chain system would also allow the cart to be made out of a lighter material, which in turn would mean that the acceleration of the cart would increase.

Noise is another component which is difficult to totally eliminate from a system. Using some form of filtering is the means by which the magnitude of the noise component can be reduced on the measured signals. Throughout this thesis it has been noted that the swing angle measurement is greatly affected by noise since a potentiometer is used to measure it. Thus it is recommended that a device which has filtering characteristics built into its structure such as a resolver or an encoder be used to measure the swing angle.

The recommendations described above have dealt with modification to the mechanics of the real-time crane in order to improve the crane's closed loop performance. These modifications do not necessarily have to be made to improve the crane's closed loop performance. It can be improved by improving the structure of the controller implemented. The following recommendations are made to improve the controller structure.

To gain a better understanding of how friction affects the system, it is recommended that a full frictional model of the crane be developed. This would result in a more complex controller, but it should negate the need to have a separate controller for dead band compensation as it would be accounted for in the design of the controller.

Throughout this thesis the velocities of the cart, swing angle, and the rope length were all estimated using an alpha-beta state estimator since they are not directly available on the real-time crane. The alpha-beta state estimator is a simple estimator which filters some of the noise component. To obtain a greater level of filtering than is provided by the alpha-beta filter, while estimating the non available states, it is recommended that a Kalman filter or a sliding mode observer be used. These techniques would produce a more accurate estimated signal as they have proved to be robust in the presence of a wide variety of uncertainties and disturbances. This would then produce a smoother control signal to the motor which in turn should improve the closed loop performance of the crane.

A simplified mathematical model of the crane was used throughout this thesis to design all the controllers. To determine if using this model is truly justified, it is recommended that a multivariable sliding mode controller be designed using the complete model of the crane. If the multivariable controller produces the same performance as the gain scheduled sliding mode controller, then using a simplified model of the crane is justified.

LQR techniques were used to design an output feedback mode following controller which achieved cart setpoint control and swing cancellation for a fixed rope length. If a rope length controller is required, then it is recommended that the LQR be reviewed to determine if there is a means by which gain scheduling can be incorporated in the controller design. The resultant controller could then achieve cart setpoint, swing cancellation and rope length control.

In this thesis it is shown that an output feedback controller which achieves cart setpoint, swing cancellation and rope length control can be designed by using a combination of H_∞ and sliding mode control techniques. To design this controller it is required to represent the system in non-minimal state space format. For MIMO systems, the non-minimal state space format produces uncontrollable modes so H_∞ control techniques could not be directly applied. To use these techniques the non-minimal representation of the system needed to be transformed into controllable/uncontrollable sub system. During the transformation the disturbance and performance weighting matrices are also

transformed. Thus, it was difficult to establish from the transformation which states are affected by a disturbance or a combination of disturbances. To gain a better understanding of which disturbances affect the controllable sub system and thus, the resultant controller, it is recommended that the effects of transforming the disturbance and performance weighting matrices be investigated.

BIBLIOGRAPHY

[1] V. I. Utkin, “Sliding modes and their application in Variable Structure Systems”, MIR, Moscow 1978.

[2] R. A. De Carlo, S. H. Zak and G. P. Matthews, “Variable Structure Control of nonlinear multivariable systems: a tutorial”, Proc IEEE, Vol 76, No 3, pages 212 – 232, 1998.

[3] C. M. Doring and A. S. I. Zinober, “Two approaches to hyperplane design in multivariable variable structure control systems”, Int J Control, Vol 44, No 1, pages 65 – 82, 1989.

[4] S. K. Spurgeon, “Temperature control of industrial processes using a variable structure design philosophy”, Trans Inst MC, Vol 14, No 5, pages 233- 237, 1992.

[5] S. K. Bag, S. K. Spurgeon and C. Edwards, “Output feedback sliding mode design for linear uncertain systems”, IEE Proc. Control theory Application, Vol 144, No 3, pages 209-216, 1997.

[6] S. K. Spurgeon and R. J. Patton, “Robust variable structure control of model reference systems”, IEE Proc. Vol 137, Part D, No 6, Pages 341 – 348, 1990.

[7] C. Edwards and S. K. Spurgeon “Robust output tracking using a sliding mode controller / observer scheme”, Int. J. Control, Vol 64, No 5, pages 967 – 983, 1996.

[8] T. Hesketh, “A state-space pole–placing self-tuning regulator using input–output values”, IEE Proc. Part D, Vol 129, pages 123 – 228, 1982.

[9] Y. A. Jiang, T. Hesketh. and D. J. Clements, “Output Feedback Sliding mode control of linear systems”, Proc. American Control Conference, Vol 3 pages 2145-2149, 1997.

[10] Y. A. Jiang, T. Hesketh. and D. J. Clements, “Non-minimal State-space Realisation in H_∞ Control Design”, Proc. Con. Decision and Control 1996.

[11] Y. A. Jiang, T. Hesketh. and D. J. Clements, “Sliding Surface Design with a D-scaled H_∞ method”, Internal paper, School of Electrical Engineering, UNSW, 1995.

[12] R. El-Khazali and R. Decarlo, “Variable Structure Output feedback control”, American Control Conference, pages 871-875, 1992.

[13] A. A. Bahnasawi, M. S. Mahmoud and S. Z. Eid, “Variable structure control of nonlinear adaptive model following systems”, Int J System Sci, Vol 22, No 2, pages 351 – 365, 1991.

[14] A. A. Bahnasawi, M. S. Mahmoud and S. Z. Eid, “Adaptive model-following control based on variable structure systems” Int J System Sci, Vol 22, No 2, pages 333 – 349, 1991.

[15] K-K. Shyu and C-Y. Liu, “Variable structure controller design for robust model following” J. Guidance and Control, Vol 19, No 6, pages 1395 – 1397, 1996.

[16] K. K. D. Young, “Design of variable structure model – following control systems”, IEEE Trans. On Automatic control, Vol 23, No 6, pages 1079 – 1085, 1978.

[17] T. H. Hopp and W. E. Schmitendorf, “Design of a linear controller for robust tracking and model following”, Journal of. Dynamic Systems, Measurement and Control, Vol 112, pages 552 – 558,1990.

[18] A. Balestrino, G. De Maria and A. S. I. Zinober,. “ Nonlinear Adaptive Model – Following Control”, Automatica, Vol. 20, No. 5, pages 559 – 568, 1984.

[19] J. K. Pieper and B. W. Surgenor, “Discrete time sliding mode control applied to a gantry crane”, Proc. IEEE Decision and Control, Vol 1, pages 829 – 834, 1994.

[20] J. W. Auernig and H. Troger, “Time optimal control of overhead cranes with ropeing”, Automatica, Vol 23, No 4, pages 437 – 447,1987.

[21] B. D’ Andrea–Novel and F. Boustany, “Adaptive control of a class of mechanical systems using linearisation and Lyapunov methods. A comparative study on the overhead crane example”, Proc. IEEE Decision and Control, pages 120 – 125, 1991.

[22] H. Butler, G. Hondered and J. Van Amerongen, “Model reference adaptive control of a gantry crane scale model”, IEEE Control system mag. pages 57 – 62, 1991 (January).

[23] F. Boustany and B. D’ Andrea–Novel, “Adaptive control of an overhead crane using dynamic feedback linearization and estimation design” Proc. IEEE Int. Conf. Robotics and Automation, pages 1963 – 1968, 1992.

[24] D. J. Woods and D. J. Clements. “Nonlinear control of overhead cranes”, I.E. Aust. Control ’92 pages 29 – 40, 1992.

[25] H. T. Nguyen, “State variable feedback controller for an overhead crane” Journal of electrical and electronic engineers, Vol 14, No 2, pages 75 – 83, 1994.

[26] T. Burg, D. Dawson, C. Rahn and W. Rhodes, “Nonlinear control of an overhead crane via the saturating control approach of Teel”, Proc. IEEE Int. Conf. Robotics and Automation, pages 3155 – 3160, 1996.

[27] W. E. Singhose, L. J. Porter and W. P. Seering, “Input shaped control of a planar gantry crane with hoisting”, Proc. American Control Conference, pages 97 – 100, 1997.

[28] A. J. Ridout, “Anti – swing control of the over head crane using linear Feedback”, Journal of Electrical and Electronic Engineering, Australia Vol 9, No 1 pages 17 – 26, 1989.

[29] D. J. Woods, “Digital Control of Nonlinear Mechanical systems” Thesis, School of Electrical Engineering, UNSW, 1990.

[30] J. Yu, F. L. Lewis and T. Huang, “Non linear feedback control of a gantry crane” Proc. American Control Conference, pages 4310 – 4315,1995.

[31] D. O. Anderson and J. B. Moore, “Optimal control. Linear quadratic methods”, second edition, Prentice Hall, 1990.

[32] K. Ogata, “Modern Control Engineering”, second edition, Prentice Hall, 1990.

[33] B. Friedland, “Control Systems Design”, McGraw Hill, 1986.

[34] M. Athans and P. L. Falb, “Optimal Control”, McGraw Hill, 1966.

[35] R. C. Dorf, “Modern Control Systems”, fourth edition, Addison – Wesley, 1986.

[36] A. Teel, “Feedback Stabilisation: Nonlinear Solutions to Inherently Nonlinear Problems”, University of California, Memorandum No, UCB/ERL M92/65, 1992.

[37] A. Teel, “Examples of saturation using saturation: An input-output approach”, NOLCOS (third IFAC symposium on nonlinear control systems design), 1995.

[38] M. L. Skolnick, "Introduction to radar systems", McGraw Hill, 1980.

[39] Makino-Toshiaki, "Study on hunting reduction of an automated guided vehicle”, JSME- Int. Journal, -series c: dynamics, control, robotic, design and manufacturing. V 36, N 3, pages 368-374, Sept 1993.

APPENDIX A

The derivation of a complete mathematical model of the gantry crane is discussed. The cart dynamics, swing dynamics and hoisting dynamics are assumed to be tightly coupled and friction is neglected.

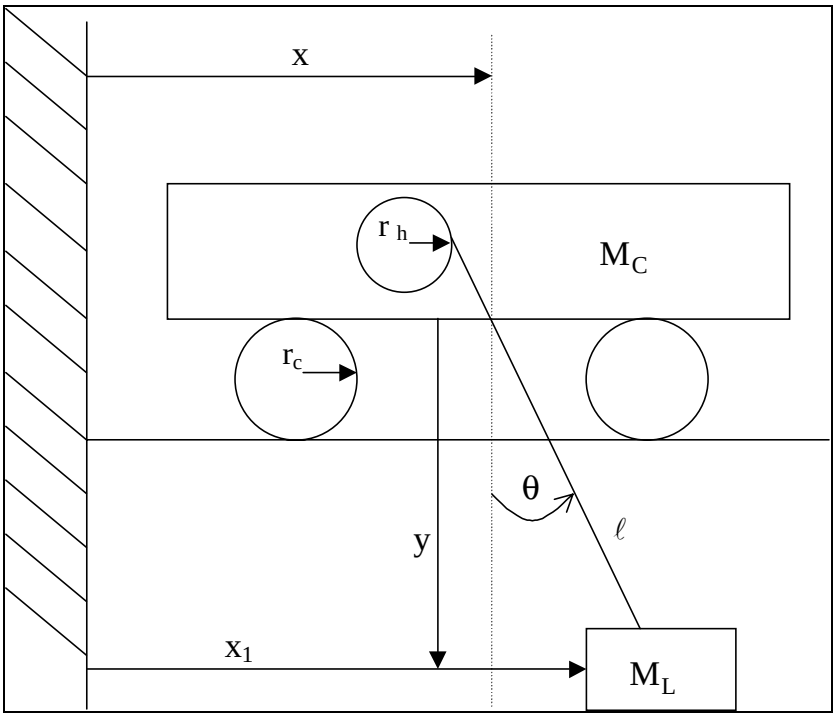

Figure A.1 Gantry crane system.

Nomenclature

x = horizontal position of cart (m) x_1 = horizontal position of load (m)

M_C = mass of cart (kg) M_L= mass of load (kg)

y = vertical position of load (m) ℓ = length of rope (m)

θ = load angle (rad)

r_C = effective radius of cart (m) r_h = effective radius of hoist (m)

J_C = total moment of inertia for cart (kg m^2)

J_h = total moment of inertia for hoist (kg m^2)

Kinetic Energy of Cart

$$T_1 = \frac{1}{2} M_c \dot{x}^2 \qquad \text{A.1}$$

Kinetic Energy of Load (Weight)

$$T_2 = \frac{1}{2} M_L (\dot{x}_1^{\ 2} + \dot{y}^2) \qquad \text{A.2}$$

where

$$x_1 = x + \ell \sin\theta \qquad y = \ell \cos\theta \qquad \text{A.3}$$

$$\dot{x}_1 = \dot{x} + \ell \dot{\theta} \cos\theta + \dot{\ell} \sin\theta \qquad \dot{y} = -\ell \dot{\theta} \sin\theta + \dot{\ell} \cos\theta \qquad \text{A.4}$$

Moment of Inertia of Cart

$$T_3 = \frac{1}{2} J_c \frac{\dot{x}^2}{r_c^{\ 2}} \qquad \text{A.5}$$

where $x = r_c \theta_1$ and θ_1 is the angular displacement of the cart.

The moment of inertia is calculated using the formula

$$J = \sum mr^2 \qquad \text{A.6}$$

where r = the radius of rotation.

m = the mass of the rigid body. Strictly, m is a mass at a point.

Moment of Inertia of Hoist

$$T_4 = \frac{1}{2} J_h \frac{\dot{\ell}^2}{r_h^{\ 2}} \qquad \text{A.7}$$

where $\ell = r_h \theta_2$ and θ_2 is the angular displacement of the hoist.

Total Kinetic Energy

$T = T_1 + T_2 + T_3 + T_4$

$$T = \frac{1}{2} M_c \dot{x}^2 + \frac{1}{2} J_c \frac{\dot{x}^2}{r_c^2} + \frac{1}{2} J_h \frac{\dot{\ell}^2}{r_h^2} + T_2 \qquad \text{A.8}$$

where

$$T_2 = \frac{1}{2} M_L [\dot{x}^2 + 2\dot{x}\ell\dot{\theta}\cos\theta + 2\dot{x}\dot{\ell}\sin\theta + (\ell\dot{\theta})^2 + \dot{\ell}^2] \qquad \text{A.9}$$

Total Potential Energy

$$U = -M_L g Y = -M_L g \ell \cos\theta \qquad \text{A.10}$$

Lagrangian Equation

Now that all the energy components within the system have been accounted for, the Lagrangian of the system is

$$L = T - U \qquad \text{A.11}$$

and so

$$L = \frac{1}{2} M_c \dot{x}^2 + \frac{1}{2} M_L [\dot{x}^2 + 2\dot{x}\ell\dot{\theta}\cos\theta + 2\dot{x}\dot{\ell}\sin\theta + (\ell\dot{\theta})^2 + \dot{\ell}^2] + \frac{1}{2} J_c \frac{\dot{x}^2}{r_c^2} + \frac{1}{2} J_h \frac{\dot{\ell}^2}{r_h^2}$$

$$+ M_L g \ell \cos\theta \qquad \text{A.12}$$

The external forces are acting on the cart and hoist dynamics. The swing dynamics do not have any directly applicable external force. The forces only act on the x and ℓ co-ordinates which are linear displacements. The θ co-ordinate of the system does not have any external forces that act directly upon it.

Thus

$$\frac{d}{dt}\left[\frac{\partial L}{\partial \dot{x}}\right] - \frac{\partial L}{\partial x} = F_1 \qquad \text{A.13}$$

$$\frac{d}{dt}\left[\frac{\partial L}{\partial \dot{\theta}}\right] - \frac{\partial L}{\partial \theta} = 0 \qquad \text{A.14}$$

$$\frac{d}{dt}\left[\frac{\partial L}{\partial \dot{\ell}}\right] - \frac{\partial L}{\partial \ell} = F_2 \qquad \text{A.15}$$

Substituting (A.12) into (A.1.13) and evaluating for the 'x' co-ordinate of the system gives

$$F_1 = \alpha\ddot{x} + M_L\ell\ddot{\theta}\cos\theta - M_L\ell\dot{\theta}\dot{\theta}\sin\theta + M_L\ddot{\ell}\sin\theta + 2M_L\dot{\ell}\dot{\theta}\cos\theta \qquad \text{A.16}$$

where $\alpha = \left(M_c + M_L + \frac{J_c}{r_c^2}\right)$

Similarly evaluating for the 'θ' co-ordinate of the system gives

$$0 = \ddot{x}\cos\theta + \ell\ddot{\theta} + g\sin\theta + 2\dot{\ell}\dot{\theta} \qquad \text{A.17}$$

And so for the 'ℓ' co-ordinate of the system as defined by (A.14)

$$F_2 = \beta\ddot{\ell} + M_L\ddot{x}\sin\theta - M_L g\cos\theta - M_L\ell\dot{\theta}^2 \qquad \text{A.18}$$

where $\beta = M_L + \frac{J_h}{r_h^2}$

Linearisation

As can be seen by (A.16), (A.17) and (A.18) the equations of motion for the gantry crane are complex and non-linear. Using small signal analysis (linearisation) for the "θ" co-ordinate the following assumptions will be made:

$\cos\theta = 1$ $\quad \sin\theta = \theta$ $\quad \theta^n = 0$ $\quad \dot{\theta}^n = 0$ where $n \geq 2$.

Thus (A.16), (A.17) and (A.18) become:

$$F_1 = \alpha\ddot{x} + M_L\ell\ddot{\theta} + M_L\ddot{\ell}\theta + 2M_L\dot{\ell}\dot{\theta} \qquad \text{A.19}$$

$$0 = \ddot{x} + \ell\ddot{\theta} + g\theta + 2\dot{\ell}\dot{\theta} \qquad \text{A.20}$$

$$F_2 = \beta\ddot{\ell} + M_L\ddot{x}\theta - M_L g \qquad \text{A.21}$$

The system states are defined as,

x_1 = cart position = x x_2 = cart velocity = $\dot{x} = \dot{x}_1$

x_3 = swing angle = θ x_4 = swing velocity = $\dot{\theta} = \dot{x}_3$

x_5 = rope length = ℓ x_6 = rope length velocity = $\dot{\ell} = \dot{x}_5$

(A.19) - (A.21) can now be expressed in terms of system states as

$$F_1 = \alpha \dot{x}_2 + M_L x_5 \dot{x}_4 + M_L \dot{x}_6 x_3 + 2M_L x_4 x_6 \qquad \text{A.22}$$

$$0 = \dot{x}_2 + x_5 \dot{x}_4 + g x_3 + 2 x_4 x_6 \qquad \text{A.23}$$

$$F_2 = \beta \dot{x}_6 + M_L \dot{x}_2 x_3 - M_L g \qquad \text{A.24}$$

Using the previous linearisation assumptions, (A.22) - (A.24) can be rewritten to produce the following state space equations.

$$\dot{x}_2 = \frac{F_1}{\alpha - M_L} + \frac{M_L g x_3}{\alpha - M_L}\left(1 - \frac{M_L}{\beta}\right) - \frac{M_L F_2 x_3}{\beta(\alpha - M_L)} \qquad \text{A.25}$$

$$\dot{x}_4 = \left(\frac{-F_1}{\alpha - M_L} - \frac{M_L g x_3}{\alpha - M_L}\left(1 - \frac{M_L}{\beta}\right) + \frac{M_L F_2 x_3}{\beta(\alpha - M_L)} - 2x_6 x_4 - g x_3 \right) / x_5 \qquad \text{A.26}$$

$$\dot{x}_6 = \frac{F_2}{\beta} - \frac{F_1 M_L x_3}{(\alpha - M_L)\beta} + \frac{M_L g}{\beta} \qquad \text{A.27}$$

From Chapter 2 the force equation of the cart motor and hoist motors are given as

$$F_1 = K_{I1}\left(\frac{V_{a1} - K_{b1}\dfrac{\dot{x}}{r_C}}{R_{a1}} \right) \qquad \text{A.28}$$

$$F_2 = K_{I2}\left(\frac{V_{a2} - K_{b2}\dfrac{\dot{\ell}}{r_h}}{R_{a2}} \right) \qquad \text{A.29}$$

where

R_{a1} = armature resistance of cart motor (Ω)

$V_{a1}(s)$ = applied armature voltage of cart motor (V)

K_{I1} and K_{b1} are cart motor constants.

R_{a2} = armature resistance of hoist motor (Ω)

$V_{a2}(s)$ = applied armature voltage of hoist motor (V)

K_{I2} and K_{b2} are hoist motor constants.

Substituting (A.28) and (A.29) into (A.25) - (A.27) gives

$$\dot{x}_2 = \frac{K_{I1}}{\alpha - M_L}\left(\frac{V_{a1} - K_{b1}\frac{x_2}{r_C}}{R_{a1}}\right) + \frac{M_L g x_3}{\alpha - M_L}\left(1 - \frac{M_L}{\beta}\right) - \frac{M_L x_3 K_{I2}}{\beta(\alpha - M_L)}\left(\frac{V_{a2} - K_{b2}\frac{x_6}{r_h}}{R_{a2}}\right) \quad \text{A.30}$$

$$\dot{x}_4 = \left(\frac{-K_{I1}}{\alpha - M_L}\left(\frac{V_{a1} - K_{b1}\frac{x_2}{r_C}}{R_{a1}}\right) - \frac{M_L g x_3}{\alpha - M_L}\left(1 - \frac{M_L}{\beta}\right) + \frac{M_L x_3 K_{I2}}{\beta(\alpha - M_L)}\left(\frac{V_{a2} - K_{b2}\frac{x_6}{r_h}}{R_{a2}}\right) - 2x_6 x_4 - g x_3\right) / x_5 \quad \text{A.31}$$

$$\dot{x}_6 = \frac{K_{I2}}{\beta}\left(\frac{V_{a2} - K_{b2}\frac{x_6}{r_h}}{R_{a2}}\right) - \frac{M_L x_3 K_{I1}}{(\alpha - M_L)\beta}\left(\frac{V_{a1} - K_{b1}\frac{x_2}{r_C}}{R_{a1}}\right) + \frac{M_L g}{\beta} \quad \text{A.32}$$

To assist with the simplification and the decoupling of (A.30) - (A.32) one final assumption can be made at this point and that is $\frac{J_h}{r_h^2} << M_L$. Making this assumption results in

$$\alpha = \left(M_c + M_L + \frac{J_c}{r_c{}^2}\right) \quad \text{A.33}$$

$$\beta = M_L \quad \text{A.34}$$

and therefore the term $(1 - \frac{M_L}{\beta})$ which appears in (A.30) and (A.31) will be equal to zero.

The state space equations are given as

$$\dot{x}_2 = \frac{K_{I1}}{\alpha - M_L}\left(\frac{V_{a1} - K_{b1}\frac{x_2}{r_C}}{R_{a1}}\right) - \frac{x_3 K_{I2}}{(\alpha - M_L)}\left(\frac{V_{a2} - K_{b2}\frac{x_6}{r_h}}{R_{a2}}\right) \qquad \text{A.35}$$

$$\dot{x}_4 = \left(\frac{-K_{I1}}{\alpha - M_L}\left(\frac{V_{a1} - K_{b1}\frac{x_2}{r_C}}{R_{a1}}\right) + \frac{x_3 K_{I2}}{(\alpha - M_L)}\left(\frac{V_{a2} - K_{b2}\frac{x_6}{r_h}}{R_{a2}}\right) - 2x_6 x_4 - g x_3\right) / x_5 \qquad \text{A.36}$$

$$\dot{x}_6 = \frac{K_{I2}}{M_L}\left(\frac{V_{a2} - K_{b2}\frac{x_6}{r_h}}{R_{a2}}\right) - \frac{x_3 K_{I1}}{(\alpha - M_L)}\left(\frac{V_{a1} - K_{b1}\frac{x_2}{r_C}}{R_{a1}}\right) + g \qquad \text{A.37}$$

To obtain a linear model of the non-linear state space equations, it is assumed that the states (x_1 - x_6) and input variables (V_{a1} and V_{a2}) only deviate slightly from the operating region. The operating region for all the states is zero, except for the rope length ℓ which is some length greater then zero ℓ . The operating region for the system is

$$x = \begin{bmatrix} 0 \\ 0 \\ 0 \\ 0 \\ \ell \\ 0 \end{bmatrix} \quad u = \begin{bmatrix} V_{a1} \\ V_{a2} \end{bmatrix} = \begin{bmatrix} 0 \\ 0 \end{bmatrix} \qquad \text{A.38}$$

The linearisation process is defined as follows

$$\begin{aligned} \Delta\dot{x} &= A\Delta x + B\Delta u \\ \Delta y &= C\Delta x \end{aligned} \qquad \text{A.39}$$

where

$$\dot{x} = f(x, V_a), \; A = \frac{\partial f}{\partial x}\Big|_{x_0, V_{a0}} \text{ and } B = \frac{\partial f}{\partial u}\Big|_{x_0, V_{a0}}$$

Therefore the linearised state space equations are

$$\dot{x}_1 = x_2 \qquad \text{A.40}$$

$$\dot{x}_3 = x_4 \qquad \text{A.41}$$

$$\dot{x}_5 = x_6 \qquad \text{A.42}$$

$$\dot{x}_2 = \frac{K_{I1}}{\alpha - M_L}\left(\frac{V_{a1} - K_{b1}\frac{x_2}{r_C}}{R_{a1}}\right) \qquad \text{A.43}$$

$$\dot{x}_4 = \left(\frac{-K_{I1}}{\alpha - M_L}\left(\frac{V_{a1} - K_{b1}\frac{x_2}{r_C}}{R_{a1}}\right) - g x_3\right)/\ell \qquad \text{A.44}$$

$$\dot{x}_6 = \frac{K_{I2}}{M_L}\left(\frac{V_{a2} - K_{b2}\frac{x_6}{r_h}}{R_{a2}}\right) \qquad \text{A.45}$$

From (A.40) - (A.45) the state space matrices of the system are

$$\dot{x} = \begin{bmatrix} 0 & 1 & 0 & 0 & 0 & 0 \\ 0 & -\eta & 0 & 0 & 0 & 0 \\ 0 & 0 & 0 & 1 & 0 & 0 \\ 0 & \frac{\eta}{\ell} & \frac{-g}{\ell} & 0 & 0 & 0 \\ 0 & 0 & 0 & 0 & 0 & 1 \\ 0 & 0 & 0 & 0 & 0 & -\varsigma \end{bmatrix}\begin{bmatrix} x_1 \\ x_2 \\ x_3 \\ x_4 \\ x_5 \\ x_6 \end{bmatrix} + \begin{bmatrix} 0 & 0 \\ \Gamma & 0 \\ 0 & 0 \\ \frac{-\Gamma}{\ell} & 0 \\ 0 & 0 \\ 0 & \xi \end{bmatrix}\begin{bmatrix} V_{a1} \\ Va_2 \end{bmatrix} \qquad \text{A.46}$$

$$y = \begin{bmatrix} 1 & 0 & 0 & 0 & 0 & 0 \\ 0 & 0 & 1 & 0 & 0 & 0 \\ 0 & 0 & 0 & 0 & 1 & 0 \end{bmatrix}\begin{bmatrix} x_1 \\ x_2 \\ x_3 \\ x_4 \\ x_5 \\ x_6 \end{bmatrix}$$

where

$$\Gamma = \frac{K_{I1}}{(\alpha - M_L)R_{a1}} \quad \text{A.47}$$

$$\eta = \frac{K_{I1}K_{b1}}{r_C(\alpha - M_L)R_{a1}} \quad \text{A.48}$$

$$\varsigma = \frac{K_{I2}K_{b2}}{r_h M_L R_{a2}} \quad \text{A.49}$$

$$\xi = \frac{K_{I2}}{M_L} \quad \text{A.50}$$

From (A.46) it can be seen that there exists two independent systems, one for the cart and swing dynamics and another for the hoist dynamics. In Chapter 2 it was initially assumed that the cart and swing dynamics were coupled to the hoisting dynamics by the a term which includes the rope length as a parameter. From this derivation of the system it is shown that this assumption is justified.

APPENDIX B

The Matlab routine for solving the generalised eigenvalue problem is detailed below. This algorithm was used to generate the feedback gain given in Chapters 9 and 10. The two functions which give the feedback gains are genlqr and lsq. Both these functions are detailed below

```
function [K,P]=genlqr(aa,bb,q,r);
ccc=zeros(size(bb));
n=length(aa);
m=size(bb)*[0;1];
aaa=[zeros(n) aa bb
aa' q ccc
bb' ccc' r];
bbb=[zeros(n) eye(n) zeros(n,m)
-eye(n) zeros(n) zeros(n,m)
zeros(m,n) zeros(m,n) zeros(m)];
[V,D]=eig(aaa,bbb);
DD=diag(D);
[Y,I]=sort(real(DD));
evalues=DD(I(1:n));
YXU=zeros((2*n+m),n);
for ii=1:n
        if abs(imag(evalues(ii)))<0.00001
        evalues(ii)=evalues(ii)-0.00001;
        end
        YXU(:,ii)=V(:,I(ii));
end
Y=YXU(1:n,:);
X=YXU((n+1):(2*n),:);
U=YXU((2*n+1):(2*n+m),:);
RK=lsq(X',U');
K=-real(RK');
```

```
PK=lsq(X',Y');
P=real(PK');
P=(P+P')/2;
end

function [X]=lsq(A,B)
[u,s,v]=svd(A);
bb=u'*B;
n=rank(s);
nn=1:n;
[k,l]=size(B);
xx=zeros(k,l);
xx(nn,:)=inv(s(nn,nn))*bb(nn,:);
X=v*xx;
```

APPENDIX C

The Matlab routine for solving the generalised H∞ control problem is detailed below. This algorithm was used to generate the feedback gain given in Chapter 10 such that an output feedback sliding mode controller could be achieved. This algorithm was developed by Dr. Y.A. Jiang at the University of New South Wales, Sydney, Australia.

```
function [r,D,K] = cdmu1(A,F,B,H,E,bsize,type,tol)
% CDMU1  Minimization of H-inf norm subject to state feedback and
%        block diagonal uncertainty scaling.
%        The system is    dx/dt = Ax + Fw + Bu
%                               z = Hx      + Eu
%        with uncertainty  w = Lz  and control  u = -Kx.
%        The uncertainty description is described by the size
%        vector and the type vector (repeated ~= 0, unrepeated = 0).
%        The parameter tol controls the accuracy.
%
% Usage:   [hinf,D] = cdmu1(A,F,B,H,E,bsize,type,tol)
%       or
%         hinf = cdmu1(A,F,B,H,E)
%
%       bsize=size of blocks
%       type =type of block (repeated~=0 and unrepeated=0)
%
% On return, hinf is the H-inf norm for the optimal scaling D.
%

nn = nargin;
if ~((nn == 5) | (nn == 8)),
   error('must have 5 or 8 arguments');
end
error(abcdchk(A,B,H,E));
error(abcdchk(A,F,H));
```

```
[n,nd] = size(F);
%
% Fix up the checking
%

  D = eye(nd);
  ls=2;
if nn == 8
   [l,m]  = size(type);
   Dt     = zeros(nd);
end
l1=1;fp=1;lp=fp;la=fp;lpp=1e10;
ru=1e9;

mu = 0;      % Inverse of square of H-inf norm
mulow = 0;   % Lower bound of inverse of square of H-inf norm
kkr = 0;     % No. of Riccati equations
kkl = 0;     % No. of Lyapounov equations
kk1 = 0;     % No. of iterations
llo = 1;     % While loop flag for termination
ru  = 1e9;   % Upper bound for H-inf norm
SE=eye(nd);

while llo > 0;
  if nn == 8
    Hs = D*H; Fs = F*inv(D); Es = D*E;
  else
    Hs = H; Fs = F; Es = E;
  end
  ND = inv(Es'*Es);
  As = A-B*ND*Es'*Hs;
  SD = eye(nd) - Es*ND*Es';
%  SD = eye(Es*Es') - Es*ND*Es';
```

```
 Q  = Hs'*SD*Hs;
 s1 = Fs*Fs';
%
%  Searching for optimal H-inf norm with Scherers' method
%
 kk  = 1;  % While loop flag for termination
 kl  = 1;  % Step size parameter
 kkk=0;
 k=0;
 while kk > 0
   Ric = [As', -Q; mu*s1-B*ND*B', -As];
   [v,d] = eig(Ric);
   kkr=kkr+1;
   d = diag(d);
   [d1,index] = sort(-real(d));
   if (~( (d1(n)<-1e-12) & (d1(n+1) > 1e-12) ))
     if kk1 > 0
       kk=0;kkk=1;
     else
       k=k/2;mu=mulow+k;
     end
   else
     kkk=0;
     chi = v(1:n,index(1:n));
     lambda = v((n+1):(2*n),index(1:n));
     P = -real(lambda/chi);
     if (min(eig(P)) < -1e-9) & (kk1 > 0);
       kk=0;kkk=1;
     else
       dP=lyap(-(As+P*Q),s1);
       kkl=kkl+1;
       k=min(eig(P/dP));
       mulow=mu;mu=k+mulow;
```

```
        if abs(k/mu) < 1e-5;kk=0;end
      end
    end
  end
  if kkk==0
     r=1/(mu^.5);
  end
%
% Searching for descent directions of scaling matrix D
%
  r = sqrt(1/mu);  % H-inf norm
  hinf=r;
  if nn == 8,
    if ru > r,
      D,r,
      [kk1,kkr,kkl],
      [v,d] = eig(P); [d1,index]=sort(diag(d));
      x = v(:,index(1)); y = v(:,index(n));
      Aq = -(As'+Q*P);
      P1 = lyap(Aq,x*x');
      kkl = kkl+1;
      U = Fs'/r; V = SD*Hs*P + Es*ND*B';
      l1 = ls; w = 0;
      for l = 2:m,
        l2 = l1+bsize(l)-1;
        u = U(l1:l2,:); v = V(l1:l2,:);
        d = u*P1*u'-v*P1*v';
        if type(l) < 1;
          KD(l1:l2,l1:l2) = eye(l2-l1+1)*trace(d);
        else
          KD(l1:l2,l1:l2) = d;
        end
        w = w+u'*KD(l1:l2,l1:l2)*u-v'*KD(l1:l2,l1:l2)*v;
```

```
      l1 = l2+1;
    end
%
% Search for Step size
%
    lpold=lp;
    P1 = lyap(Aq',w);
    kkl=kkl+1;
    P = P + eye(n,n)*1e-7;
    d = real(eig(inv(P)*P1));
    if abs(max(-d)) > 1e-5
       lp = abs(1/max(-d));
    else
       lp=1e5;
    end
    lp = lp/2;
    d = max(abs(diag(KD)*lp*fp)/2);
    if d > 2;
       lp = lp*2/d;
    end
%
% Generate scaling matrix
%
    Dtold = Dt;
    Dt = Dt+KD*lp*fp/2;
    l1=ls;
    for l=2:m,
      l2 = l1+bsize(l)-1;
      [u,d] = eig(Dt(l1:l2,l1:l2));
      D(l1:l2,l1:l2) = u*diag(exp(diag(d))')*u';
      l1 = l2+1;
    end
    kk1 = kk1+1;
```

```
      if kk1 > 3; fp = fp*1.3; end
      ee = abs(ru-r); ru = r;
      if ee < tol; llo=0; end
    else
%
% Reduce Step
%
      lp=lpold;
      fp = fp/4;
      Dt = Dtold+KD*lp*fp/2;
      l1 = ls;
      for l = 2:m,
        l2 = l1+bsize(l)-1;
        [u,d] = eig(Dt(l1:l2,l1:l2));
        D(l1:l2,l1:l2) = u*diag(exp(diag(d))')*u';
        l1 = l2+1;
      end
      if fp < 1e-2; llo = 0; end
    end
  else
    llo = 0;
  end
end
  r=hinf*1.1
  Hs = D*H; Fs = F*inv(D); Es = D*E;
  ND = inv(Es'*Es);
  As = A-B*ND*Es'*Hs;
  SD = SE - Es*ND*Es';
  Q  = Hs'*SD*Hs;
  P=lqgf(As,B*ND*B'-Fs*Fs'/(r*r),Q)
  K = ND*(B'*P+Es'*Hs)
  eig(A-B*K)
end
```